

**NUMERICAL ANALYSIS OF THE FLOWS IN
THE PEBBLE BED GEOMETRIES**

by

Aziz Takhirov

B. S. in Mathematics, National University of Uzbekistan,
2007

M. S. in Mathematics, North Dakota State University,
2009

Submitted to the Graduate Faculty of
the Kenneth P. Dietrich Graduate School of Arts and
Sciences in partial fulfillment
of the requirements for the degree of

Doctor of Philosophy

University of Pittsburgh

2014

UNIVERSITY OF PITTSBURGH
DEPARTMENT OF MATHEMATICS

This dissertation was presented

by

Aziz Takhirov

It was defended on

May 5th 2014

and approved by

William Layton, Ph.D., Professor

Ivan Yotov, Ph.D., Professor

Catalin Trenchea, Ph.D., Professor

Paolo Zunino, Ph.D., Professor

Dissertation Director: William Layton, Ph.D., Professor

NUMERICAL ANALYSIS OF THE FLOWS IN THE PEBBLE BED GEOMETRIES

Aziz Takhirov, PhD

University of Pittsburgh, 2014

Many industrial processes in engineering occur in complex fluid-solid regions. In this thesis, we discuss Finite Element algorithms for modelling the fluid flow and heat transfer in such domains. Often times, for these types of problems, the meshing (and remeshing for time-dependant problems) process is the most computationally demanding portion of the solution process. We develop and analyze various algorithms that can be applied on a uniform mesh, by incorporating information about the geometry of the flow domain into the model.

Keywords: Navier-Stokes, Brinkman, fictitious domain, Lagrange multiplier, volume penalization.

TABLE OF CONTENTS

PREFACE	ix
1.0 INTRODUCTION	1
2.0 MATHEMATICAL PRELIMINARIES	7
2.1 Elements of Functional Analysis	8
2.2 Finite Element methods	12
2.2.1 Ingredients of the Finite Element methods	12
2.2.2 Saddle-point problems	13
2.2.3 Approximation properties of FE polynomial spaces	16
3.0 THEORY AND APPROXIMATION OF FLUID FLOW	18
3.1 Navier-Stokes equations	18
3.2 Brinkman flow models	20
3.2.1 Brinkman Volume Penalization	20
3.3 Heat transfer equation	25
4.0 BRINKMAN VOLUME PENALIZATION BASED MODEL FOR SMALL <i>RE</i> FLOWS	27
4.1 Preliminaries	28
4.2 Weak formulations	30
4.2.1 Discrete subspaces	33
4.2.2 Linear system	34

4.3	Well-posedness, stability and convergence	34
4.4	Numerical experiments	41
5.0	BRINKMAN VOLUME PENALIZATION BASED MODEL	
	FOR MODERATE <i>RE</i> FLOWS	49
5.1	Weak formulations	51
5.1.1	Linear system	54
5.2	Well-posedness, stability and convergence	55
5.3	Numerical experiment	64
6.0	BRINKMAN VOLUME PENALIZATION BASED MODEL	
	FOR MODERATE <i>RE</i> FLOWS AND FORCED HEAT CON-	
	VECTION	72
6.1	Weak formulations	72
6.2	Well-posedness, stability and convergence	74
6.3	Numerical experiments	84
7.0	CONCLUSIONS AND FUTURE PROSPECTS	93
7.1	Conclusions	93
7.2	Future prospects	94
	BIBLIOGRAPHY	96

LIST OF TABLES

4.1	L^2 errors and rates	48
4.2	$L^2(\Omega_s)$ errors and rates	48
5.1	Average pressure drops across the channel, the "true" average pressure drop is around -0.57	70
5.2	The $L^2(\Omega)$ errors at $t = 1$	70
5.3	The $l^2((0, T); L^2(\Omega_s))$ errors	71
6.1	Errors in $L^2(\Omega)$ norm, at $t = t_f$	87

LIST OF FIGURES

1.1	Packed Bed Reactor used for Drinking Water Denitrification [33] . . .	3
1.2	Pebble Bed Reactor	3
1.3	Solid ball and Brinkman penalization region	5
2.1	Typical flow domain in 2d	7
4.1	The body-fitted, resolved Stokes speed contours	42
4.2	Mesh 1 ($h = 0.55$) and Ω_s	43
4.3	Mesh 2 ($h = 0.27$) and Ω_s	43
4.4	Mesh 3 ($h = 0.14$) and Ω_s	43
4.5	From top to bottom: speed contours of M2 on meshes with $h \simeq 0.11$, $h \simeq 0.055$, $h \simeq 0.027$, $\varepsilon = h^2$	44
4.6	From top to bottom: speed contour of M2, with $h = 0.014$, $\varepsilon = h^2$ and $h = 0.027$, $\varepsilon = 10^{-15}$, and of M1, with $h = 0.007$, $\varepsilon = h^2$	46
4.7	From top to bottom: speed contour of M1, with $h = 0.027$, $\varepsilon = 10^{-15}$ and $h = 0.014$, $\varepsilon = 10^{-15}$, and of M2, with $h = 0.014$, $\varepsilon = 10^{-15}$	47
5.1	Ball and an old penalization region	50
5.2	Ball and a new penalization region	50
5.3	Body-fitted mesh for the "true" solution	65
5.4	The body-fitted, resolved Navier-Stokes velocity speed contours with streamlines at $t = 1$	65

5.5	Two coarsest meshes, Ω_s and Ω_{s_h} (the shaded triangles)	67
5.6	From top to bottom: speed contours of M2 on first three meshes, $h \simeq 0.037, h \simeq 0.02, h \simeq 0.0147$	68
5.7	From top to bottom: speed contours of M1 on first three meshes, $h \simeq 0.037, h \simeq 0.02, h \simeq 0.0147$	69
6.1	The body-fitted, resolved temprature field contours at $t = t_f$	85
6.2	The body-fitted, resolved temprature field contours at $t = t_f, \kappa_{eff} = \frac{1}{6}$	86
6.3	From top to bottom: speed contours of our model on meshes with $h \simeq 0.037, h \simeq 0.02, h \simeq 0.0147$	88
6.4	From top to bottom: speed contours of Brinkman model on meshes with $h \simeq 0.037, h \simeq 0.02, h \simeq 0.0147$	89
6.5	From top to bottom: temperature contours of our model for $\kappa_{eff} = \frac{1}{6}$ on meshes with $h \simeq 0.037, h \simeq 0.02, h \simeq 0.0147$	90
6.6	From top to bottom: temperature contours of the Brinkman model for $\kappa_{eff} = \frac{1}{6}$ on meshes with $h \simeq 0.037, h \simeq 0.02, h \simeq 0.0147$	91
6.7	From top to bottom: outlet temperatures for $\kappa_{eff} = \frac{1}{6}$ on meshes with $h \simeq 0.037, h \simeq 0.02, h \simeq 0.0147$	92

PREFACE

I would like to thank my advisor, Prof. William Layton, for introducing me to the fascinating world of computational fluid dynamics. His constant encouragement, brilliant ideas and generous financial support helped me to successfully complete this and other research projects.

I am also grateful to the committee members, Prof. Catalin Trenchea, Prof. Ivan Yotov and Prof. Paolo Zunino, for their willingness to dedicate their time and efforts for this project.

1.0 INTRODUCTION

Despite being the research topic for centuries, the mathematical analysis of flow problems still contains many challenges. The Navier-Stokes equations is the correct mathematical description of incompressible fluid flows, yet, the analytic, closed form solutions are known only for a few simple flows, limiting the practicality of the analytic approach. On top of that, the well-posedness of the solutions is still an open problem [1]. Given that fluid flows occur ubiquitously in engineering, biology and other disciplines, there is a strong need for the development of robust, accurate and practical numerical models for them.

In this thesis, we are interested in developing Finite Element based numerical algorithms for the flows occurring in geometrically complex fluid-solid domains. Some of the motivating applications where such flows occur include:

- Pebble Bed Reactors (PBR) [36, 37]: PBRs are one design for power generating, which was used in Germany, South Africa and under the study in US and China. It has a much higher safety factor than current reactor designs have. The flow through the core of PBRs is not well understood yet (e.g. the temperature inside the pebble bed reactors are often off the predicted values by 200 °C and due to high reactor temperatures it is impossible to place standard measurement equipment in the core [36]);
- Packed Bed Reactors [6]: Packed bed reactors can be used in chemical reaction. These reactors are tubular and are filled with solid catalyst particles, most often

used to catalyze gas reactions [46];

- Trickle Bed Reactors [40]: Trickle beds with countercurrent flow of gas and liquid are used on a large scale for vinegar production, as biofilters for gas clean-up and deodorisation, for water purification and for ore leaching. Trickle beds can be operated with or without recycling, but recycling allows higher loading and gives better flow distribution, which is even more critical than in submerged packed bed operation;
- Other processes in chemical refining and manufacturing industry, such as in catalytic reactors, chromatographic reactors, ion exchange columns and absorption towers [14, 48, 26].

For these applications, the essential flow features such as flow start up, heat transfer and recirculation regions (in which heat concentrates) must be accurately predicted by any reasonable numerical model. The fundamental difficulty in these types of flows is the complex flow geometry. Constructing body-conforming mesh might be computationally expensive, if not impossible. Further, in many applications, the geometry of the fluid domain changes through time, making the meshing process even more challenging. An additional hurdle is the turbulent nature of these flows: they typically occur at high Re number.

For the simplicity of the mathematical presentation, we assume that the solids are mono-sized, stationary spheres. When the solid particles are not spherical, they can be represented as an equivalent sphere of the same volume, which can be characterized by the sphericity (the measure of how round an object is) [49].

Generally, the viscous flow inside fluid-solid system is described by Navier-Stokes equations in the fluid domain with no-slip boundary conditions at the solid

Figure 1.1: Packed Bed Reactor used for Drinking Water Denitri-
fication [33]

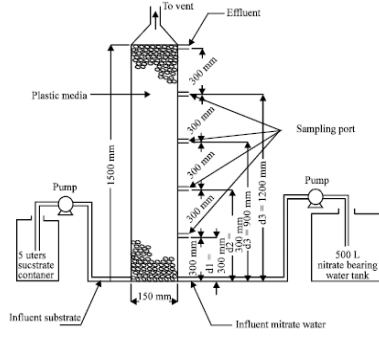
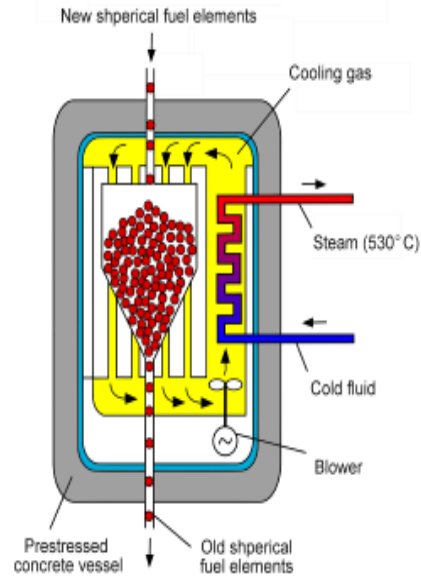


Figure 1.2: Pebble Bed Reactor



interfaces:

$$u_t + u \cdot \nabla u - \nu \Delta u + \nabla p = f \text{ in fluid domain,}$$

$$\nabla \cdot u = 0 \text{ in fluid domain,}$$

$$u = 0 \text{ on solid interface.}$$

The finite element methods based on these equations use body-fitted meshes. As mentioned above, when the number of solid bodies is large, meshing such region becomes computationally very demanding (e.g. pebble-bed reactors contain nearly 400,000 graphite covered uranium spheres [41, 42]).

One alternative approach is the Darcy based models. But they are inadequate since

a) the Darcy models are appropriate for the flows with [7], [16]

$$Re_{porous} := \frac{qd}{\nu} \leq 1,$$

where d is the diameter of pore, ν is the kinematic viscosity and q is the specific discharge. Since the diameters of the pores are too big and velocity can be too large in many industrial processes, the Darcy model can be inaccurate model.

b) Darcy models fail to predict recirculation regions (where the heat concentrates). Since

$$\mathbf{u} = -K\nabla p \Rightarrow \nabla \times \mathbf{u} = 0.$$

Another approach with some promise is the Brinkman model [12] used as volume penalization of the flow in the solid bodies [4, 5]. In this method the original domain is embedded inside a geometrically simple fictitious auxiliary domain, in which flow obeys the Navier-Stokes-Brinkman equations. The particular medium is then taken into account by its characteristic permeability and viscosity, i.e. infinite permeability in the fluid region, zero permeability in the solid region and very large viscosity in the solid region. That is, for a fixed small penalty parameter $\varepsilon > 0$, the Brinkman parameters are

$$\tilde{\nu} = \begin{cases} \nu & \text{if } x \text{ in Fluid region,} \\ \frac{1}{\varepsilon} + \nu & \text{if } x \text{ in Solid region,} \end{cases}$$

and

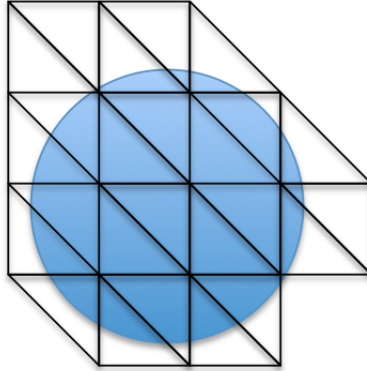
$$K = \begin{cases} \infty & \text{if } x \text{ in Fluid region,} \\ \varepsilon & \text{if } x \text{ in Solid region.} \end{cases}$$

The Navier-Stokes-Brinkman volume penalization of flow in solid domain is given by the following system

$$\begin{aligned} u_t + u \cdot \nabla u - \nabla \cdot (\tilde{\nu} \nabla \mathbf{u}) + \frac{1}{K} \mathbf{u} + \nabla p &= \mathbf{f} \text{ in Solid} \cup \text{Fluid region,} \\ \nabla \cdot \mathbf{u} &= 0 \text{ in Solid} \cup \text{Fluid region,} \end{aligned}$$

where \mathbf{f} is the body force.

Figure 1.3: Solid ball and Brinkman penalization region



The Finite Element approximation of Brinkman volume penalization method is straightforward to analyze and implement. However, the Brinkman model based Finite Element methods on meshes non-conforming to the fluid-solid interface, investigated in [31], concluded that, *if the finite element mesh does not resolve fluid solid interface, Brinkman simulations can fail to predict reliably flow start up, heat transfer and recirculation regions*. The fundamental reason for the Brinkman Volume Penalization model's failure is that on non-conforming mesh the penalization regions extend beyond the actual solid ball to all the elements having non-empty intersection with the solid, Figure 1.3, see Chapter 5 for further elaboration.

For very small values of ε , this results in flow being obstructed in the elements shared by the solids. This often dramatically changes the entire flow structures and yields very underresolved solutions. On the other hand, picking larger values of ε is not satisfactory either, as the fluid is allowed to flow too fast through the solid region. In the next chapters, we discuss three methods for improving the Brinkman volume penalization model.

In Chapter 4, we develop an algorithm for small Re flows. In order to capture

more geometry of the solid region, in addition to Brinkman penalization, we enforce the weak no-flow in the solids through minimally chosen Lagrange multipliers space. To ensure the inf-sup stability on the coarse meshes, we also augment the discrete velocity space with special spherical bubble functions. The goal then consists of picking a ε such that, the combination of all the ingredients yields improved results compared to the Brinkman model.

In Chapter 5, we develop an algorithm for moderate Re flows. The natural extension of the model of Chapter 4 did not yield numerical results as good as in the case creeping flow. Thus, we improve the model by restricting the volume penalization region to the finite elements that are entirely contained in the solid region. The Lagrange multiplier will enforce the weak no-flow in the remainings parts of the solids.

In Chapter 6, we develop an algorithm for the convective heat transfer, where the convecting velocity is computed via the approach of Chapter 5. In order to stabilize the discrete solution for convection dominated flows, we apply the Streamline Diffusion FEM.

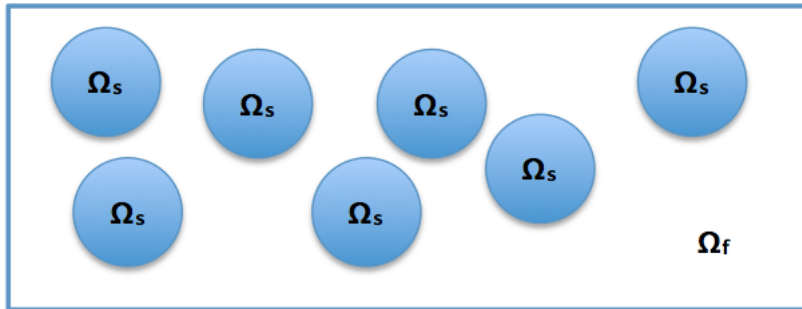
2.0 MATHEMATICAL PRELIMINARIES

This chapter introduces some fundamental concepts and common notations used extensively in this thesis. The specifics will be introduced as needed.

Let $\Omega \subset R^d, d = 2, 3$, denote an open, simply connected, bounded domain, with Lipschitz continuous boundary. We often break down Ω (Fig. 2.1) into a purely fluid domain Ω_f and purely solid domain $\Omega_s = \bigcup_{i=1}^S B_i$, where $B_i := \{\mathbf{x} \in R^d : |\mathbf{x} - \mathbf{x}_i| < r\}, B_i \cap B_j = \emptyset, i \neq j$ is a d-ball centered at \mathbf{x}_i and with a radius r .

The usual notation χ_ω will be used for the characteristic function of the set ω and \mathbf{e}_i will be used for the standard i -th basis vector of R^d . For a given region ω , the outer unit normal to the boundary $\partial\omega$ will be denoted by $\mathbf{n}_{\partial\omega}$. For Ω and its subsets, we make further simplifications: if $\omega = \{\Omega, \Omega_f, \Omega_s\}$, then correspondingly $\mathbf{n}_{\partial\omega} = \{\mathbf{n}, \mathbf{n}_f, \mathbf{n}_s\}$.

Figure 2.1: Typical flow domain in 2d



Throughout this thesis, the letter C (with or without subscripts), will be used

to denote a generic constant, independent of h , which assumes different values at different places.

2.1 ELEMENTS OF FUNCTIONAL ANALYSIS

Definition 2.1.1. Let $1 \leq p \leq \infty$, and suppose $f : \omega \rightarrow \mathbb{R}$ is a measurable function. The $L^p(\omega)$ -norm of f is defined as

$$\|f\|_{L^p(\omega)} := \begin{cases} \left(\int_{\omega} |f|^p dx \right)^{1/p} & \text{if } 1 \leq p < \infty, \\ \text{ess sup}_{\omega} |f| & \text{if } p = \infty, \end{cases}$$

and space of all measurable functions for which

$$\|f\|_{L^p(\omega)} < \infty$$

is denoted by $L^p(\omega)$.

Definition 2.1.2. Let $\alpha = (\alpha_1, \dots, \alpha_N) \in \mathcal{N}^N$ and $|\alpha| = \sum_{n=1}^N \alpha_n$. For given integer $m \geq 0$ and real $p \in [1, \infty]$, we say that $f \in L^p(\omega)$ belongs to the Sobolev space $W^{m,p}(\omega)$ if and only if

$$\partial^{\alpha} f \in L^p(\omega) \quad \forall |\alpha| \leq m,$$

where, $\partial^{\alpha} v = \frac{\partial^{|\alpha|} v}{\partial x_1^{\alpha_1} \dots \partial x_N^{\alpha_N}}$ is the distributional α -th partial derivative of f . $W^{m,p}(\omega)$ is a Banach space for the norm

$$\|f\|_{W^{m,p}(\omega)} := \begin{cases} \left(\sum_{|\alpha| \leq m} \int_{\omega} |\partial^{\alpha} f|^p dx \right)^{1/p} & \text{if } 1 \leq p < \infty, \\ \max_{|\alpha| \leq m} \left(\text{ess sup}_{\omega} |f| \right) & \text{if } p = \infty. \end{cases}$$

Further, $W^{m,p}(\omega)$ is equipped with the following seminorm

$$|f|_{W^{m,p}(\omega)} := \left(\sum_{|\alpha|=m} \int_{\omega} |\partial^{\alpha} f|^p dx \right)^{1/p} \quad \text{if } 1 \leq p < \infty.$$

When $p = 2$, we identify $H^m(\omega) := W^{m,2}(\omega)$, $\|f\|_{m,\omega} := \|f\|_{W^{m,2}(\omega)}$ and $|f|_{m,\omega} := |f|_{W^{m,2}(\omega)}$. In particular, if $m = 0$, then $|f|_{m,\omega} = \|f\|_{W^{m,2}(\omega)}$. $H^m(\omega)$ is a Hilber space with the following inner product

$$(f, g)_{m,\omega} := \sum_{|\alpha| \leq m} \int_{\omega} \partial^{\alpha} f \partial^{\alpha} g dx.$$

If $m = 0$, this reduces to standard $L^2(\omega)$ inner product, and we will omit the m subscript.

Lemma 2.1.3. (*Trace theorem*)[2] *Let $1 \leq p < \infty$. Assume ω is bounded, open with Lipschitz boundary $\partial\omega$. Then there exists a bounded linear operator $\gamma_0 : W^{1,p}(\omega) \rightarrow W^{\frac{1}{p},p}(\partial\omega)$, $\frac{1}{p} + \frac{1}{p} = 1$, such that*

(i) $\gamma_0 f = f|_{\partial\omega}$ if $f \in W^{1,p}(\omega) \cap C(\bar{\omega})$,

(2) $\|\gamma_0 f\|_{W^{\frac{1}{p},p}(\partial\omega)} \leq C \|f\|_{W^{1,p}(\omega)}$,

(3) γ_0 is surjective,

(4) $\text{Ker} \gamma_0 = W_0^{1,p}(\omega)$,

for each $f \in W^{1,p}(\omega)$, with the constant C depending only on p and ω . $\gamma_0 f$ is called the trace of f on $\partial\omega$.

The range of the trace operator γ_0 forms a proper subset of $L^p(\partial\omega)$ and for $p = 2$ it is denoted by $H^{1/2}(\partial\omega)$. The norm on $H^{1/2}(\partial\omega)$ is defined as follows

$$\|g\|_{1/2,\partial\omega} := \inf_{f \in H^1(\omega), \gamma_0 f = g} \|f\|_{1,\omega}.$$

$W_0^{1,2}(\omega)$ is denoted by $H_0^1(\omega)$. One important property of $H_0^1(\omega)$ is the Poincarè's inequality.

Lemma 2.1.4. (*Poincaré's inequality*)[39] *There exists a constant $C_\omega = \frac{2\text{diam}(\omega)}{d}$ such that*

$$\|f\|_\omega \leq C_\omega |f|_{1,\omega}. \quad (2.1.1)$$

One of the consequence of the Poincaré's inequality is that the seminorm $|\cdot|_{1,\omega}$ is a norm on $H_0^1(\omega)$.

We shall also be interested in the dual spaces of $H_0^1(\omega)$ and $H^{1/2}(\partial\omega)$. The dual space of $H_0^1(\omega)$ is $H^{-1}(\omega)$ with a dual norm

$$\|\phi\|_{-1,\omega} := \sup_{f \in H_0^1(\omega), f \neq 0} \frac{\langle \phi, f \rangle}{|f|_{1,\omega}}.$$

where $\langle \cdot, \cdot \rangle$ is duality pairing between $H_0^1(\omega)$ and $H^{-1}(\omega)$. $H^{-1/2}(\partial\omega)$, the dual of $H^{1/2}(\partial\omega)$, is equipped with similar dual norm:

$$\|\psi\|_{-1/2,\partial\omega} := \sup_{g \in H^{1/2}(\partial\omega), g \neq 0} \frac{\langle \psi, g \rangle}{\|g\|_{1/2,\partial\omega}},$$

where $\langle \cdot, \cdot \rangle$ is duality pairing between $H^{1/2}(\partial\omega)$ and $H^{-1/2}(\partial\omega)$. In general, the dual space of Y will be denoted by Y' . We apply the same notations for the norms and inner products of scalars, vectors and tensors and let the context determine the appropriate spaces.

Mostly we will be dealing with integral and inner products over Ω and its subsets. In order to further simplify the notation, when $\omega = \Omega$, we simply omit Ω in the subscripts. Moreover, for subsets of Ω , we only use the respective letters in the subscripts, e.g., if $\omega = \Omega_s$, then $(\cdot, \cdot)_\omega = (\cdot, \cdot)_s$ and so on.

Next we define the standard spaces used in the finite element analysis of our models.

Definition 2.1.5. Let $\Omega_* = \Omega_f, \Omega_s, \Omega$ if $*$ = f, s or $*$ is omitted, respectively.

$$L_0^2(\Omega_*) := \left\{ q \in L^2(\Omega_*) : \int_{\Omega_*} q = 0 \right\},$$

$$V(\Omega_*) := \{v \in H_0^1(\Omega_*) : (\nabla \cdot v, q) = 0 \forall q \in L_0^2(\Omega_*)\},$$

$$X_* := H_0^1(\Omega_*), \quad Q_* := L_0^2(\Omega_*), \quad L := L^2(\Omega_s).$$

For space-time functions $f(x, t), x \in \omega, t \in (0, t_f), t_f > 0$, it is natural to introduce the following Banach space

$$L^q((0, t_f); H^m(\Omega)) = \left\{ v : (0, t_f) \rightarrow H^m(\Omega) \text{ such that } \int_0^{t_f} \|v(t)\|_m^q dt < \infty \right\}$$

endowed with the norm

$$\|v\|_{q,m} = \left(\int_0^{t_f} \|v(t)\|_m^q dt \right)^{1/q}$$

and a seminorm

$$|v|_{q,m} = \left(\int_0^{t_f} |v(t)|_{m,\Omega}^q dt \right)^{1/q}.$$

We also introduce the following discrete-in-time analog of $|v|_{q,m}$ seminorm on the time interval $(0, t_f)$

$$|v|_{m,k} := \left(\Delta t \sum_{n=0}^N |v^n|_k^m \right)^{1/m},$$

where Δt is the timestep and $N\Delta t = t_f$.

2.2 FINITE ELEMENT METHODS

In this section we collect some necessary facts from the theory of the Finite Element Methods (FEM).

2.2.1 Ingredients of the Finite Element methods

Finite Element (FE) based approaches are one of the very common and efficient ways of solving partial differential equations numerically [11, 17]. In FEM, the problem domain ω is decomposed into elementary pieces, which are called *elements*. Formally, this is expressed as $\omega = \mathcal{T}_h = \bigcup_{K \in \mathcal{T}_h} K$. \mathcal{T}_h is called the mesh of the domain ω . Most commonly used meshes are triangular (tetrahedral), quadrilateral and hexahedral meshes [20]. The parameter $h > 0$ is called the *meshwidth* of \mathcal{T}_h and is defined as follows

$$h_K := \text{diam}K, \quad h = \max_{K \in \mathcal{T}_h} h_K.$$

Our theory will be developed for the triangular (or tetrahedral) meshes, but they can be extended to quadrilateral ones with appropriate modifications. Throughout the analysis, we assume that the family of grids $\{\mathcal{T}_h\}$ satisfies the following conditions

1. *Regularity*: For each $K \in \mathcal{T}_h$, let ρ_K be the diameter of the ball inscribed in K . Then there exists $\delta > 0$ such that

$$\frac{h_K}{\rho_K} \leq \delta \quad \forall K \in \mathcal{T}_h.$$

2. *Quasi-uniformity*: \mathcal{T}_h is shape regular and there exist constants $c_1, c_2 > 0$ such that

$$\forall K_1, K_2 \in \mathcal{T}_h \Rightarrow c_1 h_{K_1} \leq h_{K_2} \leq c_2 h_{K_1}.$$

The second aspect of FE methods is the discrete solution space. Given triangulation (tetrahedralization) \mathcal{T}_h of ω , the solution of the partial differential equation is approximated within each element with a low-degree polynomial. We denote by P_k the space of globally continuous polynomials, which have global degree less than or equal to k when restricted to elements of the mesh

$$P_k = \left\{ p(x) \in C(\bar{\omega}) : \sum_{i,j,k \geq 0, i+j+m \leq k} a_{ijm} x^i y^j z^m \text{ with } a_{ijm} \in R \right\}.$$

Similar to norm notations, P_k will be used for scalar, vector and tensor polynomials of global degree less than or equal to k .

2.2.2 Saddle-point problems

We next briefly discuss the theory of the saddle-point problems, which are important in the analysis of many flow problems. Saddle-point problems have the following general form. Assume X and M are Hilbert spaces with the norms $\|\cdot\|_X$ and $\|\cdot\|_Q$. Let $a : X \times X \rightarrow R, b : X \times Q \rightarrow R$ be bilinear forms, find $(u, p) \in (X, Q)$ such that

$$a(u, v) + b(v, p) = \langle f, v \rangle \quad \forall v \in X, \quad (2.2.1)$$

$$b(u, q) = \langle g, q \rangle \quad \forall q \in Q, \quad (2.2.2)$$

where $f \in X', g \in Q'$ and $\langle \cdot, \cdot \rangle$ is the appropriate duality pairing. Equivalently, the above problem can be expressed in the operator form. To this end, we define linear operators $A \in \mathcal{L}(X, X'), B \in \mathcal{L}(X, Q')$ associated with bilinear forms $a(\cdot, \cdot), b(\cdot, \cdot)$ in the following way

$$\langle Aw, v \rangle = a(w, v) \quad \forall v, w \in X,$$

$$\langle Bv, \mu \rangle = b(v, \mu) \quad \forall v \in X, \mu \in Q.$$

The well-posedness of saddle-point problems depends on the fulfillment of the following inf-sup condition

$$\exists \beta > 0 \text{ such that } \inf_{q \in Q} \sup_{v \in X} \frac{b(v, q)}{\|v\|_X \|q\|_Q} \geq \beta. \quad (2.2.3)$$

Let

$$X^0 = \{v \in X : b(v, q) = 0 \ \forall q \in Q\}.$$

Then (2.2.3) can be restated in terms of linear operators A, B [22].

Lemma 2.2.1. *The three following statements are equivalent:*

- (2.2.3) holds;
- the operator B^T is an isomorphism from Q onto $X_{polar}^0 := \{g \in X' : \langle g, v \rangle = 0 \ \forall v \in X^0\}$; moreover,

$$\|B^T \mu\|_{X'} = \sup_{v \in X, v \neq 0} \frac{\langle B^T \mu, v \rangle}{\|v\|_X} \geq \beta^* \|\mu\|_Q \ \forall \mu \in Q;$$

- the operator B is an isomorphism from $(X_{polar}^0)^\perp$ onto Q' ; moreover,

$$\|Bv\|_{Q'} = \sup_{\mu \in Q, \mu \neq 0} \frac{\langle Bv, \mu \rangle}{\|\mu\|_Q} \geq \beta^* \|v\|_X \ \forall v \in (X^0)^\perp.$$

Assume the bilinear forms $a(\cdot, \cdot), b(\cdot, \cdot)$ are continuous, i.e., $\exists c_1, c_2 > 0$ such that

$$|a(u, v)| \leq c_1 \|u\|_X \|v\|_X, \quad |b(v, q)| \leq c_2 \|v\|_X \|q\|_Q, \quad \forall u, v \in X, \ q \in Q. \quad (2.2.4)$$

Theorem 2.2.2. *Assume (2.2.3) holds and let the bilinear forms $a(\cdot, \cdot), b(\cdot, \cdot)$ satisfy the continuity condition (2.2.4). Moreover, let $a(\cdot, \cdot)$ be coercive on the space X^0 , that is*

$$\exists \alpha > 0 : a(v, v) \geq \alpha \|v\|_X^2 \ \forall v \in X^0. \quad (2.2.5)$$

Then for every $f \in X'$ and $g \in Q'$, there exists a unique solution (u, p) to the saddle-point problem (2.2.2) with

$$\|u\|_X + \|p\|_Q \leq C (\|f\|_{X'} + \|g\|_{Q'}). \quad (2.2.6)$$

Often times the saddle-point problem needs to be solved along with addition constraint on the variable u . The additional constraint can be enforced via new Lagrange space Q_2 , giving rise to twofold or nested saddle-point problem of the following form: Find $(u, p_1, p_2) \in (X, Q_1, Q_2)$ such that

$$\begin{cases} a(u, v) + b_1(v, p_1) + b_2(v, p_2) = \langle f, v \rangle & \forall v \in X, \\ b_1(u, q_1) = \langle g, q_1 \rangle & \forall q_1 \in Q_1, \\ b_2(u, q_2) = \langle l, q_2 \rangle & \forall q_2 \in Q_2, \end{cases}$$

with $g \in Q'_1, l \in Q'_2$, where the third equation is the weak form of the additional constraint that u must satisfy. Defining

$$b : X \times (Q_1 \times Q_2) \Rightarrow R \text{ as } b(v, (q_1, q_2)) = b_1(v, q_1) + b_2(v, q_2)$$

and

$$G : Q'_1 \times Q'_2 \Rightarrow R \text{ as } G(q_1, q_2) := \langle g, q_1 \rangle + \langle l, q_2 \rangle,$$

the twofold saddle-point problem can be rewritten as

$$\begin{cases} a(u, v) + b(v, (p_1, p_2)) = \langle f, v \rangle & \forall v \in X, \\ b(u, (q_1, q_2)) = \langle G, (q_1, q_2) \rangle & \forall (q_1, q_2) \in Q_1 \times Q_2. \end{cases}$$

Thus the corresponding twofold inf-sup condition becomes

$$\exists \gamma > 0 \text{ such that } \inf_{(q_1, q_2) \in (Q_1, Q_2)} \sup_{v \in X} \frac{b_1(v, q_1) + b_2(v, q_2)}{\|v\|_X (\|q_1\|_{Q_1} + \|q_2\|_{Q_2})} \geq \gamma. \quad (2.2.7)$$

The next theorem holds about the two-fold inf-sup conditions [53].

Theorem 2.2.3. *Let X, Q_1 and Q_2 be reflexive Banach spaces, and let $b_i : X \times Q_i \rightarrow R$ be linear and continuous. Let $Z_i = \{v \in X : b_i(v, q_i) = 0 \forall q_i \in Q_i\}$, then the following are equivalent:*

(1) *There exists $c > 0$ such that*

$$\inf_{(q_1, q_2) \in (Q_1, Q_2)} \sup_{v \in X} \frac{b_1(v, q_1) + b_2(v, q_2)}{\|v\|_X (\|q_1\|_{Q_1} + \|q_2\|_{Q_2})} \geq c; \quad (2.2.8)$$

(2) *There exists $c > 0$ such that*

$$\inf_{q_1 \in Q_1} \sup_{v \in X} \frac{b_1(v, q_1)}{\|v\|_X \|q_1\|_{Q_1}} \geq c \text{ and } \inf_{q_2 \in Q_2} \sup_{v \in Z_1} \frac{b_2(v, q_2)}{\|v\|_X \|q_2\|_{Q_2}} \geq c; \quad (2.2.9)$$

(3) *There exists $c > 0$ such that*

$$\inf_{q_2 \in Q_2} \sup_{v \in X} \frac{b_2(v, q_2)}{\|v\|_X \|q_2\|_{Q_2}} \geq c \text{ and } \inf_{q_1 \in Q_1} \sup_{v \in Z_2} \frac{b_1(v, q_1)}{\|v\|_X \|q_1\|_{Q_1}} \geq c; \quad (2.2.10)$$

(3) *There exists $c > 0$ such that*

$$\inf_{q_1 \in Q_1} \sup_{v \in Z_2} \frac{b_1(v, q_1)}{\|v\|_X \|q_1\|_{Q_1}} \geq c \text{ and } \inf_{q_2 \in Q_2} \sup_{v \in Z_1} \frac{b_2(v, q_2)}{\|v\|_X \|q_2\|_{Q_2}} \geq c. \quad (2.2.11)$$

2.2.3 Approximation properties of FE polynomial spaces

Theorem 2.2.4. [11] *Assume $\{\mathcal{T}_h\}$ is a family of regular grids, $u \in H^m(\omega)$, $m \geq 1$ and $0 \leq r \leq m$. There exists a constant $C > 0$ and a FE interpolant $I_h u \in P_{m-1}$ such that*

$$\begin{aligned} |u - I_h u|_{r,K} &\leq Ch_K^{m-r} |u|_{m,K}, \\ |u - I_h u|_{r,\omega} &\leq Ch^{m-r} |u|_{m,\omega}. \end{aligned}$$

Often times we will be working with functions that have low regularity. In such cases, special interpolants are required. We list the approximation properties of two such interpolants.

Theorem 2.2.5. [47, 15] Let Π_{SZ} be the Scott-Zhang interpolation operator. Then, for small enough h , for given $\frac{1}{2} < \beta < 1$ and $0 \leq m \leq \beta$, the following local approximability result holds

$$\forall K \in \mathcal{T}_h, \forall q \in H^\beta(S_K), \|q - \Pi_{SZ}q\|_{H^m(K)} \leq Ch_K^{\beta-m} |q|_{H^\beta(S_K)},$$

where $S_K \supset K$ is suitable macroelement containing K .

Theorem 2.2.6. [24] Let $X_h = P_k, Q_h = P_{k-1}$ be the Taylor-Hood spaces with $k \leq 2, d = 2$ or $k \leq 3, d = 3$. Then the Scott-Girault interpolation operator Π_{SG} satisfies the following

- a) $\forall w \in H_0^1(\Omega) \quad |\Pi_{SG}w|_1 \leq C|w|_1,$
- b) $\forall w \in H_0^1(\Omega), \forall q_h \in Q_h \quad (q_h, \nabla \cdot (\Pi_{SG}w - w)) = 0,$
- c) $\forall w \in H^s(\Omega) \quad \|\Pi_{SG}w - w\|_{H^m(K)} \leq Ch_K^{s-m} |w|_{H^s(S_K)}$

for all real $s, 1 \leq s \leq k + 1$ and integer $m = 0$ or 1 such that $H^s(\Omega) \subset H^m(\Omega)$, where $S_K \supset K$ is suitable macroelement containing K .

3.0 THEORY AND APPROXIMATION OF FLUID FLOW

In the chapter, we discuss various aspects of the equations describing the fluid flow and the heat transfer.

3.1 NAVIER-STOKES EQUATIONS

The motion of an incompressible fluid with constant density ρ and constant viscosity μ in a domain $\omega \subset \mathbb{R}^d$ is described by Navier-Stokes equations (NSE):

$$u_t + u \cdot \nabla u - \nu \Delta u + \nabla p = f, \quad x \in \omega, t > 0, \quad (3.1.1)$$

$$\nabla \cdot u = 0, \quad x \in \omega, t > 0, \quad (3.1.2)$$

$u = u(x, t)$ being the fluid velocity, $p = p(x, t)$ the pressure divided by the density (which will simply be called "pressure"), $\nu = \frac{\mu}{\rho}$ the kinematic viscosity, μ the dynamic viscosity, and $f = f(x, t)$ a forcing term per unit mass. The equation (3.1.1) is a mathematical realization of conservation of linear momentum principle and linear stress-strain relation, while the equation (3.1.2) follows from the principle of conservation of mass [9]. Additional boundary and initial conditions are imposed for the well-posedness of (3.1.1)-(3.1.2). We will be using two types of boundary conditions

1. *Dirichlet*: $u(x, t) = \phi(x, t)$,

2. *Do-nothing*: $\left(\nu \frac{\partial u}{\partial \mathbf{n}_{\partial\omega}} - p \mathbf{n}_{\partial\omega}\right)(x, t) = \psi(x, t)$,

and standard initial conditions of the form $u(x, 0) = u^0(x)$, $\forall x \in \omega$ with $\nabla \cdot u^0 = 0$.

For $d = 2$, the Navier-Stokes equations with the boundary conditions previously indicated yield well-posed problems, provided all of the data (initial condition, forcing term, boundary data) are regular enough [18, 19]. As for $d = 3$, the existence and uniqueness of classical solutions have been proven only for a sufficiently small time interval [18, 19]. The existence of weak solutions has been proven [52, 44], but the uniqueness is an open question in R^3 [1].

Our analysis will be based on the weak formulation of Navier-Stokes equations:

Suppose that ω is locally Lipschitz, $f(x, t) \in L^2((0, t_f); H^{-1}(\omega))$, $u^0(x) \in V(\omega)$.

Then weak NS-solutions satisfy

$$(u_t, v)_\omega + (u \cdot \nabla u, v)_\omega + \nu(\nabla u, \nabla v)_\omega - (p, \nabla \cdot v)_\omega = (f, v)_\omega, \quad \forall v \in X$$

$$\nabla \cdot u = 0, \quad a.e. (x, t) \in \omega \times [0, T],$$

$$u(x, 0) = u^0(x), \quad a.e. x \in \omega.$$

Moreover, the solution satisfy $u \in L^2((0, t_f); H_0^1(\omega)) \cap V$, $u \in L^\infty((0, t_f); L^2(\omega))$, $u_t \in L^{d/4}((0, t_f); H^{-1}(\omega))$ and $p \in H^{-1}((0, t_f); L_0^2(\omega))$.

The dimensionless parameter $Re := \frac{UL}{\nu}$, called the Reynolds number, gives a rough indication of the relative magnitudes of two key terms in the equations of motion (3.1.1) - (3.1.2). Here U is the typical flow speed and L is characteristic length scale of the flow. Flows with different Re numbers have different general characteristics. If $Re \ll 1$, then the convective term $u \cdot \nabla u$ and u_t can be omitted (as these type of flows tend to be steady), and NSE reduces to Stokes equation

$$-\nu \Delta u + \nabla p = f, \quad x \in \omega, \tag{3.1.3}$$

$$\nabla \cdot u = 0, \quad x \in \omega. \tag{3.1.4}$$

On the other hand, if $Re \gg 1$, the flow will become very sensitive to small perturbations in the data and turbulent flows occur [9, 43].

3.2 BRINKMAN FLOW MODELS

Darcy model is often used to model flows in porous media with small permeabilities and small Re number [7]

$$u = -\frac{K}{\mu}\nabla p,$$

where u is the average velocity, K is the permeability, μ is the dynamic viscosity and p is the pressure. However, the Darcy's model neglects the viscous shearing stresses acting on a volume element of fluid [12]. Brinkman suggested (in the absence of convective term)

$$\nabla p = -\frac{\mu}{K}u + \bar{\mu}\Delta u.$$

The coefficient $\bar{\mu}$ is an effective viscosity. The ratio $\frac{\bar{\mu}}{\mu}$ depends on the geometry of the medium [8] and usually exceeds unity [34]. Some theoretical justifications exist for the Brinkman model as an asymptotic approximation to the NSE, e.g. see [3, 27].

3.2.1 Brinkman Volume Penalization

Starting in 1980s, number of algorithms for fluid flow have been developed for implementing the no-slip boundary conditions on the obstacle interface, e.g. [38, 21, 25]. For the high Re flows around solid obstacles, if implemented by penalization, some numerical experiments suggest that in order to obtain physically correct solutions, the penalization must be extended to the volume of the obstacle [45]. Our algorithms will be built on the penalized Brinkman problem formulated and described in [32] and analyzed in [5]. Recall from the introduction that, for a

fixed small penalty parameter $\varepsilon > 0$, the Brinkman viscosity and permeability are defined as

$$\tilde{\nu} = \begin{cases} \nu & \text{if } x \in \Omega_f, \\ \frac{1}{\varepsilon} + \nu & \text{if } x \in \Omega_s \end{cases}$$

and

$$K = \begin{cases} \infty & \text{if } x \in \Omega_f, \\ \varepsilon & \text{if } x \in \Omega_s. \end{cases}$$

That is, the viscosity is large and the permeability is small in the solid region. Then the Navier-Stokes-Brinkman volume penalization model considered in this thesis is given by

$$u_t + u \cdot \nabla u - \nabla \cdot (\tilde{\nu} \nabla u) + \frac{1}{K} u + \nabla p = f \text{ in } \Omega, \quad (3.2.1)$$

$$\nabla \cdot u = 0 \text{ in } \Omega, \quad (3.2.2)$$

where f is a forcing term. Other types of penalizations are also possible, see Definition 3.2.3, Definition 3.2.6.

(3.2.1)-(3.2.2) allows the use of the structured meshes that are not conforming to the boundary of the solids. As in the case of Navier-Stokes equations, for $Re \ll 1$, the time derivative and the convective term can be dropped, yielding Stokes-Brinkman volume penalization equation.

Next we list some variants of the continuous Navier-Stokes-Brinkman volume penalization model (3.2.1)-(3.2.2) and relevant results that have been established in the literature.

Theorem 3.2.1. [4] *Let Ω be bounded open set, of class \mathcal{C}^1 . Let $(u_\varepsilon, p_\varepsilon)$ be the solution Stokes-Brinkman volume penalization system*

$$\nu(\nabla u_\varepsilon, \nabla v) - (p_\varepsilon, \nabla \cdot v) = (f, v), \quad \forall v \in X$$

$$(q_\varepsilon, \nabla \cdot u_\varepsilon) = 0, \quad \forall q_\varepsilon \in Q,$$

and let (u, p) be the solution of the Stokes equation in the fluid region, extended by zero to solid region. Then

$$\|u - u_\varepsilon\|_1 = \mathcal{O}(\varepsilon^{1/4}), \quad \|u_\varepsilon\|_s = \mathcal{O}(\varepsilon^{3/4}).$$

Theorem 3.2.2. [4] Let Ω_f be of class \mathcal{C}^2 . Let $(u_\varepsilon, p_\varepsilon)$ and (u, p) be as in the previous theorem. Denote the resulting global force F exerted by the fluid on the obstacle by

$$F = - \int_{\partial\Omega_s} (-p\mathbf{n}_f + \nu\nabla\mathbf{u}\mathbf{n}_f).$$

Further, define the Darcy 'drag' as

$$F_\varepsilon = \int_{\Omega_s} \frac{\nu}{\varepsilon} u_\varepsilon dx - \int_{\Omega_s} f dx.$$

Then

$$|F - F_\varepsilon|_{R^d} = \mathcal{O}(\varepsilon^{1/4}).$$

Definition 3.2.3. (L^2 penalization)[5] $(u_\varepsilon, p_\varepsilon)$ is the solution of Navier-Stokes-Brinkman L^2 volume penalization of the flow if

$$\begin{aligned} u_{\varepsilon,t} + u_\varepsilon \cdot \nabla u_\varepsilon - \nu \Delta u_\varepsilon + \frac{1}{K} u_\varepsilon + \nabla p_\varepsilon &= f \text{ in } R^+ \times \Omega, \\ \nabla \cdot u_\varepsilon &= 0 \text{ in } R^+ \times \Omega, \\ u_\varepsilon(x, 0) &= u^0(x) \text{ in } \Omega, \\ u_\varepsilon &= 0 \text{ on } R^+ \times \partial\Omega. \end{aligned} \tag{3.2.3}$$

Expanding formally $u_\varepsilon = u + \varepsilon\tilde{u}$, $p_\varepsilon = p + \varepsilon\tilde{p}$, it can be shown that [5]

$$\begin{aligned}\Delta p &= 0 \text{ in } \Omega_s, \\ p|_{\Omega_s} &= p|_{\Omega_f} \text{ on } \partial\Omega_s, \\ \tilde{u} + \nabla p &= 0 \text{ in } \Omega_s.\end{aligned}$$

and

$$\begin{aligned}\tilde{u}_t + u \cdot \nabla \tilde{u} + \tilde{u} \cdot \nabla u - \nu \Delta \tilde{u} + \nabla \tilde{p} &= 0 \text{ in } \Omega_f, \\ \nabla \cdot \tilde{u} &= 0 \text{ in } \Omega_f, \\ \tilde{u}|_{\Omega_s} &= \tilde{u}|_{\Omega_f} \text{ on } \partial\Omega_s, \\ \tilde{u}(x, 0) &= 0.\end{aligned}$$

and (u, p) solve NSE in Ω_f .

Further, the following theorems hold.

Theorem 3.2.4. [5] *When $\varepsilon \rightarrow 0$, the sequence $\{u_\varepsilon\}_\varepsilon$ converges to a limit u which satisfies ‘*

$$u = 0 \text{ in } \Omega_s,$$

and $u|_{\Omega_f}$ is the unique weak solution of Navier-Stokes equation in Ω_f .

Define $H := \{u \in L^2(\Omega) : \nabla \cdot u = 0, u \cdot \mathbf{n} = 0 \text{ on } \partial\Omega\}$.

Theorem 3.2.5. [5] *Let*

$$u \in L^\infty((0, t_f); X_f) \cap L^2((0, t_f); H^2(\Omega_f))$$

be the solution of NSE in Ω_f , prolonged by zero to solid region. Then there exists v_ε bounded in $L^\infty((0, t_f); H) \cap L^2((0, t_f); V)$ such that

$$u_\varepsilon = u + \varepsilon^{\frac{1}{4}} v_\varepsilon.$$

Moreover there exists a generic function $g \in C^0(\mathbb{R}^+)$ such that

$$|v_\varepsilon|_{L^2((0, t_f); L^2(\Omega_s))} \leq g(t) \varepsilon^{\frac{1}{2}}.$$

Let $\sigma(u, p) = \frac{\nu(\nabla u + \nabla u^t)}{2} - pI$ be the stress tensor.

Definition 3.2.6. (H^1 penalization)[5] $(u_\varepsilon, p_\varepsilon)$ is the solution of Navier-Stokes-Brinkman H^1 volume penalization of the flow if

$$\begin{aligned} \left(1 + \frac{\chi_s}{\varepsilon}\right) u_{\varepsilon,t} + u_\varepsilon \cdot \nabla u_\varepsilon - \nabla \cdot \left(\left(1 + \frac{\chi_s}{\varepsilon}\right) \sigma(u_\varepsilon, p_\varepsilon) \right) + \frac{\chi_s}{\varepsilon} u_\varepsilon &= f \text{ in } R^+ \times \Omega, \\ \nabla \cdot u_\varepsilon &= 0 \text{ in } R^+ \times \Omega, \\ u_\varepsilon(x, 0) &= u^0(x) \text{ in } \mathfrak{B}.2.4 \\ u_\varepsilon &= 0 \text{ on } R^+ \times \partial\Omega. \end{aligned}$$

As in the case of L^2 penalization, from the expansion form of u_ε and p_ε , $u_\varepsilon = u + \varepsilon \tilde{u}$, $p_\varepsilon = p + \varepsilon \tilde{p}$, it can be shown that [5]

$$\begin{aligned} \tilde{u}_t - \nabla \cdot \sigma(\tilde{u}, \tilde{p}) + \tilde{u} &= 0 \text{ in } R^+ \times \Omega_s, \\ \nabla \cdot \tilde{u} &= 0 \text{ in } R^+ \times \Omega_s, \\ \sigma(\tilde{u}, \tilde{p}) \cdot \mathbf{n}_s &= \sigma(u, p) \cdot \mathbf{n}_f \text{ on } R^+ \times \partial\Omega_s, \\ \tilde{u}(x, 0) &= 0 \text{ in } \Omega_s, \end{aligned}$$

and

$$\begin{aligned} \tilde{u}_t + u \cdot \nabla \tilde{u} + \tilde{u} \cdot \nabla u - \nabla \cdot \sigma(\tilde{u}, \tilde{p}) &= 0 \text{ in } R^+ \times \Omega_f, \\ \nabla \cdot \tilde{u} &= 0 \text{ in } R^+ \times \Omega_f, \\ \tilde{u}|_{\Omega_s} &= \tilde{u}|_{\Omega_f} \text{ on } R^+ \times \partial\Omega_s, \\ \tilde{u}(x, 0) &= 0 \text{ in } \Omega_f, \end{aligned}$$

where u solves the NSE in Ω_f and $u = 0$ in Ω_s .

Theorem 3.2.7. [5] *Let u and \tilde{u} be defined as above. Then there exists $\{v_\varepsilon\}_\varepsilon$ bounded in $L^\infty((0, t_f); X_f) \cap L^2((0, t_f); V)$ such that*

$$u_\varepsilon = u + \varepsilon \tilde{u} + \varepsilon^{3/2} v_\varepsilon.$$

Moreover there exists a generic function $g \in C^0(R^+)$ such that

$$\|v_\varepsilon\|_{L^\infty(0, t_f; L^2(\Omega_s))} \leq g(t) \varepsilon^{\frac{1}{2}},$$

$$\|\nabla v_\varepsilon\|_{L^\infty(0, t_f; L^2(\Omega_s))} \leq g(t) \varepsilon^{\frac{1}{2}}.$$

3.3 HEAT TRANSFER EQUATION

Heat transfer is the movement of heat from one object to another by means of radiation, convection or conduction. Thermal radiation is the only way of heat transfer from one place to another that does not require a medium. Thermal conduction is the transfer of internal energy by microscopic diffusion and collisions of particles within a body due to a temperature gradient. Thermal convection or convective heat transport is the transfer of heat with a fluid movement. We will be considering only the latter kind of heat transfer.

Thermal convection can further be divided into two categories: natural convection and forced convection. Natural convection occurs as a consequence of natural means, such as temperature gradients and buoyancy. On the other hand, forced convection occurs when the fluid motion is generated by an external force. We will consider FE approximation to heat transfer equation in fluid-solid domain. Assuming incompressible flow with constant density, the nondimensionalized, coupled system for convective heat transport in Ω is given by the following equations:

1) Momentum equation in the fluid domain

$$\begin{aligned}
u_t + u \cdot \nabla u - Pr \Delta u + \nabla p &= \tilde{f} + Pr Ra g T \text{ in } \Omega_f \times (0, t_f], \\
\nabla \cdot u &= 0 \text{ in } \Omega_f \times [0, t_f], \\
u &= u^0(x) \text{ on } \Omega_f \times \{t = 0\}, \\
u &= 0 \text{ on } \partial\Omega_f \times [0, t_f];
\end{aligned} \tag{3.3.1}$$

2) Fluid temperature equation

$$\begin{aligned}
T_{f,t} + u \cdot \nabla T_f - \nabla \cdot (\kappa_f \nabla T_f) &= \Upsilon_f \text{ in } \Omega_f \times (0, t_f], \\
T_f &= T_f^0(x) \text{ on } \Omega_f \times \{t = 0\}, \\
T_f &= 0 \text{ on } \partial\Omega_f \times [0, t_f];
\end{aligned} \tag{3.3.2}$$

3) Solid temperature equation

$$\begin{aligned}
T_{s,t} - \nabla \cdot (\kappa_s \nabla T_s) &= \Upsilon_s \text{ in } \Omega_s \times (0, t_f], \\
T_s &= T_s^0(x) \text{ on } \Omega_s \times \{t = 0\}, \\
T_f &= 0 \text{ on } \partial\Omega_s \times [0, t_f],
\end{aligned} \tag{3.3.3}$$

where

- Pr is the Prandtl number, which describes the relationship between momentum diffusivity and thermal diffusivity;
- Ra is the Rayleigh number, which is the product of Grashof which describes the relationship between buoyancy and viscosity within a fluid and Prandtl number;
- κ_f, κ_s are thermal conductivities of the fluid and solid, respectively;
- Υ_f, Υ_s are heat sources of the fluid and solid, respectively.

When $Ra \gg 1$, then (3.3.1)-(3.3.3) describes natural convection, while for $Ra \ll 1$ it describes the forced convection and (3.3.1) can be replaced with NSE.

4.0 BRINKMAN VOLUME PENALIZATION BASED MODEL FOR SMALL Re FLOWS

This chapter is devoted to the analysis of the numerical algorithm for low Re flows in PBG and it is based on the author's article [50].

Recall the continuous Stokes-Brinkman equations are given by the following system:

$$-\nabla \cdot (\tilde{\nu} \nabla u) + \frac{1}{K} u + \nabla p = f \text{ in } \Omega, \quad (4.0.1)$$

$$\nabla \cdot u = 0 \text{ in } \Omega, \quad (4.0.2)$$

where f is the body force, K is the permeability of the medium and $\tilde{\nu}$ is the Brinkman viscosity.

We show herein that for the Stokes-Brinkman problem by *imposing the no-flow condition in the solid bodies weakly through Lagrange multipliers and enhancing the velocity space by spherical bubble functions more accurate numerical results can be obtained*. Moreover, when our proposed algorithm is used, *i)* the method is more accurate compared to the Stokes-Brinkman Volume Penalization, *ii)* the convergence rate of the velocity is decoupled from the Lagrange multiplier and *iii)* less fluid flows through the solid region, a critical test of model fidelity.

4.1 PRELIMINARIES

We assume that $f \in H^{-1}(\Omega_f)$, $\mathbf{g} \in H^{1/2}(\partial\Omega)$ and g satisfies the compatibility condition

$$\int_{\partial\Omega} g \cdot \mathbf{n} = 0.$$

We extend the forcing term f by zero to Ω_s . We denote the extension of the boundary data g by $Eg \in H^1(\Omega)$, which is assumed to satisfy $Eg = 0$ in Ω_s , $\nabla \cdot Eg = 0$ and $\|Eg\|_1 \leq C\|g\|_{1/2}$. Such extension can be obtained by using smooth cut-off functions and the property of the divergence operator, as shown below.

Lemma 4.1.1. [23, p. 288] *Let ω be a bounded domain of R^d , $d \leq 4$ with a Lipschitz-continuous boundary Γ . For $\forall \varepsilon > 0$ there exists a function $\theta_\varepsilon \in C^2(\bar{\omega})$ such that*

$$\begin{cases} \theta_\varepsilon = 1, & \text{in a neighborhood of } \Gamma, \\ \theta_\varepsilon = 0, & \text{if } d(x; \Gamma) \geq 2 \exp(-\frac{1}{\varepsilon}), \\ |\nabla \theta_\varepsilon| \leq C \frac{\varepsilon}{d(x; \Gamma)}, & \text{if } d(x; \Gamma) \leq 2 \exp(-\frac{1}{\varepsilon}), \end{cases}$$

where $d(x; \Gamma) = \inf_{y \in \Gamma} |x - y|$ is the distance function.

Lemma 4.1.2. *There exists an extension $\tilde{E}g \in H^1(\Omega)$ of the boundary data $g \in H^{1/2}(\partial\Omega)$ such that $\tilde{E}g = 0$ in Ω_s and $\|\tilde{E}g\|_1 \leq C\|g\|_{1/2}$.*

Proof. Let E' be the right inverse of the standard trace operator $\gamma_0 : H^1(\Omega) \rightarrow H^{1/2}(\partial\Omega)$, for which $\exists C > 0$ such that $\|E'g\|_1 \leq C\|g\|_{1/2}$. Set

$$d := \min\{d(\partial\Omega_s; \partial\Omega), 1\}.$$

Let $\varepsilon > 0$ be such that $d = 2 * \exp(-\frac{1}{\varepsilon})$. By Lemma 4.1.1, there exists $\theta_\varepsilon \in C^2(\bar{\Omega})$, with $\theta_\varepsilon = 0$ in Ω_s , $\theta_\varepsilon|_{\partial\Omega} = 1$. Set $\tilde{E}g = \theta_\varepsilon E'g$. It easy to see that $\tilde{E}g$ has the desired properties. \square

Lemma 4.1.3. [23, p. 24] Suppose $d \leq 3$ and $\omega \subset R^d$ is open and connected. Then, the divergence operator is an isomorphism between $V^\perp(\omega)$, where $V(\omega) = \{\mathbf{v} \in H_0^1(\omega) : \nabla \cdot \mathbf{v} = 0\}$, and $L_0^2(\omega)$. Further, $\exists \beta > 0$ such that

$$\forall q \in L_0^2(\omega) \exists! \mathbf{v} \in V^\perp(\omega), |\mathbf{v}|_{1,\omega} \leq \frac{1}{\beta} \|q\|_\omega. \quad (4.1.1)$$

Lemma 4.1.4. There exists an extension $Eg \in H^1(\Omega)$ of the boundary data $g \in H^{1/2}(\partial\Omega)$ such that $Eg = 0$ in Ω_s , $\nabla \cdot Eg = 0$ and $\|Eg\|_1 \leq C\|g\|_{1/2}$.

Proof. Note that for $\tilde{E}g$ obtained in Lemma 4.1.2, we have $\nabla \cdot \tilde{E}g \in Q_f$, because

$$\int_{\Omega_f} \nabla \cdot \tilde{E}g = \int_{\Omega} \nabla \cdot \tilde{E}g = \int_{\partial\Omega} g \cdot \mathbf{n} = 0. \quad (4.1.2)$$

By Lemma 4.1.3, $\exists! v_g \in X_f$ such that $\nabla \cdot v_g = \nabla \cdot \tilde{E}g$ and $|v_g|_{1,f} \leq \frac{1}{\beta} \|\nabla \cdot \tilde{E}g\|_f \leq \frac{\sqrt{d}}{\beta} |\tilde{E}g|_{1,f}$. Extend v_g by zero to Ω_s . Then v_g belongs to X . Let $Eg = \tilde{E}g - v_g$. Then $Eg = g$ on $\partial\Omega$, $Eg = 0$ in Ω_s , $\nabla \cdot Eg = 0$ and $\|Eg\|_1 \leq C\|g\|_{1/2}$. \square

4.2 WEAK FORMULATIONS

Definition 4.2.1. Let g_h be an interpolant of g . Define

$$a(\cdot, \cdot) : X \times X \rightarrow R, \quad a(u, v) := (\tilde{\nu} \nabla u, \nabla v) + (K^{-1}u, v)_s,$$

$$b(\cdot, \cdot) : Q \times X \rightarrow R, \quad b(q, v) := -(q, \nabla \cdot v),$$

$$c(\cdot, \cdot) : L \times X \rightarrow R, \quad c(\mu, v) := (\mu, v)_s,$$

$$l(\cdot) : X \rightarrow R, \quad l(v) := \langle f, v \rangle - \nu(\nabla E g, \nabla v)_f,$$

$$l_h(\cdot) : X \rightarrow R, \quad l_h(v) := \langle f, v \rangle - \nu(\nabla E g_h, \nabla v)_f,$$

for some fixed parameter $0 < \varepsilon \ll 1$, $\|\cdot\|_\varepsilon^2 := \nu|\cdot|_1^2 + \frac{1}{\varepsilon}\|\cdot\|_{1,s}^2$,

$$W_h := \left\{ v_h \in V_h : \int_{\Omega_s} v_h dx = 0 \right\}.$$

We denote by (u, p) the solution of the Stokes problem in Ω_f :

$$\begin{aligned} -\nu \Delta u + \nabla p &= f \text{ in } \Omega_f, \\ \nabla \cdot u &= 0 \text{ in } \Omega_f, \\ u &= g \text{ on } \partial\Omega, \\ u &= 0 \text{ on } \partial\Omega_s, \end{aligned} \tag{4.2.1}$$

prolongated by $(u, p) = (0, 0)$ inside Ω_s .

Now we define the weak formulation of Stokes equation. Since the discrete model is going to be defined on the entire Ω , we use the test functions $(v, q) \in (X, Q)$ in all of the weak formulations.

Problem 1. Find $(\tilde{u}, p) \in (X_f, Q_f)$ such that $\tilde{u} = u - Eg$, $(\tilde{u}, p)_{\Omega_s} = (0, 0)$ and

$$\begin{aligned} & \nu(\nabla\tilde{u}, \nabla v)_f - (p, \nabla \cdot v)_f + \langle \tau(\tilde{u}, p) \cdot \mathbf{n}, v \rangle \\ & = \langle f, v \rangle - \nu(\nabla Eg, \nabla v)_f + \langle \nu \nabla Eg \cdot \mathbf{n}_f, v \rangle \quad \forall v \in X, \end{aligned} \quad (4.2.2)$$

$$(q, \nabla \cdot \tilde{u})_f = 0 \quad \forall q \in Q. \quad (4.2.3)$$

where $\tau(\tilde{u}, p) \cdot \mathbf{n}_f := p\mathbf{n}_f - \nu \nabla \tilde{u} \cdot \mathbf{n}_f$ is a pseudo-traction on $\partial\Omega_s$. In this chapter we assume that $\tau(\tilde{u}, p) \cdot \mathbf{n}_f \in H^{-1/2}(\partial\Omega_s)$.

Since $\tilde{u} \in X_f$ and $\tilde{u} = 0$ in Ω_s , we have that $\tilde{u} \in X$. Further, as $p|_{\Omega_s} = 0$, we also have $p \in Q$. These observations allow us to rewrite (4.2.2)-(4.2.3) in terms of linear operators and bilinear forms defined in Definition 4.2.1.

Problem 2. Find $(\tilde{u}, p) \in (X, Q)$ such that $\tilde{u} = u - Eg$, $(\tilde{u}, p)_{\Omega_s} = (0, 0)$ and

$$a(\tilde{u}, v) + b(p, v) + \langle \tau(\tilde{u}, p) \cdot \mathbf{n}, v \rangle = l(v) + \langle \nu \nabla Eg \cdot \mathbf{n}, v \rangle \quad \forall v \in X, \quad (4.2.4)$$

$$b(q, \tilde{u}) = 0 \quad \forall q \in Q. \quad (4.2.5)$$

The continuous Lagrange multiplier formulation of Problem 2. Consider the following Neumann problem:

$$\begin{aligned} -\Delta\lambda + \lambda &= 0 \text{ in } \Omega_s, \\ \frac{\partial\lambda}{\partial\mathbf{n}_s} &= \tau \cdot \mathbf{n}_f \text{ on } \partial\Omega_s. \end{aligned}$$

Multiplying through by $\mu \in H^1(\Omega_s)$ and integrating by parts, we find

$$(\lambda, \mu)_{1,s} = \langle \tau \cdot \mathbf{n}_f, \mu \rangle \quad \forall \mu \in H^1(\Omega_s). \quad (4.2.6)$$

In particular, since $X \subset H^1(\Omega_s)$, we have $(\lambda, v)_{1,s} = \langle \tau \cdot \mathbf{n}_f, v \rangle \quad \forall v \in X$. Inserting this into (4.2.4), and noting that $(\mu, u)_{1,s} = 0 \quad \forall \mu \in H^1(\Omega_s)$, we can restate the Problem 2 as:

Problem 3. Find $(u, p, \lambda) \in (X, Q, H^1(\Omega_s))$ such that $(u, p)_{\Omega_s} = (0, 0)$ and

$$a(u, v) + b(p, v) + (\lambda, v)_{1,s} = (f, v) \quad \forall v \in X \quad (4.2.7)$$

$$b(q, u) = 0 \quad \forall q \in Q, \quad (4.2.8)$$

$$(\mu, u)_{1,s} = 0 \quad \forall \mu \in H^1(\Omega_s). \quad (4.2.9)$$

The discrete model. We enhance the Stokes-Brinkman Volume Penalization model (4.0.1)-(4.0.2) with two new ingredients:

1. We impose $u \simeq 0$ in the each ball weakly through a Lagrange Multiplier space

$$L^h := \text{span} \{ \mathbf{e}_i \chi_{B_j} : \text{for } i = \overline{1, d}, j = \overline{1, S} \} :$$

$$\int_{\Omega_s} u \mu = 0 \quad \forall \mu \in L^h \quad \Rightarrow \quad \int_{B_i} u = 0 \quad \forall B_i.$$

2. In order to capture the geometry of the solid region and ensure the inf-sup stability on a coarse mesh, we augment the discrete velocity space with bubble functions described in the next subsection.

Problem 4. Find $(\tilde{u}_h, p_h, \lambda_h) \in (X_h, Q_h, L_h) \subset (X, Q, L)$ such that $u_h = \tilde{u}_h + E g_h$ and

$$a(\tilde{u}_h, v_h) + b(p_h, v_h) + c(\lambda_h, v_h) = l_h(v_h) \quad \forall v_h \in X_h, \quad (4.2.10)$$

$$b(q_h, \tilde{u}_h) = 0 \quad \forall q_h \in Q_h, \quad (4.2.11)$$

$$c(\mu_h, \tilde{u}_h) = 0 \quad \forall \mu_h \in L_h. \quad (4.2.12)$$

4.2.1 Discrete subspaces

We denote conforming velocity, pressure finite element polynomial spaces based on an edge to edge triangulations of Ω (with maximum element diameter h) by

$$Y_h \subset X, Q_h \subset Q.$$

We assume that Y_h, Q_h satisfy the usual inf-sup stability condition (2.2.3). This means the velocity-pressure spaces Y_h, Q_h , before augmentation by spherical bubbles, would be div-stable for Stokes flow in Ω . In order to capture the geometry of the solid region, we additionally augment the velocity space with the spherical bubbles described below.

When choosing the spherical bubbles two things must be taken into account. First, each such basis function must be in X . Next, it should be able to capture the geometry of the balls. So ideally each such basis function ξ_i must vanish outside $\overline{B_i}$.

For a ball B_i , define

$$\phi_i := \max \left\{ 1 - \frac{|\mathbf{x} - \mathbf{x}_i|^2}{r^2}, 0 \right\}.$$

For each B_i of radius r , centered at \mathbf{x}_i , we let $\xi_i^j = \phi_i \mathbf{e}_j, j = \overline{1, d}, i = \overline{1, S}$.

Let

$$Z_h = \text{span}\{\xi_1^1, \xi_2^1, \dots, \xi_S^1, \dots, \xi_1^d, \xi_2^d, \dots, \xi_S^d\}$$

and $X_h := Y_h \oplus Z_h$.

4.2.2 Linear system

With the above choice of subspaces, the formulation of Problem 4 in matrix notation corresponds to

$$\begin{pmatrix} A_{Y_h Y_h} & A_{Z_h Y_h} & B_{Q_h Y_h} & C_{L_h Y_h} \\ A_{Z_h Y_h}^T & A_{Z_h Z_h} & B_{Q_h Z_h} & C_{L_h Z_h} \\ B_{Q_h Y_h}^T & B_{Q_h Z_h}^T & C_{L_h Z_h}^T & 0 \\ C_{L_h Y_h}^T & C_{L_h Z_h}^T & 0 & 0 \end{pmatrix} \begin{pmatrix} \mathbf{U}_p \\ \mathbf{U}_b \\ \mathbf{P} \\ \mathbf{\Lambda} \end{pmatrix} = \begin{pmatrix} \mathbf{F}_p \\ \mathbf{F}_b \\ \mathbf{0} \\ \mathbf{0} \end{pmatrix}.$$

Here \mathbf{U}_p , \mathbf{U}_b , \mathbf{P} and $\mathbf{\Lambda}$ are the degrees of freedom of the polynomial part of \tilde{u}^h , bubble part of \tilde{u}^h , p^h and l^h , respectively. Assuming that $Y_h = \{\phi_i\}$, $Z_h = \{\xi_i\}$, $Q_h = \{q_i\}$ and $L_h = \{\mu_i\}$, the entries of matrix blocks are given by

$$\begin{aligned} (A_{Y_h Y_h})_{ij} &= a(\phi_i, \phi_j), (A_{Z_h Y_h})_{ij} = a(\xi_i, \phi_j), (B_{Q_h Y_h})_{ij} = b(q_j, \phi_i), \\ (C_{L_h Y_h})_{ij} &= c(\mu_j, \phi_i), (C_{L_h Z_h})_{ij} = c(\mu_j, \xi_i), A_{Z_h Z_h} = cI_{d \times d}, \end{aligned}$$

where c is a $\mathcal{O}(1)$ constant.

4.3 WELL-POSEDNESS, STABILITY AND CONVERGENCE

In this section, we prove well-posedness of the system (4.2.10)-(4.2.12), along with stability and convergence results.

Lemma 4.3.1. *The linear functionals $l(\cdot)$, $l_h(\cdot)$ are continuous. In particular, for any $v \in X$, $q \in Q$*

$$\begin{aligned} l(v) &\leq C(\|f\|_{-1} + \nu\|g\|_{1/2})|v|_1, \\ l_h(v) &\leq C(\|f\|_{-1} + \nu\|g_h\|_{1/2})|v|_1. \end{aligned}$$

Proof. The results follow directly by applying Cauchy-Schwarz and Poincaré inequalities. \square

Lemma 4.3.2. *The bilinear functionals $a(\cdot, \cdot)$, $b(\cdot, \cdot)$ and $c(\cdot, \cdot)$ are continuous. Further, $a(\cdot, \cdot)$ is coercive. In particular, for any $\mathbf{u}, \mathbf{v} \in X$, $q \in Q$ and $\mu \in L$,*

$$\begin{aligned} a(v, v) &= \|v\|_\varepsilon^2, \\ a(u, v) &\leq \|u\|_\varepsilon \|v\|_\varepsilon, \\ b(q, v) &\leq \sqrt{d} \|q\| \|v\|_1, \\ c(\mu, v) &\leq C(\Omega) \|\mu\|_s |v|_1. \end{aligned}$$

Proof. As in the last lemma, all the inequalities are directly obtained by applying Cauchy-Schwarz and Poincaré inequalities. \square

The Problem 4 is a twofold saddle point problem and its stability and convergence depends on the fulfillment of the twofold inf-sup condition (2.2.7). Usually, proving them is notoriously difficult [53]. This is even harder for the methods on the nonboundary conforming meshes. E.g., when mesh is non-conforming to the boundary, for the Poisson problem the stability considerations require the mesh-width of the multiplier space to be three times larger than that of the primal variable [21] and this is just a saddle-point problem. Ensuring these type of requirements is not always easy in practice. We establish in Lemma 4.3.4 the twofold inf-sup condition for particular choice of subspaces and geometric configuration of the solids. For the general case, we assume that it holds.

Lemma 4.3.3. *(Inf-sup condition between X_h and L_h) (Y_h, L_h) satisfy the inf-sup conditions, i.e.,*

$$\exists c_1 > 0 \sup_{v_h \in Y_h} \frac{(\mu_h, v_h)_s}{|v_h|_{1,s}} \geq c_1 r \|\mu_h\|_s, \quad \forall \mu_h \in L_h, \quad (4.3.1)$$

$$\exists c_2 > 0 \sup_{v_h \in Y_h} \frac{(\mu_h, v_h)_s}{\|v_h\|_{1,s}} \geq c_2 \frac{r}{r+1} \|\mu_h\|_s, \quad \forall \mu_h \in L_h. \quad (4.3.2)$$

Proof. Pick arbitrary $\mu_h \in L_h$. Then

$$\mu = \sum_{i=1}^d \sum_{j=1}^S m_j^i \chi_{B_j} \mathbf{e}_i$$

for some $m_j^i \in R$. Set

$$v_h = \sum_{i=1}^d \sum_{j=1}^S m_j^i \xi_j^i \mathbf{e}_i \in Y_h.$$

Simple calculations show that

$$\frac{(\mu_h, v_h)_s}{|v_h|_{1,s} \|\mu_h\|_s} \geq c_1 r,$$

and

$$\frac{(\mu_h, v_h)_s}{\|v_h\|_{1,s} \|\mu_h\|_s} \geq c_2 \frac{r}{r+1}.$$

□

Theorem 4.3.4. (*Twofold inf-sup condition*) Let $X_h = P_2 \oplus Y_h$, $Q_h = P_0$. Assume $B \cap K \neq \emptyset \iff B \subset \bar{K}$, where $K \in \mathcal{T}_h$. Then $\exists c_1 > 0, c_2 > 0$ such that $\forall (q_h, \mu_h) \in (Q_h, L_h)$

$$\sup_{v_h \in X_h} \frac{(\mu_h, v_h)_s}{|v_h|_1} \geq c_1 \|\mu_h\|_s \text{ and} \quad (4.3.3)$$

$$\sup_{v_h \in W_h} \frac{(q_h, \nabla \cdot v_h)}{|v_h|_1} \geq c_2 \|q_h\|. \quad (4.3.4)$$

Proof. Note that (4.3.3) is the result of the Lemma 4.3.3. Further, by div-stability assumption on (Y_h, Q_h) , $\exists \gamma > 0 \forall q_h \in Q_h, \exists w_h \in Y_h$ such that

$$\frac{(q_h, \nabla \cdot w_h)}{|w_h|_1} \geq \gamma \|q_h\|.$$

Now let $v_h := w_h + \sum_{i=1}^d \sum_{j=1}^S \alpha_j^i \xi_j^i \mathbf{e}_i$ such that $v_h \in W_h$. This is accomplished by choosing

$$\alpha_j^i = -\frac{\int_{B_j} w_h \mathbf{e}_i}{\int_{B_j} \xi_j^i} = \frac{c_d}{r^d} \int_{B_j} w_h \mathbf{e}_i.$$

Hölder's inequality gives $|v_h|_1 \leq C|w_h|_1$. The last ingredient that makes things work is the fact that

$$\int_{B_j} \frac{\partial \xi_j^i}{\partial x_m} = 0, \quad m = \overline{1, d}, \quad i = \overline{1, d} \Rightarrow$$

$$\int_K \frac{\partial \xi_j^i}{\partial x_m} = 0 \quad \forall K \in \mathcal{T}_h, \quad m = \overline{1, d}, \quad i = \overline{1, d}, \quad j = \overline{1, S}.$$

Combining the above facts we obtain that

$$\gamma \leq \frac{(q_h, \nabla \cdot w_h)}{|w_h|_1} = \frac{(q_h, \nabla \cdot v_h)}{|w_h|_1} \leq \frac{C(q_h, \nabla \cdot v_h)}{|v_h|_1}.$$

□

For the analysis we assume that (X_h, Q_h, L_h) satisfy the twofold inf-sup condition (2.2.8), i.e., $\exists \beta_h > 0$ such that

$$\inf_{q_h \in Q_h, \mu_h \in L_h} \sup_{v_h \in X_h} \frac{b(q_h, v_h) + c(\mu_h, v_h)}{|v_h|_1 (\|\mu_h\|_s + \|q_h\|)} \geq \beta_h. \quad (4.3.5)$$

Theorem 4.3.5. *Assume (4.3.5) holds. Then $\exists!$ $(\tilde{u}_h, p_h, \lambda_h) \in (X_h, Q_h, L_h)$ solution of the Problem 4. Moreover, $(\tilde{u}_h, p_h, \lambda_h)$ satisfy*

$$|\tilde{u}_h|_1 \leq C \left(\frac{1}{\nu} \|f\|_{-1} + \|g_h\|_{1/2} \right), \quad (4.3.6)$$

$$\|\tilde{u}_h\|_\varepsilon \leq C \left(\frac{1}{\sqrt{\nu}} \|f\|_{-1} + \sqrt{\nu} \|g_h\|_{1/2} \right), \quad (4.3.7)$$

$$\|\tilde{u}_h\|_{1,s} \leq C \sqrt{\varepsilon} \left(\sqrt{\frac{1}{\nu}} \|f\|_{-1} + \sqrt{\nu} \|g_h\|_{1/2} \right), \quad (4.3.8)$$

$$\|\lambda_h\|_s \leq C \left(\left(\nu + \frac{1}{\varepsilon} \right) |\tilde{u}_h|_1 + \nu \|g_h\|_{1/2} + \|f\|_{-1} \right), \quad (4.3.9)$$

$$\|p_h\| \leq C \left(\left(\nu + \frac{1}{\varepsilon} \right) |\tilde{u}_h|_1 + \nu \|g_h\|_{1/2} + \|f\|_{-1} \right). \quad (4.3.10)$$

Proof. We first obtain the bounds (4.3.6)-(4.3.8). Restricting the test functions to W_h reduces the Problem 4 to finding $\tilde{u}_h \in W_h$ such that

$$a(\tilde{u}_h, v_h) = l_h(v_h) \quad \forall v_h \in W_h. \quad (4.3.11)$$

Setting $v_h = \tilde{u}_h$ yields

$$\|\tilde{u}_h\|_\varepsilon^2 = l_h(\tilde{u}_h). \quad (4.3.12)$$

Applying the results of Lemmas 4.3.1, 4.3.2 and the definition of $\|\cdot\|_\varepsilon$, we obtain (4.3.6)-(4.3.8). By assumption (4.3.5)

$$\begin{aligned} \|p_h\| + \|\lambda_h\|_s &\leq \frac{C}{\beta_h} \sup_{v_h \in X_h} \frac{|b(p_h, v_h) + c(\lambda_h, v_h)|}{|v_h|_1} \\ &\leq \frac{C}{\beta_h} \sup_{v_h \in X_h} \frac{|a(\tilde{u}_h, v_h)| + |l_h(v_h)|}{|v_h|_1} \\ &\leq C \left(\left(\nu + \frac{1}{\varepsilon} \right) |\tilde{u}_h|_1 + \nu \|g_h\|_{1/2} + \|f\|_{-1} \right). \end{aligned}$$

In order to show existence and uniqueness of the solution, we set $f = g_h = 0$. Then (4.3.6)-(4.3.10) imply that $(\tilde{u}_h, p_h, \lambda_h) = (0, 0, 0)$. \square

Next we obtain a bound for an error $e := u - u_h$ under the following assumptions

$$u \in H^{1+\alpha}(\Omega) \cap H^{k+1}(\Omega_f), \quad p \in H^\beta(\Omega) \cap H^k(\Omega_f),$$

with $0 < \alpha < 1, \frac{1}{2} < \beta < 1, k \geq 1$.

Depending on whether $\nabla u|_{\partial\Omega_s} = 0$ and $p|_{\partial\Omega_s} = 0$, we might have $u \in H^2(\Omega), p \in H^1(\Omega)$. But in general these are not true. Thus, the true solution may fail to have more global regularity than assumed above.

Theorem 4.3.6. *Let (\tilde{u}, p) be the solution of Stokes Problem 2, $X_h = P_{k+1}, Q_h = P_k, k \geq 1$. Then we have*

$$\|\tilde{u} - \tilde{u}_h\|_\varepsilon \leq C \left(\inf_{w_h \in W_h} \|\tilde{u} - w_h\|_\varepsilon + h^\beta + \sqrt{\varepsilon} + \|g - g_h\|_{1/2} \right) \quad (4.3.13)$$

$$\inf_{w_h \in W_h} |\tilde{u} - w_h|_1 \leq C \inf_{v_h \in X_h} (|\tilde{u} - v_h|_1 + \|\tilde{u} - v_h\|_s) \quad (4.3.14)$$

$$\inf_{w_h \in W_h} \|\tilde{u} - w_h\|_{1,s} \leq C \inf_{v_h \in X_h} \|\tilde{u} - v_h\|_s \quad (4.3.15)$$

$$\inf_{w_h \in W_h} \|\tilde{u} - w_h\|_\varepsilon \leq C \inf_{v_h \in X_h} \|\tilde{u} - v_h\|_\varepsilon \quad (4.3.16)$$

$$\|\tilde{u} - \tilde{u}_h\|_\varepsilon \leq C \left(\inf_{v_h \in X_h} \|\tilde{u} - v_h\|_\varepsilon + h^\beta + \sqrt{\varepsilon} + \|g - g_h\|_{1/2} \right) \quad (4.3.17)$$

Proof. Consider $v_h, w_h \in W_h, q_h = \Pi_{SZ} p \in Q_h$. By subtracting (4.2.10) from (4.2.4), then adding and subtracting $a(w_h, v_h)$ we find

$$\begin{aligned} a(\tilde{u}_h - w_h, v_h) &= a(\tilde{u} - w_h, v_h) + b(p - q_h, v_h) + \langle \tau \cdot \mathbf{n}_f, v_h \rangle \\ &\quad - \nu \langle \nabla E g \cdot \mathbf{n}_f, v_h \rangle + (\nabla E(g - g_h), \nabla v_h)_f. \end{aligned} \quad (4.3.18)$$

Let us now choose $v_h = \tilde{u}_h - w_h \in W_h$. The regularity assumption on pseudo-traction $\tau(\tilde{u}, p)$, Lemma 4.3.2, (4.2.12) and standard inequalities imply

$$\begin{aligned} \|\tilde{u}_h - w_h\|_\varepsilon &\leq C \left(\|\tilde{u} - w_h\|_\varepsilon + \frac{1}{\sqrt{\nu}} \|p - q_h\| \right) + \frac{C}{\sqrt{\nu}} \|g - g_h\|_{1/2} \\ &\quad + C\sqrt{\varepsilon} (\|\tau \cdot \mathbf{n}_f\|_{-1/2,s} + \nu \|\nabla E g \cdot \mathbf{n}_f\|_{-1/2,s}), \end{aligned} \quad (4.3.19)$$

and therefore

$$\begin{aligned} \|\tilde{u}_h - \tilde{u}\|_\varepsilon &\leq C \left(\|\tilde{u} - w_h\|_\varepsilon + \frac{1}{\sqrt{\nu}} \|p - q_h\| \right) + \frac{C}{\sqrt{\nu}} \|g - g_h\|_{1/2} \\ &\quad + C\sqrt{\varepsilon} (\|\tau \cdot \mathbf{n}_f\|_{-1/2,s} + \nu \|\nabla E g \cdot \mathbf{n}_f\|_{-1/2,s}), \end{aligned} \quad (4.3.20)$$

$$\leq C (\|\tilde{u} - w_h\|_\varepsilon + h^\beta + \sqrt{\varepsilon} + \|g - g_h\|_{1/2}). \quad (4.3.21)$$

Next we establish (4.3.14)-(4.3.16). To this end, pick $\forall v_h \in X_h, \forall w_h \in W_h$. By applying the second statement of the Lemma 2.2.1 to the twofold saddle-point problems, we have that

$$\begin{aligned} |v_h - w_h|_1 &\leq \frac{1}{\beta_h} \sup_{(q_h, \mu_h) \in (Q_h, L_h)} \frac{b(q_h, v_h - w_h) + c(\mu_h, v_h - w_h)}{\|q_h\| + \|\mu_h\|} \\ &= \frac{1}{\beta_h} \sup_{(q_h, \mu_h) \in (Q_h, L_h)} \frac{b(q_h, v_h - \tilde{u}) + c(\mu_h, v_h - \tilde{u})}{\|q_h\| + \|\mu_h\|} \\ &\leq C (|\tilde{u} - v_h|_1 + \|u - v_h\|_s), \end{aligned} \quad (4.3.22)$$

as $b(q_h, \tilde{u}) = c(\mu_h, \tilde{u}) = 0 \forall (q_h, \mu_h) \in (Q_h, L_h)$. Another application of the triangle inequality gives (4.3.14).

Similar to the previous argument

$$\begin{aligned} \|v_h - w_h\|_{1,s} &\leq C \sup_{\mu_h \in L_h} \frac{c(\mu_h, v_h - w_h)}{\|\mu_h\|} \\ &= C \sup_{\mu_h \in L_h} \frac{c(\mu_h, v_h - \tilde{u})}{\|\mu_h\|} \\ &\leq C \|\tilde{u} - v_h\|_s, \end{aligned} \quad (4.3.23)$$

for any $v_h \in X_h, w_h \in W_h$. Triangle inequality yields (4.3.15). (4.3.16) is obtained in the similar manner, and (4.3.17) is a combination of (4.3.13) and (4.3.16). \square

Remark 4.3.7. If \mathcal{T}_h is conforming to the fluid-solid interface, then we can pick $v_h = 0, q_h = 0$ in Ω_s and obtain the standard error bound

$$\|\tilde{u} - \tilde{u}_h\|_\varepsilon \leq C (h^k |\tilde{u}|_{k+1,f} + h^k |p|_{k,f} + \sqrt{\varepsilon} + \|g - g_h\|_{1/2}).$$

In general, (4.3.8) guarantees that RHS of (4.3.17) is uniformly bounded. Further, using the fact that $\tilde{u} = 0$ in Ω_s , from

$$\|\tilde{u} - v_h\|_\varepsilon^2 = \nu |\tilde{u} - v_h|_{1,f}^2 + \nu |v_h|_{1,s}^2 + \frac{1}{\varepsilon} \|v_h\|_{1,s}^2$$

we observe that the last two terms measure how well the mesh captures the fluid-solid interface.

4.4 NUMERICAL EXPERIMENTS

For our computations, we used

$$X_h = Y_h \oplus Z_h, Q_h \text{ and } L_h := \text{span} \left\{ \begin{pmatrix} \chi_{B_i} \\ 0 \end{pmatrix}, \begin{pmatrix} 0 \\ \chi_{B_j} \end{pmatrix} \right\},$$

where (Y_h, Q_h) are P3-P2 Taylor-Hood elements which are known to satisfy the inf-sup condition [11, 13]. We used FreeFEM++ [28] in our computations. Our tests here are preliminary proof of concept, tested in 2d with spheres simple enough to allow a mesh-conforming "true" solution to be obtained.

Two key comparisons of Brinkman (M1) vs. our model (M2) are the 1) amount of fluid flowing through the spheres and 2) the size of the dead zones behind the spheres caused by the spheres acting like a solid obstacles.

Flow through a thin channel. Our experiment is for two-dimensional flow around seven balls placed in the channel, with small distance apart from each other. The domain is $([0, 1] \times [0.39, 0.61]) - \Omega_s$, where Ω_s is the union of seven balls with radii 0.03 and centered at $(0.16, 0.49)$, $(0.23, 0.52)$, $(0.28, 0.43)$, $(0.1, 0.44)$, $(0.13, 0.56)$, $(0.35, 0.48)$ and $(0.39, 0.54)$. We assume no-slip boundary conditions on the top and bottom boundaries, a parabolic inflow given by $((y - 0.39)(0.61 - y)/25, 0)^T$ and do-nothing outflow. We take $\nu = 100$, $f = (y, 0)^T \chi_f$. In Figure 4.1 we present the speed contour of the true solution. We ran tests on few mesh refinements (Fig. 4.4) for two different values of the penalty parameter ε . The speed contours of M1 and M2 are presented in Figures 4.5, 4.6 and 4.7. We also list the tables of errors in Tables 4.1, 4.2.

From the numerical experiments, we can observe the following:

- On the coarsest mesh, for both values of ε the proposed method gives improved results than M1. In the case of $\varepsilon = h^2$, M2 gives reasonable speed contours

Figure 4.1: The body-fitted, resolved Stokes speed contours

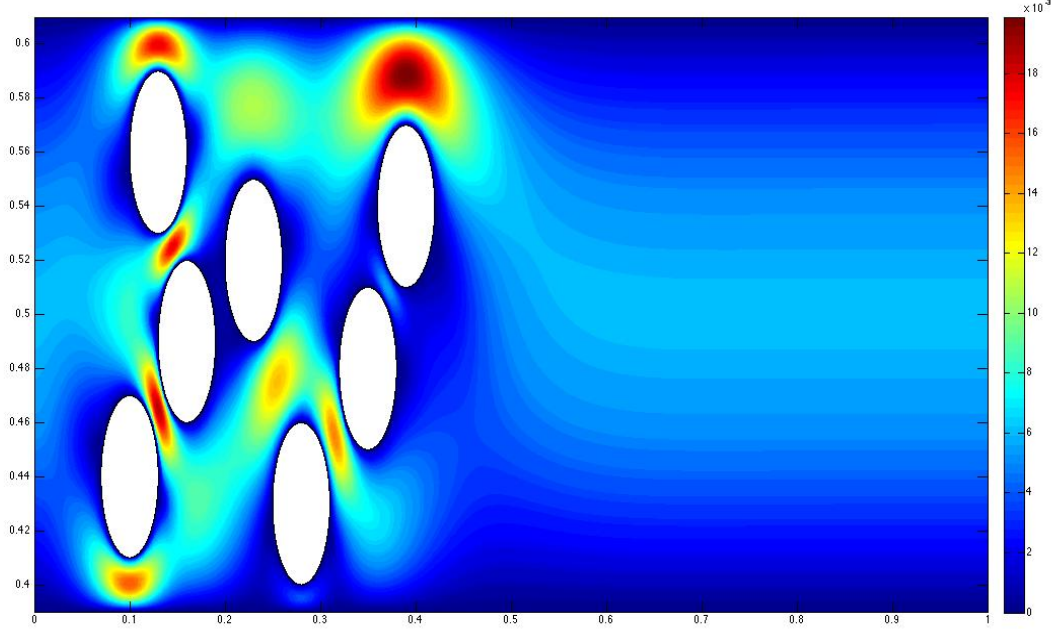


(Fig 4.5), while M1 yields very poor approximation even on the finest mesh (Fig. 4.6). Further, M1 also produces more accurate approximation (Tables 4.1-4.2). This is due to the new ingredients added to Stokes-Brinkman model.

- For very small value of the penalty parameter ε , both methods give very similar, poor results. In particular note the *polygonal no-flow regions* in Figures 4.6 - 4.7. Further, the flow has been choked off in some of the pores. One advantage of the method herein is that less flow goes through the solid domain. This improvement is due to the addition of the bubbles because, by Hölder's inequality $\int_B u \leq \left| \int_B u \right| \leq C \|u\|_s \leq C \sqrt{\varepsilon}$ by (4.3.8), so that weak no-flow is almost satisfied for both methods.
- For larger value of ε , M2 gives very good approximations, while M1 gives very underresolved solution even on the finest mesh. As it was pointed out above, these improvements are due to the combinations of Lagrange multiplier,

Figure 4.2: Mesh 1 ($h = 0.55$) and Ω_s

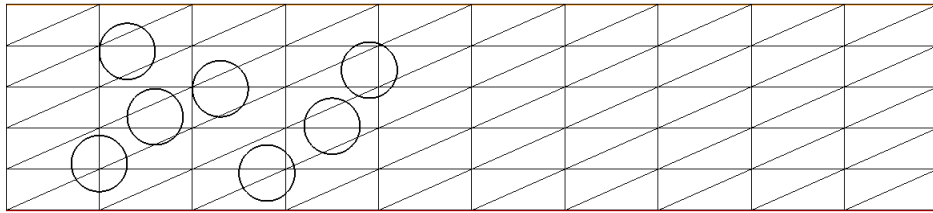


Figure 4.3: Mesh 2 ($h = 0.27$) and Ω_s



Figure 4.4: Mesh 3 ($h = 0.14$) and Ω_s

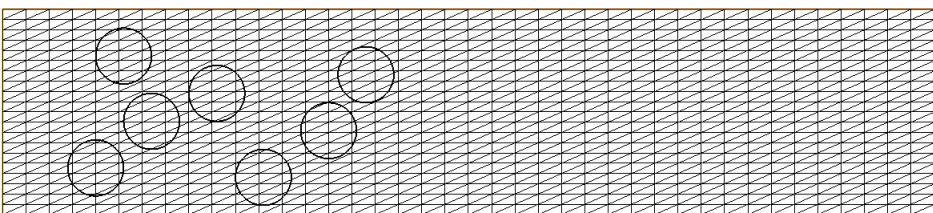
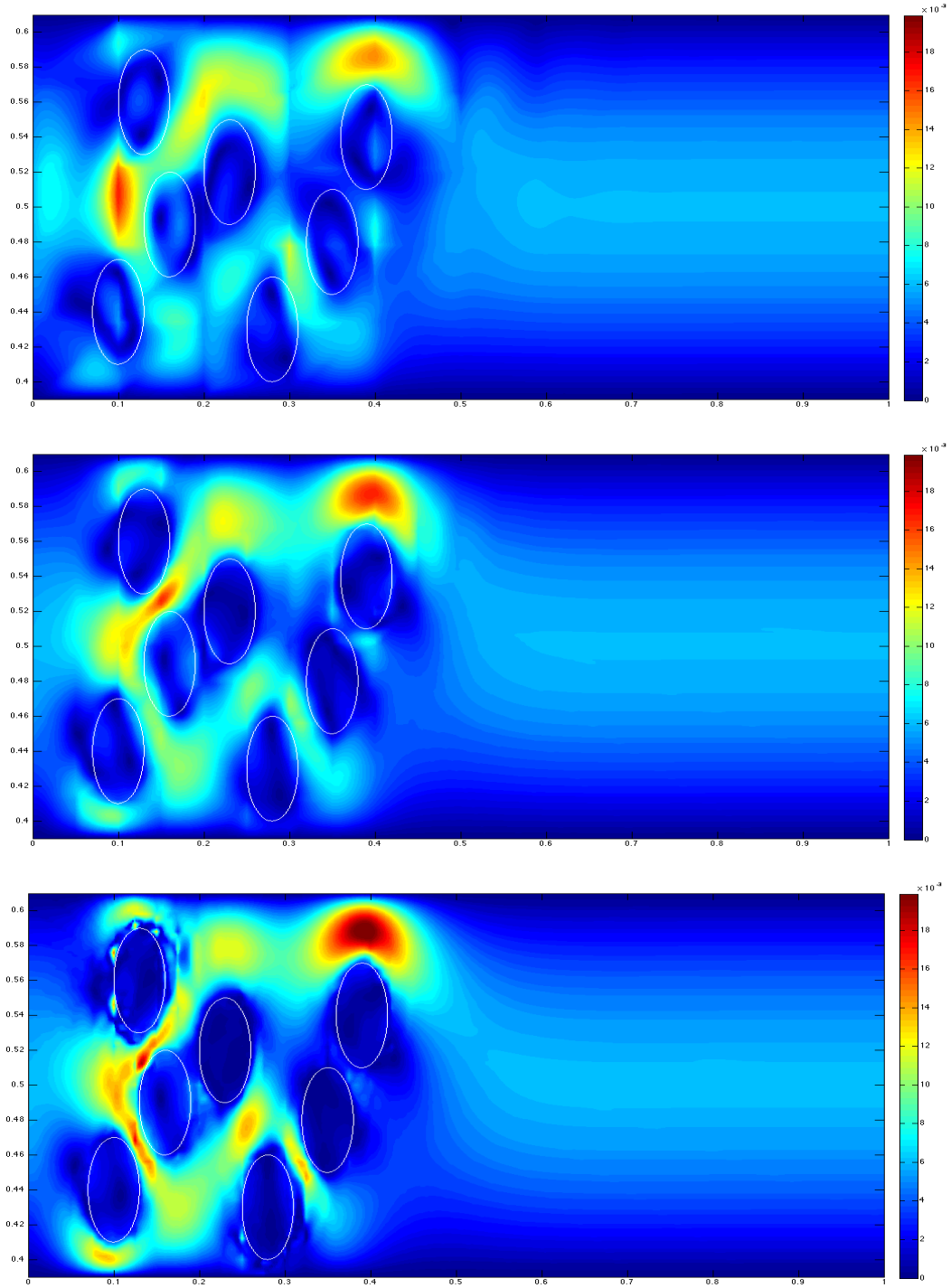


Figure 4.5: From top to bottom: speed contours of M2 on meshes with $h \simeq 0.11$, $h \simeq 0.055$, $h \simeq 0.027$, $\varepsilon = h^2$



penalization terms and the spherical bubbles. This is because the penalization terms by themselves gave poor results, as it can be observed from the plots of M1 method.

Figure 4.6: From top to bottom: speed contour of M2, with $h = 0.014, \varepsilon = h^2$ and $h = 0.027, \varepsilon = 10^{-15}$, and of M1, with $h = 0.007, \varepsilon = h^2$

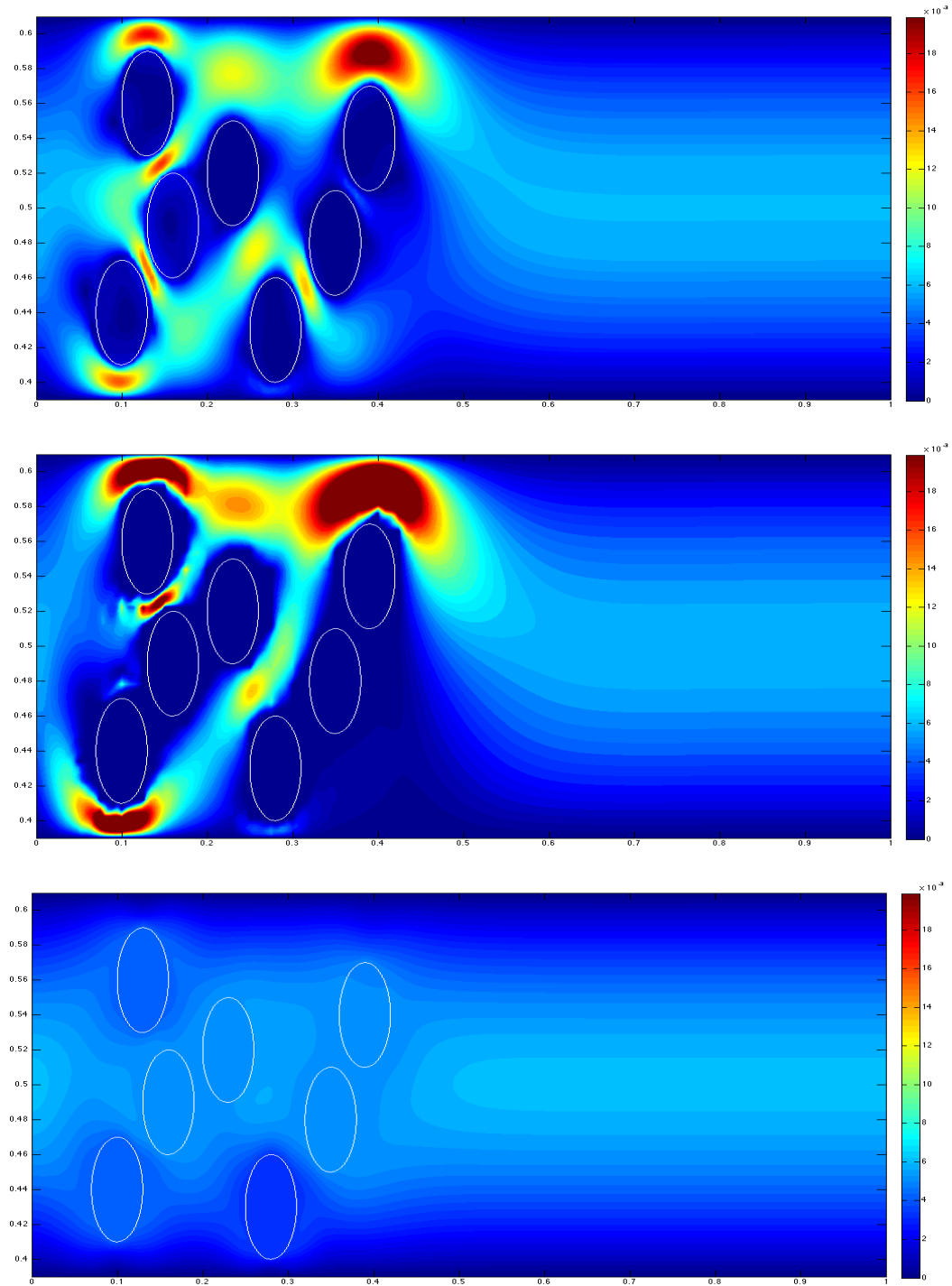
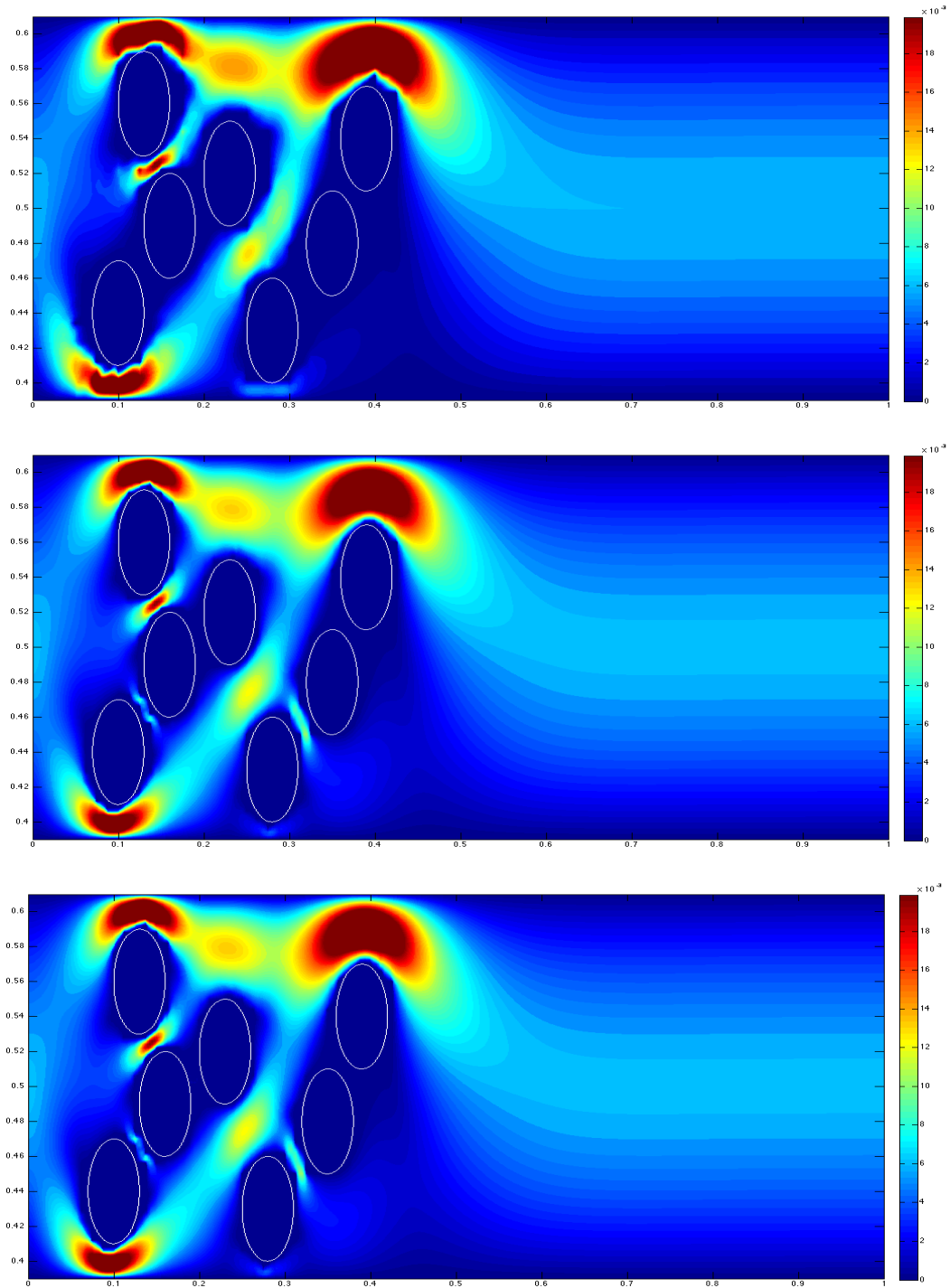


Figure 4.7: From top to bottom: speed contour of M1, with $h = 0.027, \varepsilon = 10^{-15}$ and $h = 0.014, \varepsilon = 10^{-15}$, and of M2, with $h = 0.014, \varepsilon = 10^{-15}$



	$\varepsilon = 1e - 15$				$\varepsilon = h^2$			
	M1	rate	M2	rate	M1	rate	M2	rate
h								
0.11	3.79e-2	4.0316	2.43e-3	-0.1226	1.59e-3	0.0288	9.33e-4	0.3656
0.055	2.32e-3	0.7407	2.65e-3	0.9002	1.55e-3	0.0258	7.24e-4	0.1983
0.027	1.39e-3	0.4225	1.42e-3	0.4496	1.52e-3	0.0131	6.31e-4	1.2753
0.014	1.04e-3	-	1.04e-3	-	1.51e-3	0.001	2.6e-4	0.5746
0.007	Out of memory				1.5e-3	-	1.75e-4	-

Table 4.1: L^2 errors and rates

	$\varepsilon = 1e - 15$				$\varepsilon = h^2$			
	M1	rate	M2	rate	M1	rate	M2	rate
h								
0.11	2.03e-3	3.99	9.15e-6	-0.782	6.971e-4	0.022	4.548e-4	0.322
0.055	3.761e-5	1.465	1.57e-5	2.205	6.82e-4	0.021	3.6373e-4	0.586
0.027	8.694e-6	2.187	2.77e-6	2.897	6.682e-4	0.011	2.4238e-4	1.371
0.014	9.762e-7	-	3.72e-7	-	6.608e-4	-	9.37e-5	1.815
0.007	Out of memory				1.5e-3	-	2.6632e-5	-

Table 4.2: $L^2(\Omega_s)$ errors and rates

5.0 BRINKMAN VOLUME PENALIZATION BASED MODEL FOR MODERATE *RE* FLOWS

In this chapter, we develop an algorithm from the model of the previous chapter. The new aspect of the model is that we implement the volume penalization (i.e., the strong enforcement of $u \simeq 0$) only in the elements contained in the solid region. Unlike [31], this prevents the flow obstruction in the regions between the solids. As for the rest of the solid, the no-flow is enforced weakly via characteristic functions of the balls, applied as the Lagrange multipliers.

To introduce the ideas, for given penalty parameter $0 < \varepsilon \ll 1$, again consider the Navier-Stokes-Brinkman volume penalization equation (3.2.1)-(3.2.2):

$$\begin{aligned} u_t + u \cdot \nabla u - \nabla \cdot (\tilde{\nu} \nabla u) + \frac{1}{K} u + \nabla p &= f \text{ in } \Omega_f, \\ \nabla \cdot u &= 0 \text{ in } \Omega_s, \end{aligned}$$

where f is the forcing term, and the Brinkman viscosity $\tilde{\nu}$ and permeability K are defined as before

$$\tilde{\nu} = \begin{cases} \nu & \text{if } x \text{ in fluid region,} \\ \frac{1}{\varepsilon} + \nu & \text{if } x \text{ in solid region,} \end{cases} \quad \text{and } K = \begin{cases} \infty & \text{if } x \text{ in fluid region,} \\ \varepsilon & \text{if } x \text{ in solid region.} \end{cases}$$

On a non-conforming mesh, the finite element discretization of (3.2.1) - (3.2.2) extends the penalization beyond the intended solid ball to the elements having non-empty intersection with that ball, Figure 5.1. That is because a polynomial is

Figure 5.1: Ball and an old penalization region

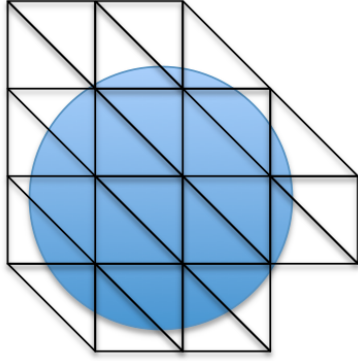
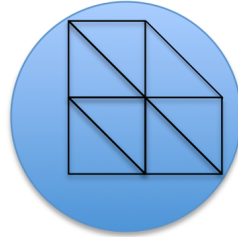


Figure 5.2: Ball and a new penalization region



identically zero if it vanishes at finitely many points, and Brinkman penalization makes polynomial representation of the velocity almost zero (for a very small ε) in a region with a positive measure, i.e., at infinitely many points. As a result, the flow is obstructed in some of the pores between the solids, changing the flow properties [31].

We propose the following approach: instead of applying the penalization in the entire ball, we restrict the penalization region to those elements which are entirely contained in the closure of the ball, Figure 5.2. Such elements exist if *meshwidth* \leq *radius*. As for the flow elsewhere in the ball, as in Chapter 4, we use the Lagrange Multipliers to enforce the no-flow weakly.

We combine these ideas with Navier-Stokes-Brinkman equations (3.2.1)-(3.2.2). For a given ball B , let $B^h \subset B$ be the union of elements that entirely lie in B . Set

$$\tilde{\nu}^h := \begin{cases} \nu & \text{if } x \text{ in fluid region,} \\ \frac{1}{\varepsilon} + \nu & \text{if } x \text{ in } B^h, \forall B, \end{cases} \quad \text{and } K^h := \begin{cases} \infty & \text{if } x \text{ in fluid region,} \\ \varepsilon & \text{if } x \text{ in } B^h, \forall B. \end{cases}$$

Then the continuous algorithm is given by

$$u_t + u \cdot \nabla u - \nabla \cdot (\tilde{\nu}^h \nabla u) + \frac{1}{K^h} u + \nabla p = f \text{ in solid} \cup \text{fluid region, (5.0.1)}$$

$$\nabla \cdot u = 0 \text{ in solid} \cup \text{fluid region, (5.0.2)}$$

$$u \simeq 0 \text{ in solid. (5.0.3)}$$

We will give the precise definition of our algorithm in the next section, once the notations are introduced.

5.1 WEAK FORMULATIONS

Definition 5.1.1. For a given ball B_j , we define the discrete ball B_j^h as $B_j^h := \{\bigcup_i K_i^j : K_i^j \subset \overline{B_j}, K_i^j \in \mathcal{T}^h\}$. Further, we set

$$\chi_s^h := \sum_j \chi_{B_j^h}^h, \tilde{\nu}^h := \chi_s^h \varepsilon^{-1} + \nu, K^h := \varepsilon \chi_s^h, \Omega_s^h := \bigcup_j B_j^h.$$

Let

$$a(\cdot, \cdot) : X \times X \rightarrow R, a(u, v) := (\tilde{\nu} \nabla u, \nabla v) + (K^{-1} u, v)_s,$$

$$a^h(\cdot, \cdot) : X \times X \rightarrow R, a^h(u, v) := (\tilde{\nu}^h \nabla u, \nabla v) + \left(\frac{1}{K^h} u, v \right)_{s_h},$$

$$b(\cdot, \cdot) : Q \times X \rightarrow R, b(q, v) := -(q, \nabla \cdot v),$$

$$c(\cdot, \cdot) : L \times X \rightarrow R, c(\mu, v) := (\mu, v)_s,$$

$$d(\cdot, \cdot, \cdot) : X \times X \times X \rightarrow R, d(u, v, w) := (u \cdot \nabla v, w),$$

$$d^*(\cdot, \cdot, \cdot) : X \times X \times X \rightarrow R, d^*(u, v, w) := \frac{1}{2}(d(u, v, w) - d(u, w, v)),$$

for some fixed parameter $0 < \varepsilon \ll 1$, $\|\cdot\|_{\varepsilon_h}^2 := \nu \|\cdot\|_1^2 + \frac{1}{\varepsilon} \|\cdot\|_{1, s_h}^2$.

For given $u^0(x) \in V(\Omega_f)$, let $(u(x, t), p(x, t))$ be the solution of the Navier-Stokes equation in $\overline{\Omega_f} \times [0, t_f]$:

$$\begin{aligned} u_t + u \cdot \nabla u - \nu \Delta u + \nabla p &= f \text{ in } \Omega_f \times (0, t_f], \\ \nabla \cdot u &= 0 \text{ in } \Omega_f \times [0, t_f], \\ u &= u^0(x) \text{ on } \Omega_f \times \{t = 0\}, \\ u &= 0 \text{ on } \partial\Omega_f \times [0, t_f], \end{aligned} \quad (5.1.1)$$

prolongated by $(u, p) = (0, 0)$ inside $\Omega_s \times [0, t_f]$. The weak formulation of the above Navier-Stokes equation is defined as follows:

Problem 5. Find $(u, p) \in (X_f, Q_f)$ such that $u(x, 0) = u^0(x)$, $(u(x, t), p(x, t))_{\Omega_s} = (0, 0)$ and

$$\begin{aligned} (u_t, v)_f + (u \cdot \nabla u, v)_f + \nu(\nabla u, \nabla v)_f - (p, \nabla \cdot v)_f + \langle \tau(u, p) \cdot \mathbf{n}_f, v \rangle \\ = (f, v)_f, \quad \forall v \in X, \end{aligned} \quad (5.1.2)$$

$$(q, \nabla \cdot u)_f = 0 \quad \forall q \in Q. \quad (5.1.3)$$

where $\tau \cdot \mathbf{n}_f = \tau(u, p) \cdot \mathbf{n}_f := p\mathbf{n}_f - \nu \nabla u \cdot \mathbf{n}_f$ is a pseudo-traction on $\partial\Omega_s$, $\langle \cdot, \cdot \rangle$ is the duality pairing between $H^{-1/2}(\partial\Omega_s) \times H^{1/2}(\partial\Omega_s)$.

Since $u \in X_f$ and $u = 0$ in Ω_s , we have that $u \in X$. Further, as $p|_{\Omega_s} = 0$, we also have $p \in Q$. These observations allow us to rewrite (5.1.2)-(5.1.3) in terms of linear operators and bilinear forms defined in the Definition 5.1.1.

Problem 6. Find $(u, p) \in (X, Q)$ such that $(u(x, t), p(x, t))_{\Omega_s} = (0, 0)$, $u(x, 0) = u^0$ and

$$(u_t, v) + d(u, u, v) + a(u, v) + b(p, v) + \langle \tau(u, p) \cdot \mathbf{n}_f, v \rangle = (f, v) \quad \forall v \in X, \quad (5.1.4)$$

$$b(q, u) = 0 \quad \forall q \in Q. \quad (5.1.5)$$

The continuous Lagrange multiplier formulation of Problem 6. Consider the following Neumann problem, $\forall t > 0$

$$\begin{aligned} -\Delta\lambda + \lambda &= 0 \text{ in } \Omega_s, \\ \frac{\partial\lambda}{\partial\mathbf{n}_s} &= \tau \cdot \mathbf{n}_f \text{ on } \partial\Omega_s. \end{aligned}$$

Multiplying through by $\mu \in H^1(\Omega_s)$ and integrating by parts, we find

$$(\lambda, \mu)_{1,s} = \langle \tau \cdot \mathbf{n}_f, \mu \rangle \quad \forall \mu \in H^1(\Omega_s). \quad (5.1.6)$$

In particular, since $X \subset H^1(\Omega_s)$, we have $(\lambda, v)_{1,s} = \langle \tau \cdot \mathbf{n}_f, v \rangle \quad \forall v \in X$. Inserting this into (5.1.4), and noting that $(\mu, u)_{1,s} = 0 \quad \forall \mu \in H^1(\Omega_s)$, we can restate the Problem 6 as

Problem 7. Find $(u, p, \lambda) \in (X, Q, H^1(\Omega_s))$ such that $(u(x, t), p(x, t))_{\Omega_s} = (0, 0)$, $u(x, 0) = u^0$ and

$$(u_t, v) + d(u, u, v) + a(u, v) + b(p, v) + (\lambda, v)_{1,s} = (f, v) \quad \forall v \in X \quad (5.1.7)$$

$$b(q, u) = 0 \quad \forall q \in Q, \quad (5.1.8)$$

$$(\mu, u)_{1,s} = 0 \quad \forall \mu \in H^1(\Omega_s). \quad (5.1.9)$$

As in the case Stokes flow, at each time step, the well-posedness and stability of discrete-in-time FE approximation of the Problem 7 depends on the fulfillment of the twofold inf-sup condition (2.2.7). In the current algorithm, it is assumed that X_h does not contain the spherical bubble of Chapter 4.0, as the mesh is finer. Therefore, inf-sup condition between X_h and L_h is not as straightforward as in Lemma 4.3.3, see Lemma 5.2.1. In the general case, we again assume that the twofold inf-sup condition (5.2.3) is satisfied.

The discrete model. Assume that (X_h, Q_h) is a div-stable pair.

Problem 8. Find $(u_h^{n+1}, p_h^{n+1}, \lambda_h^{n+1}) \in (X_h, Q_h, L_h) \subset (X, Q, L)$, $n = 0, 1, \dots, N-1$ satisfying

$$\begin{aligned} \left(\frac{u_h^{n+1} - u_h^n}{\Delta t}, v_h \right) + a^h(u_h^{n+1}, v_h) + b(p_h^{n+1}, v_h) + c(\lambda_h^{n+1}, v_h) \\ + d^*(u_h^n, u_h^{n+1}, v_h) = (f^{n+1}, v_h) \quad \forall v_h \in X_h, \end{aligned} \quad (5.1.10)$$

$$b(q_h, u_h^{n+1}) = 0 \quad \forall q_h \in Q_h, \quad (5.1.11)$$

$$c(\mu_h, u_h^{n+1}) = 0 \quad \forall \mu_h \in L_h, \quad (5.1.12)$$

where u_h^0 is an approximation of u^0 .

Remark 5.1.2. One could choose the test functions such that $v_h = 0, q_h = 0$ in Ω_s^h , drop the penalty term in (5.1.10) and set $u_h = 0$ in Ω_s^h . We advocate the current version of (5.1.10) for two reasons. Firstly, it is much easier to implement in FreeFEM++ package [28]. Secondly, in the case of moving solids (which will be studied in the future projects), the model enforces rigid body motion in each B , i.e., $u_h = U + \omega \times r$, where U, ω are the translational and angular velocities of the ball, respectively. Additionally, there will be a new set of equations for these new variables and they are solved for simultaneously with u, p .

5.1.1 Linear system

With the above choice of subspaces, at each timestep, the formulation of Problem 8 in matrix notation corresponds to

$$\begin{pmatrix} A_{X_h X_h} + \tilde{A}_{X_h X_h}^{n+1} & B_{Q_h X_h} & C_{L_h X_h} \\ B_{Q_h X_h}^T & 0 & 0 \\ C_{L_h X_h}^T & 0 & 0 \end{pmatrix} \begin{pmatrix} \mathbf{U}^{n+1} \\ \mathbf{P}^{n+1} \\ \mathbf{\Lambda}^{n+1} \end{pmatrix} = \begin{pmatrix} \mathbf{F}^{n+1} \\ \mathbf{0} \\ \mathbf{0} \end{pmatrix}.$$

Here \mathbf{U}^{n+1} , \mathbf{P}^{n+1} and $\mathbf{\Lambda}^{n+1}$ are the degrees of freedom of u_h^{n+1} , p_h^{n+1} and λ_h^{n+1} , respectively. Assuming that $X_h = \{\phi_i\}$, $Q_h = \{q_i\}$ and $L_h = \{\mu_i\}$, the entries of matrix blocks are given by

$$\begin{aligned} (A_{X_h X_h})_{ij} &= a(\phi_i, \phi_j), \left(\tilde{A}_{X_h X_h}^{n+1} \right)_{ij} = d^*(u_h^n, \phi_i, \phi_j), \\ (B_{Q_h X_h})_{ij} &= b(q_j, \phi_i), (C_{L_h X_h})_{ij} = c(\mu_j, \phi_i). \end{aligned}$$

Note that only $\tilde{A}_{X_h X_h}^{n+1}$ must be assembled at each timestep, other blocks in the matrix can be pre-assembled. Further, only the integrals corresponding to $C_{L_h X_h}$ block require integration over the intersection of spheres with the triangles (tetrahedrons).

5.2 WELL-POSEDNESS, STABILITY AND CONVERGENCE

In this section we establish well-posedness of (5.1.10)-(5.1.12) and obtain stability and convergence results. We first prove the inf-sup condition between X_h and L_h .

Lemma 5.2.1. *Let $X_h = P_k$, $k \geq 2$ and L_h as above. If $h < Cr$ for some $C = \mathcal{O}(1)$, then $\exists \alpha_h = \alpha_h(h) > 0$, $\lim_{h \rightarrow 0} \alpha_h = Cr$, such that*

$$\inf_{\mu_h \in L_h} \sup_{v_h \in X_h} \frac{(\mu_h, v_h)}{\|\mu_h\|_s |v_h|_1} \geq \alpha_h. \quad (5.2.1)$$

Proof. Pick arbitrary $\mu_h \in L_h$. Then $\mu_h = \sum_{j=1}^d \sum_{i=1}^S a_j^i \chi_{B_i} \mathbf{e}_j$. Set

$$\phi_i := \max \left\{ 1 - \frac{|\mathbf{x} - \mathbf{x}_i|}{r^2}, 0 \right\} \in X, \text{ and } w := \sum_{j=1}^d \sum_{i=1}^S a_j^i \phi_i \mathbf{e}_j.$$

Simple calculation shows that

$$\frac{(\mu_h, w)}{\|\mu_h\|_s |w|_1} \geq Cr. \quad (5.2.2)$$

Now let Π_{SG} be the Scott-Girault interpolating operator (Lemma 2.2.6) and $w_h := \Pi_{SG}w \in X_h$. Then

$$\begin{aligned} \sup_{v_h \in X_h} \frac{(\mu_h, v_h)}{|v_h|_1} &\geq \frac{|(\mu_h, w_h)|}{|w_h|_1} \geq \frac{|(\mu_h, w_h)|}{C_1|w|_1} \\ &= \frac{|(\mu_h, w) + (\mu_h, w_h - w)|}{C_1|w|_1} \geq \frac{(\mu_h, w)}{C_1|w|_1} - \frac{|(\mu_h, w_h - w)|}{C_1|w|_1} \\ &\geq Cr\|\mu_h\|_s - \frac{\|\mu_h\|_s\|w_h - w\|}{C_1|w|_1} \geq Cr\|\mu_h\|_s - C_2h\|\mu_h\|_s =: \alpha_h > 0, \end{aligned}$$

provided h is small enough. \square

We assume that (X_h, Q_h, L_h) satisfy the twofold inf-sup condition (2.2.8), i.e., $\exists \beta_h > 0$ such that

$$\inf_{q_h \in Q_h, \mu_h \in L_h} \sup_{v_h \in X_h} \frac{b(q_h, v_h) + c(\mu_h, v_h)}{|v_h|_1 (\|\mu_h\|_s + \|q_h\|)} \geq \beta_h. \quad (5.2.3)$$

Lemma 5.2.2. *The bilinear functionals $a_h(\cdot, \cdot)$, $b(\cdot, \cdot)$ and $c(\cdot, \cdot)$ are continuous. Further, $a_h(\cdot, \cdot)$ is coercive. In particular, for any $u, v \in X$, $q \in Q$ and $\mu \in L$,*

$$\begin{aligned} a^h(v, v) &= \|v\|_{\varepsilon_h}^2, \\ a^h(u, v) &\leq \|u\|_{\varepsilon_h} \|v\|_{\varepsilon_h}, \\ b(q, v) &\leq \sqrt{d}\|q\| |v|_1, \\ c(\mu, v) &\leq C(\Omega)\|\mu\|_s |v|_1. \end{aligned}$$

Proof. All the statements are directly obtained by using definition of $\|\cdot\|_{\varepsilon_h}$, or by applying Cauchy-Schwarz and Poincaré inequalities. \square

Theorem 5.2.3. *There exists a unique $(u_h^n, p_h^n, \lambda_h^n) \in (X_h, Q_h, L_h)$ solution of the Problem 8. Moreover, $(u_h^n, p_h^n, \lambda_h^n)$ satisfy*

$$\|u_h^N\| \leq \frac{\|f\|_{2,-1}}{\sqrt{\nu}} + \|u_h^0\|, \quad (5.2.4)$$

$$\Delta t \sum_{n=0}^{N-1} \|u_h^{n+1}\|_{\varepsilon_h}^2 \leq \frac{\|f\|_{2,-1}}{\nu} + \|u_h^0\|^2, \quad (5.2.5)$$

$$|u_h|_{2,1} \leq \frac{\|f\|_{2,-1}}{\nu} + \frac{1}{\sqrt{\nu}} \|u_h^0\|, \quad (5.2.6)$$

$$|u_h|_{2,0,s_h} \leq \sqrt{\varepsilon} \left(\frac{\|f\|_{2,-1}}{\sqrt{\nu}} + \|u_h^0\| \right), \quad (5.2.7)$$

$$\|\lambda_h^{n+1}\|_s \leq C \left(\nu |u_h^{n+1}|_1 + \frac{\|u_h^{n+1}\| + \|u_h^n\|}{\Delta t} + \|f^{n+1}\|_{-1} + |u_h^{n+1}|_1 |u_h^n|_1 \right), \quad (5.2.8)$$

$$\|p_h^{n+1}\| \leq C \left(\nu |u_h^{n+1}|_1 + \frac{\|u_h^{n+1}\| + \|u_h^n\|}{\Delta t} + \|f^{n+1}\|_{-1} + |u_h^{n+1}|_1 |u_h^n|_1 \right). \quad (5.2.9)$$

Proof. Setting $v_h = u_h^{n+1}$, $q_h = p_h^{n+1}$, $\mu_h = \lambda_h^{n+1}$ in (5.1.10)-(5.1.12) and adding the equations gives

$$\frac{(u_h^{n+1} - u_h^n, u_h^{n+1})}{\Delta t} + \|u_h^{n+1}\|_{\varepsilon_h}^2 = (f^{n+1}, u_h^{n+1}). \quad (5.2.10)$$

Applying polarization identity to the first term on the LHS and Cauchy-Schwarz to the RHS in (5.2.10), we obtain

$$\|u_h^{n+1}\|^2 - \|u_h^n\|^2 + \|u_h^{n+1} - u_h^n\|^2 + \Delta t \|u_h^{n+1}\|_{\varepsilon_h}^2 \leq \frac{\Delta t \|f^{n+1}\|_{-1}^2}{\nu}. \quad (5.2.11)$$

Summing over n from 0 to $N - 1$ yields

$$\|u_h^N\|^2 + \sum_{n=0}^{N-1} \|u_h^{n+1} - u_h^n\|^2 + \Delta t \sum_{n=0}^{N-1} \|u_h^{n+1}\|_{\varepsilon_h}^2 \leq \frac{\Delta t \sum_{n=0}^{N-1} \|f^{n+1}\|_{-1}^2}{\nu} + \|u_h^0\|^2, \quad (5.2.12)$$

which imply (5.2.4)-(5.2.7). Now we derive the bounds on the pressure and the Lagrange multiplier. By inf-sup condition (5.2.3), $\exists \beta_h > 0$ such that

$$\begin{aligned} & \|p_h^{n+1}\| + \|\lambda_h^{n+1}\|_s \\ & \leq \frac{C}{\beta_h} \sup_{v_h \in X_h} \frac{\left| \frac{(u_h^{n+1} - u_h^n, v_h)}{\Delta t} + a^h(u_h^{n+1}, v_h) + d^*(u_h^n, u_h^{n+1}, v_h) - (f^{n+1}, v_h) \right|}{|v_h|_1}. \end{aligned} \quad (5.2.13)$$

Since the mesh is conforming to the discrete solid region, in (5.2.13) we can pick $v_h = 0$ in Ω_{s_h} , implying that $a^h(u_h^{n+1}, v_h) = \nu(\nabla u_h^{n+1}, \nabla v_h)$ and

$$\|p_h^{n+1}\| + \|\lambda_h^{n+1}\|_s \leq C \left(\nu |u_h^{n+1}|_1 + \frac{\|u_h^{n+1}\| + \|u_h^n\|}{\Delta t} + \|f^{n+1}\|_{-1} + |u_h^{n+1}|_1 |u_h^n|_1 \right). \quad (5.2.14)$$

In order to show existence and uniqueness of the solution, we set $f = u_h^0 = 0$. Then (5.2.4)-(5.2.9) imply that $(u_h^{n+1}, p_h^{n+1}, \lambda_h^{n+1}) = (0, 0, 0)$. Thus, there exists a unique solution of the system at each timestep. \square

Next we obtain an asymptotic result for the error $e^n = u^n - u_h^n$ under the following regularity assumptions

$$\begin{aligned} u, u_t &\in L^2(0, T; H^{1+\alpha}(\Omega)), \quad u \in L^4(0, T; H^{1+\alpha}(\Omega)), \quad p \in L^2(0, T; H^\beta(\Omega)), \\ u &\in L^2(0, T; H^2(\Omega_f)), \quad p \in L^2(0, T; H^1(\Omega_f)), \\ u, u_t &\in L^\infty(0, T; H^1(\Omega)), \quad u_{tt} \in L^2(0, T; L^2(\Omega)), \end{aligned}$$

with $0 < \alpha < 1, \frac{1}{2} < \beta < 1$.

Lemma 5.2.4. *Let $h < r$. Then for a d -dimensional ball B , d -Lebesgue measure of $B \setminus B_h$ satisfies $\mu_d(B \setminus B_h) \leq Ch$ where $C = C(d, r)$.*

Proof. Let $\omega_h^B := \{\cup K : K \in \mathcal{T}_h, K \cap \partial B \neq \emptyset\}, \omega_h = \bigcup_B \omega_h^B$ Then

$$\mu_d(B \setminus B_h) \leq \mu_d(\omega_h^B) \leq \frac{\pi^{d/2}}{\Gamma(\frac{d}{2} + 1)} ((r+h)^d - (r-h)^d) \leq C(d, r)h.$$

□

Theorem 5.2.5. *Let (u, p) be the solution of the Problem 6. Then*

$$\lim_{h \rightarrow 0} \left(\|e^N\|^2 + \Delta t \sum_{n=0}^{N-1} \|e^{n+1}\|_{\varepsilon_h}^2 \right) = \mathcal{O}(\varepsilon + \Delta t^2). \quad (5.2.15)$$

Proof. At time t_{n+1} , the solution of Navier-Stokes equation (5.1.4)-(5.1.5) satisfies

$$\begin{aligned} \left(\frac{u^{n+1} - u^n}{\Delta t}, v_h \right) &+ d^*(u^{n+1}, u^{n+1}, v_h) - (p^{n+1}, \nabla \cdot v_h) + a^h(u^{n+1}, v_h) \\ &+ \langle \tau^{n+1} \cdot \mathbf{n}_f, v_h \rangle = (f^{n+1}, v_h) + Intp(u^{n+1}; v_h) \end{aligned} \quad (5.2.16)$$

for all $v_h \in X_h$, where $Intp(u^{n+1}; v_h)$ denotes

$$Intp(u^{n+1}; v_h) = \left(\frac{u^{n+1} - u^n}{\Delta t} - \frac{\partial u}{\partial t}(t_{n+1}), v_h \right). \quad (5.2.17)$$

Subtracting (5.1.10) from (5.2.16) and restricting $v_h \in V_h$ gives

$$\begin{aligned}
& \left(\frac{e^{n+1} - e^n}{\Delta t}, v_h \right) + d^*(u^{n+1}, u^{n+1}, v_h) - d^*(u_h^n, u_h^{n+1}, v_h) \\
& - b(p^{n+1} - q_h^{n+1}, v_h) + a^h(e^{n+1}, v_h) + \langle \tau^{n+1} \cdot \mathbf{n}_f, v_h \rangle \\
& = \text{Intp}(u^{n+1}; v_h), \forall q_h^{n+1} \in Q_h.
\end{aligned} \tag{5.2.18}$$

Now decompose the error as $e^n = (u^n - U^n) + (U^n - u_h^n) := \eta^n + \phi_h^n$, where U^n is the Scott-Girault interpolant of u^n . In particular this means $U^n = 0$ in Ω_{s_n} . Inserting $e^n = \eta^n + \phi_h^n$ into (5.2.18), picking $v_h = \phi_h^{n+1}$, $\forall q_h^{n+1} \in Q_h$ and combining the results gives

$$\begin{aligned}
& \frac{\|\phi_h^{n+1}\|^2 - \|\phi_h^n\|^2 + \|\phi_h^{n+1} - \phi_h^n\|^2}{2\Delta t} + \|\phi_h^{n+1}\|_{\varepsilon_h}^2 = - \left(\frac{\eta^{n+1} - \eta^n}{\Delta t}, \phi_h^{n+1} \right) \\
& - a^h(\eta^{n+1}, \phi_h^{n+1}) + b(p^{n+1} - q_h^{n+1}, \phi_h^{n+1}) - \langle \tau^{n+1} \cdot \mathbf{n}_f, \phi_h^{n+1} \rangle \\
& - d^*(u^{n+1}, u^{n+1}, \phi_h^{n+1}) + d^*(u_h^n, u_h^{n+1}, \phi_h^{n+1}) + \text{Intp}(u^{n+1}; \phi_h^{n+1}).
\end{aligned} \tag{5.2.19}$$

We bound the terms on RHS individually.

$$\begin{aligned}
\left(\frac{\eta^{n+1} - \eta^n}{\Delta t}, \phi_h^{n+1} \right) & \leq \frac{\|\eta^{n+1} - \eta^n\|}{\Delta t} \|\phi_h^{n+1}\| \\
& \leq \nu \theta |\phi_h^{n+1}|_1^2 + \frac{C}{\nu \Delta t} \int_{t^n}^{t^{n+1}} \|\eta_t\|^2 \\
& \leq \nu \theta |\phi_h^{n+1}|_1^2 + \frac{Ch^{2(1+\alpha)}}{\nu \Delta t} \int_{t^n}^{t^{n+1}} |u_t|_{1+\alpha}^2.
\end{aligned} \tag{5.2.20}$$

By Lemma 5.2.2

$$\begin{aligned}
a^h(\eta^{n+1}, \phi_h^{n+1}) & \leq \|\eta^{n+1}\|_{\varepsilon_h} \|\phi_h^{n+1}\|_{\varepsilon_h} \\
& = \sqrt{\nu} |\eta^{n+1}|_1 \|\phi_h^{n+1}\|_{\varepsilon_h} \leq \frac{\nu |\eta^{n+1}|_1^2}{2} + \frac{\|\phi_h^{n+1}\|_{\varepsilon_h}^2}{2} \\
& \leq C\nu h^{2\alpha} |u^{n+1}|_{1+\alpha}^2 + \frac{\|\phi_h^{n+1}\|_{\varepsilon_h}^2}{2}.
\end{aligned} \tag{5.2.21}$$

Using $\|\nabla \cdot v_h\| \leq \sqrt{d}|\nabla v_h|_1$ and picking $q_h^{n+1} = \Pi_{SZ} p^{n+1}$, we obtain

$$\begin{aligned}
b(p^{n+1} - q_h^{n+1}, \phi_h^{n+1}) &\leq \|p^{n+1} - q_h^{n+1}\| \|\nabla \cdot \phi_h^{n+1}\| \\
&\leq \theta\nu |\phi_h^{n+1}|_1^2 + \frac{C}{\nu} \|p^{n+1} - q_h^{n+1}\|^2 \\
&\leq \theta\nu |\phi_h^{n+1}|_1^2 + \frac{Ch^{2\beta}}{\nu} |p^{n+1}|_\beta^2.
\end{aligned} \tag{5.2.22}$$

We now bound the traction term. Using $\phi_h^n = -u_h^n$ in Ω_{s_h} and (5.1.6), the traction term can be expressed as

$$\begin{aligned}
\langle \tau^{n+1} \cdot \mathbf{n}_f, \phi_h^{n+1} \rangle &= (\lambda^{n+1}, \phi_h^{n+1})_{1,s} = (\lambda^{n+1}, u_h^{n+1})_{1,s_h} + (\lambda^{n+1}, \phi_h^{n+1})_{1,s \setminus s_h} \\
&\leq \|\lambda^{n+1}\|_{1,s_h} \|u_h^{n+1}\|_{1,s_h} + C \|\lambda^{n+1}\|_{1,s \setminus s_h} |\phi_h^{n+1}|_1 \\
&\leq \|\lambda^{n+1}\|_{1,s_h} \|u_h^{n+1}\|_{1,s_h} + \frac{C}{\nu} \|\lambda^{n+1}\|_{1,s \setminus s_h}^2 + \theta\nu |\phi_h^{n+1}|_1^2.
\end{aligned} \tag{5.2.23}$$

By Taylor series expansion

$$\text{Intp}(u^{n+1}; \phi_h^{n+1}) \leq \theta\nu |\phi_h^{n+1}|_1^2 + \frac{C\Delta t}{\nu} \int_{t^n}^{t^{n+1}} \|u_{tt}\|^2 dt. \tag{5.2.24}$$

Now consider the nonlinear terms. By adding and subtracting terms, they can be rewritten as

$$\begin{aligned}
&d^*(u^{n+1}, u^{n+1}, \phi_h^{n+1}) - d^*(u_h^n, u_h^{n+1}, \phi_h^{n+1}) \\
&= d^*(u^{n+1}, u^{n+1} - u_h^{n+1}, \phi_h^{n+1}) + d^*(u^{n+1}, u_h^{n+1}, \phi_h^{n+1}) - d^*(u_h^n, u_h^{n+1}, \phi_h^{n+1}) \\
&= d^*(u^{n+1}, \eta^{n+1}, \phi_h^{n+1}) + d^*(u^{n+1} - u^n, u^{n+1}, \phi_h^{n+1}) - d^*(u^{n+1} - u^n, \eta^{n+1}, \phi_h^{n+1}) \\
&+ d^*(e^n, u^{n+1}, \phi_h^{n+1}) - d^*(e^n, \eta^{n+1}, \phi_h^{n+1}) \\
&= d^*(u^{n+1}, \eta^{n+1}, \phi_h^{n+1}) + d^*(u^{n+1} - u^n, u^{n+1}, \phi_h^{n+1}) - d^*(u^{n+1} - u^n, \eta^{n+1}, \phi_h^{n+1}) \\
&+ d^*(\eta^n, u^{n+1}, \phi_h^{n+1}) + d^*(\phi_h^n, u^{n+1}, \phi_h^{n+1}) \\
&- d^*(\eta^n, \eta^{n+1}, \phi_h^{n+1}) - d^*(\phi_h^n, \eta^{n+1}, \phi_h^{n+1}).
\end{aligned} \tag{5.2.25}$$

The terms in (5.2.25) can be dealt with as follows:

$$\begin{aligned}
d^*(u^{n+1}, \eta^{n+1}, \phi_h^{n+1}) &\leq C|u^{n+1}|_1|\eta^{n+1}|_1|\phi_h^{n+1}|_1 \\
&\leq \theta\nu|\phi_h^{n+1}|_1^2 + \frac{C}{\nu}|u^{n+1}|_1^2|\eta^{n+1}|_1^2 \\
&\leq \theta\nu|\phi_h^{n+1}|_1^2 + \frac{Ch^{2\alpha}}{\nu}|u^{n+1}|_1^2|u^{n+1}|_{1+\alpha}^2 \\
&\leq \theta\nu|\phi_h^{n+1}|_1^2 + \frac{Ch^{2\alpha}}{\nu}|u|_{\infty,1}^2|u^{n+1}|_{1+\alpha}^2 \\
&\leq \theta\nu|\phi_h^{n+1}|_1^2 + \frac{Ch^{2\alpha}}{\nu}|u^{n+1}|_{1+\alpha}^2,
\end{aligned} \tag{5.2.26}$$

$$\begin{aligned}
d^*(u^{n+1} - u^n, u^{n+1}, \phi_h^{n+1}) &\leq C|u^{n+1} - u^n|_1|u^{n+1}|_1|\phi_h^{n+1}|_1 \\
&\leq \theta\nu|\phi_h^{n+1}|_1^2 + \frac{C\Delta t^2}{\nu}|u_t|_{\infty,1}^2|u^{n+1}|_1^2 \\
&\leq \theta\nu|\phi_h^{n+1}|_1^2 + \frac{C\Delta t^2}{\nu}|u^{n+1}|_1^2,
\end{aligned} \tag{5.2.27}$$

$$\begin{aligned}
d^*(u^{n+1} - u^n, \eta^{n+1}, \phi_h^{n+1}) &\leq C|u^{n+1} - u^n|_1|\eta^{n+1}|_1|\phi_h^{n+1}|_1 \\
&\leq \theta\nu|\phi_h^{n+1}|_1^2 + \frac{C\Delta t^2}{\nu}|u_t|_{\infty,1}^2|\eta^{n+1}|_1^2 \\
&\leq \theta\nu|\phi_h^{n+1}|_1^2 + \frac{C\Delta t^2 h^{2\alpha}}{\nu}|u^{n+1}|_{1+\alpha}^2,
\end{aligned} \tag{5.2.28}$$

$$\begin{aligned}
d^*(\eta^n, u^{n+1}, \phi_h^{n+1}) &\leq C|\eta^n|_1|u^{n+1}|_1|\phi_h^{n+1}|_1 \\
&\leq \theta\nu|\phi_h^{n+1}|_1^2 + \frac{C}{\nu}|\eta^n|_1^2|u^{n+1}|_1^2
\end{aligned} \tag{5.2.29}$$

$$\begin{aligned}
&\leq \theta\nu|\phi_h^{n+1}|_1^2 + \frac{Ch^{2\alpha}}{\nu}|u^n|_{1+\alpha}^2|u^{n+1}|_1^2 \\
&\leq \theta\nu|\phi_h^{n+1}|_1^2 + \frac{Ch^{2\alpha}}{\nu}|u^n|_{1+\alpha}^2,
\end{aligned} \tag{5.2.30}$$

$$\begin{aligned}
d^*(\eta^n, \eta^{n+1}, \phi_h^{n+1}) &\leq C|\eta^n|_1|\eta^{n+1}|_1|\phi_h^{n+1}|_1 \\
&\leq \theta\nu|\phi_h^{n+1}|_1^2 + \frac{C}{\nu}|\eta^n|_1^2|\eta^{n+1}|_1^2
\end{aligned} \tag{5.2.31}$$

$$\begin{aligned}
&\leq \theta\nu|\phi_h^{n+1}|_1^2 + \frac{Ch^{4\alpha}}{\nu}|u^n|_{1+\alpha}^2|u^{n+1}|_{1+\alpha}^2 \\
&\leq \theta\nu|\phi_h^{n+1}|_1^2 + \frac{Ch^{4\alpha}}{\nu}|u^{n+1}|_{1+\alpha}^2,
\end{aligned} \tag{5.2.32}$$

and

$$\begin{aligned}
d^*(\phi_h^n, u^{n+1}, \phi_h^{n+1}) &\leq C\sqrt{|\phi_h^n|_1\|\phi_h^n\|}|u^{n+1}|_1|\phi_h^{n+1}|_1 \\
&\leq \theta\nu|\phi_h^{n+1}|_1^2 + \frac{C}{\nu}\|\phi_h^n\|\|\phi_h^n|_1|u^{n+1}|_1^2 \\
&\leq \theta\nu|\phi_h^{n+1}|_1^2 + \tilde{\theta}\nu|\phi_h^n|_1^2 + \frac{C}{\nu^2}\|\phi_h^n\|^2|u^{n+1}|_1^4,
\end{aligned} \tag{5.2.33}$$

$$\begin{aligned}
d^*(\phi_h^n, \eta^{n+1}, \phi_h^{n+1}) &\leq C\sqrt{|\phi_h^n|_1\|\phi_h^n\|}|\eta^{n+1}|_1|\phi_h^{n+1}|_1 \\
&\leq \theta\nu|\phi_h^{n+1}|_1^2 + \tilde{\theta}\nu|\phi_h^n|_1^2 + \frac{C}{\nu^2}\|\phi_h^n\|^2|\eta^{n+1}|_1^4 \\
&\leq \theta\nu|\phi_h^{n+1}|_1^2 + \tilde{\theta}\nu|\phi_h^n|_1^2 + \frac{Ch^{4\alpha}}{\nu^2}\|\phi_h^n\|^2|u^{n+1}|_{1+\alpha}^4.
\end{aligned} \tag{5.2.34}$$

Applying the obtained estimates to (5.2.19), summing from $n = 0$ to $N - 1$ and picking $\theta = \frac{1}{32}$, $\tilde{\theta} = \frac{1}{8}$ we obtain

$$\begin{aligned}
&\|\phi_h^N\|^2 + \Delta t \sum_{n=0}^{N-1} \|\phi_h^{n+1}\|_{\varepsilon_h}^2 + \sum_{n=0}^{N-1} \|\phi_h^{n+1} - \phi_h^n\|^2 \\
&\leq C \left(\frac{h^{2(1+\alpha)}}{\nu} \|u_t\|_{2,1+\alpha}^2 + h^{2\alpha}\nu \|u\|_{2,1+\alpha}^2 + \frac{h^{2\beta}}{\nu} \|p\|_{2,\beta}^2 \right. \\
&\quad + \|\lambda\|_{2,1,s_h} \|u_h\|_{2,0,s_h} + \frac{\|\lambda\|_{2,1,s}^2}{\nu} + \frac{\Delta t^2}{\nu} \|u_{tt}\|_{2,0}^2 + \frac{\Delta t^2}{\nu} \|u\|_{2,1}^2 + \frac{h^{2\alpha}}{\nu} \|u\|_{2,1+\alpha}^2 \\
&\quad \left. + \frac{\Delta t}{\nu^2} \sum_{n=0}^{N-1} \|\phi_h^n\|^2 (|u^{n+1}|_1^4 + h^{4\alpha}|u^{n+1}|_{1+\alpha}^4) \right).
\end{aligned} \tag{5.2.35}$$

Applying the Gronwall's inequality, (5.2.7) and simplifying further, we get

$$\begin{aligned} & \|\phi_h^N\|^2 + \Delta t \sum_{n=0}^{N-1} \|\phi_h^{n+1}\|_\varepsilon^2 + \sum_{n=0}^{N-1} \|\phi_h^{n+1} - \phi_h^n\|^2 \\ & \leq C \left(\frac{\|\lambda\|_{2,1,s \setminus s_h}^2}{\nu} + \sqrt{\varepsilon} + \frac{h^{2\alpha}}{\nu} + \frac{\Delta t^2}{\nu} \right) \exp \left(\frac{\|u\|_{4,1}^4}{\nu^2} + \frac{h^{4\alpha} \|u\|_{4,1+\alpha}^4}{\nu^2} \right). \end{aligned} \quad (5.2.36)$$

Note that $\lim_{h \rightarrow 0} \mu_d(\Omega_s \setminus \Omega_{s_h}) = 0$ by Lemma 5.2.4, and thus $\|\lambda\|_{2,1,s \setminus s_h}^2 \rightarrow 0$ as $h \rightarrow 0$. The triangle inequality completes the proof. \square

5.3 NUMERICAL EXPERIMENT

We test the proposed algorithm with two-dimensional flow around nine balls placed in the channel. We compare the results with the solution of NSE found on a fine, conforming mesh (Fig. 5.3), which we refer to as a "true" solution. The problem setup is as follows: $\Omega_f = ((0, 1) \times (0.39, 0.61)) \setminus \Omega_s$, where Ω_s is the union of nine balls with radii 0.03 and centered at (0.16, 0.49), (0.73, 0.54), (0.27, 0.45), (0.1, 0.44), (0.13, 0.56), (0.35, 0.48), (0.34, 0.56), (0.45, 0.5) and (0.52, 0.45). The boundary conditions are no-slip on the top and bottom boundaries, a parabolic inflow given by $(10(y - 0.39)(0.61 - y), 0)^T$ and do-nothing outflow. The flow and model parameters are $\nu = 0.005$, $f = (\exp(xy + t), 0)^T \chi_f$, $t_f = 1$ and $\varepsilon = 1e - 15$. The discrete spaces are the standard $(X_h, Q_h) = (P_2, P_1)$ Taylor-Hood pair [11, 13], and the Lagrange multiplier space is $L_h := \text{span} \left\{ \begin{pmatrix} \chi_{B_i} \\ 0 \end{pmatrix}, \begin{pmatrix} 0 \\ \chi_{B_j} \end{pmatrix} \right\}$, as in [50]. The experiments were performed on FreeFEM++ package [28]. We compare the speed contours and the pressure drops of Navier-Stokes-Brinkman model (M1), the proposed algorithm (M2) and the "true" solution. We also compare the errors between M1, M2 and the "true" solution. The tests are performed on four successive

Figure 5.3: Body-fitted mesh for the "true" solution

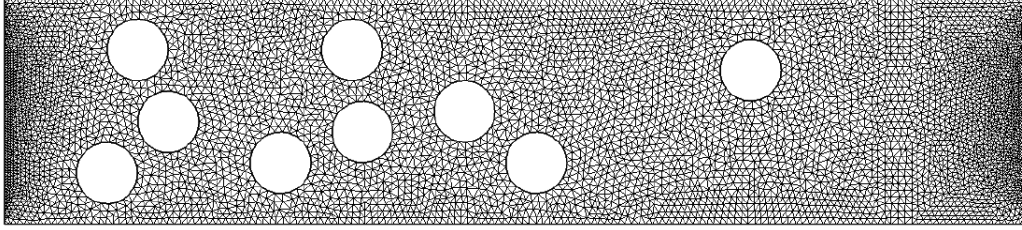
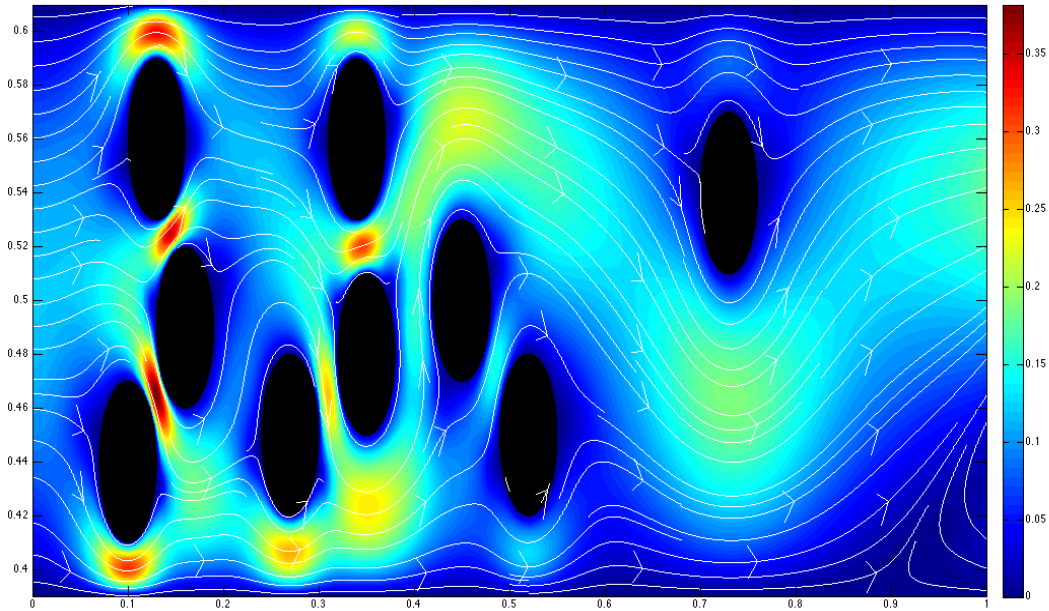


Figure 5.4: The body-fitted, resolved Navier-Stokes velocity speed contours with streamlines at $t = 1$



uniform mesh and timestep refinements with initial mesh size $h \simeq 0.037 > r$ and timestep $\Delta t = 0.02$.

Speed contours. We first compare the speed contours at the final time. The speed contours of M1 and M2 are presented in Figures 5.6, and 5.7, respectively. As it can be seen, the Brinkman model chokes off the flow in some of the pores, and

alters the entire flow structure. Specifically, it fails to capture the flow structure between the two balls, located in the bottom of the channel near the inlet, on all three meshes. On the other hand, the proposed algorithm predicts the flow structures more accurately, including the pores between the balls. In the plots we also observe the polygonal no-flow regions, similar to those described in 5.1 and 5.2. We also observe that our model allows flow through the solid region, which in turn causes smaller maximum speed values in some of the pores. This is due to the minimal choice of Lagrange multiplier space (some ideas for possible ways of improving this is mentioned below).

Pressure drops. The M2 algorithm also predicts more accurate pressure drop across the channel compared to M1, see the Table 5.1.

Errors. We next list the errors in both models in the Tables 5.2, 5.3. The Brinkman model gives excellent accuracy in the solid region at the cost of the global error, while M2 approach yields more accurate global approximation. From the Table 5.3, we also observe the slower convergence of M2 in Ω_s . This is so because, the no-flow in $\Omega_s \setminus \Omega_{s_n}$ is enforced by the same Lagrange multiplier space without refinements as $h \rightarrow 0, \Delta t \rightarrow 0$. Therefore, a possible improvement to the model would be to refine or enrich the multiplier space as $h \rightarrow 0, \Delta t \rightarrow 0$, while being computationally feasible (this might also require a stabilization for the multiplier space as locking might occur otherwise). We briefly mention two ideas herein

1. Incorporating the ideas from Glowinski et. al. [25], i.e., meshing the solid region with a different triangulation and then enforcing the weak no-flow on each triangle in Ω_s .
2. With the current model, u is made orthogonal to χ_B , which is 0-th degree spherical harmonic function. So another possibility is to carefully enrich the LM space with more spherical harmonics of lower order.

Figure 5.5: Two coarsest meshes, Ω_s and Ω_{s_h} (the shaded triangles)

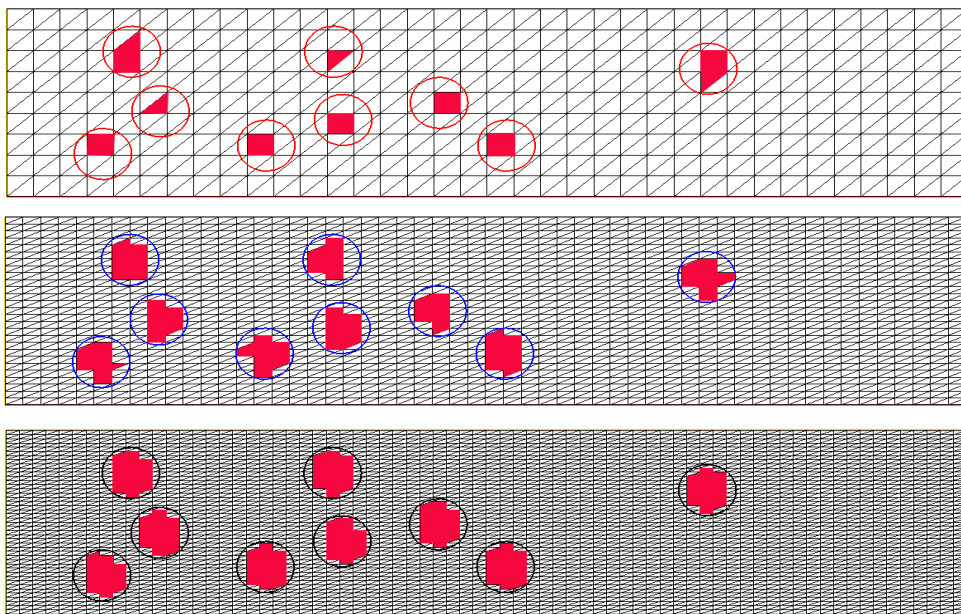


Figure 5.6: From top to bottom: speed contours of M2 on first three meshes, $h \simeq 0.037$, $h \simeq 0.02$, $h \simeq 0.0147$

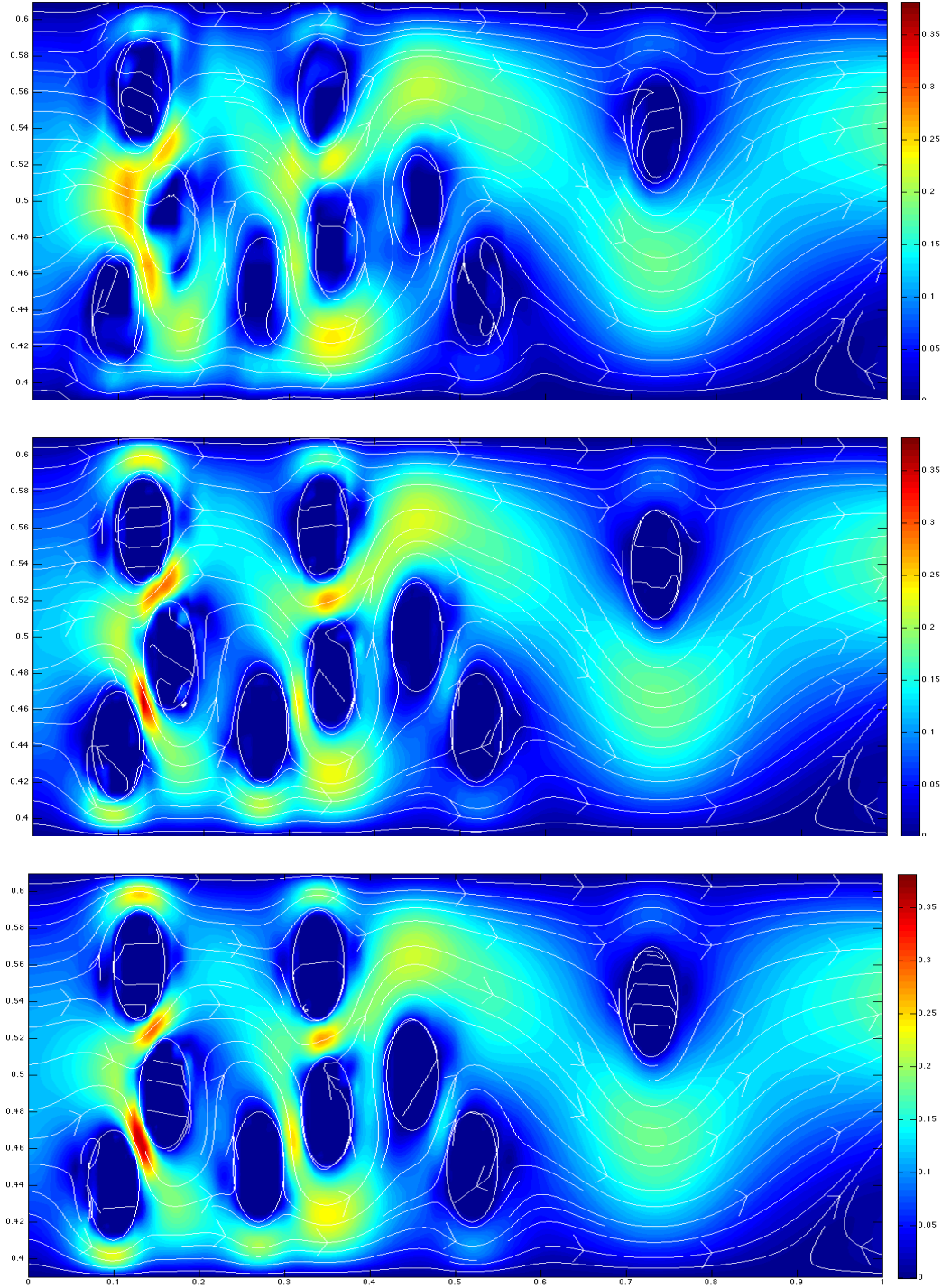
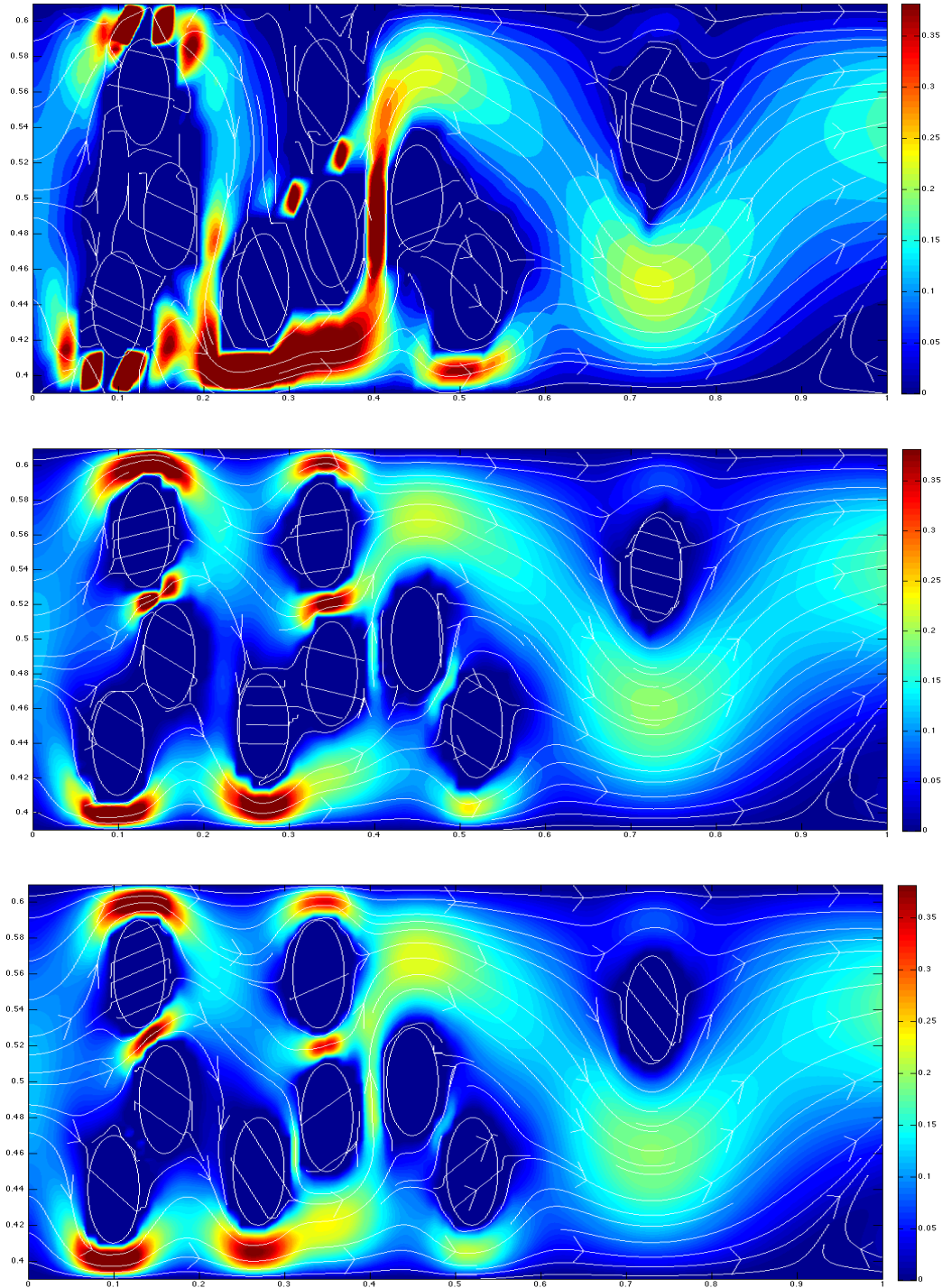


Figure 5.7: From top to bottom: speed contours of M1 on first three meshes, $h \simeq 0.037$, $h \simeq 0.02$, $h \simeq 0.0147$



	M1	M2
h		
0.037	-28.5	-2.2
0.02	-5.19	-1.5
0.0147	-2.44	-1.36
0.0072	-0.9	-0.9

Table 5.1: Average pressure drops across the channel, the "true" average pressure drop is around -0.57

	M1	M2
$h \ \& \ \Delta t$		
$h = 0.037$ $\Delta t = 0.02$	$5.8381e - 2$	$1.75244e - 2$
$h = 0.02$ $\Delta t = 0.01$	$2.50133e - 2$	$8.59639e - 3$
$h = 0.0147$ $\Delta t = 0.005$	$1.96568e - 2$	$6.96201e - 3$
$h = 0.0072$ $\Delta t = 0.0025$	$1.063e - 2$	$3.02426e - 3$

Table 5.2: The $L^2(\Omega)$ errors at $t = 1$

	M1	M2
h & Δt		
$h = 0.037$ $\Delta t = 0.02$	$1.05867e - 3$	$8.05326e - 3$
$h = 0.02$ $\Delta t = 0.01$	$1.44405e - 5$	$3.52782e - 3$
$h = 0.0147$ $\Delta t = 0.005$	$1.74799e - 6$	$2.71275e - 3$
$h = 0.0072$ $\Delta t = 0.0025$	$7.51459e - 9$	$9.47e - 4$

Table 5.3: The $l^2((0, T); L^2(\Omega_s))$ errors

6.0 BRINKMAN VOLUME PENALIZATION BASED MODEL FOR MODERATE *RE* FLOWS AND FORCED HEAT CONVECTION

In this chapter, we develop an algorithm for forced convective heat transfer. For the flow part, we adapt the approach of Chapter 5, and for the convective heat transfer, we employ the Streamline Diffusion finite element method (SDFEM) (also known as SUPG) [10, 29].

6.1 WEAK FORMULATIONS

Definition 6.1.1. Let

$$\begin{aligned}
 Y_* &:= H_0^1(\Omega_*), Y_h \subset Y, \\
 w(\cdot, \cdot, \cdot) &: X \times Y \times Y \rightarrow R, \quad w(u, \theta, \phi) := (u \cdot \nabla \theta, \phi), \\
 w^*(\cdot, \cdot, \cdot) &: X \times Y \times Y \rightarrow R, \quad w^*(u, \theta, \phi) := \frac{1}{2}(w(u, \theta, \phi) - w(u, \phi, \theta)), \\
 \kappa &:= \kappa_f \chi_f + \kappa_s \chi_s, \\
 \Upsilon(x, t) &:= \Upsilon_f(x, t) \chi_f + \Upsilon_s(x, t) \chi_s, \\
 T^0(x) &:= T_f^0(x) \chi_f + T_s^0(x) \chi_s.
 \end{aligned}$$

Note that Y_* is the space of scalar $H_0^1(\Omega_*)$ functions, while X_* is that of vector functions.

The weak formulation of the heat transfer equation is obtained by multiplying the sum of the equations (3.3.2) and (3.3.3) by $\theta \in Y$, and integrating by parts. Letting

$$T(x, t) := T_f(x, t)\chi_f + T_s(x, t)\chi_s,$$

we obtain that (u, p, T) satisfy the following system.

Problem 9. Find $(u, p, T) \in (X, Q, Y)$ such that $(u(x, t), p(x, t))_{\Omega_s} = (0, 0)$, $u(x, 0) = u^0, T(x, 0) = T^0, T$ - continuous across $\partial\Omega_s$, and

$$(u_t, v) + d^*(u, u, v) + a(u, v) + b(p, v) + \langle \tau(u, p) \cdot \mathbf{n}_f, v \rangle = (f, v) \quad \forall v \in X, \quad (6.1.1)$$

$$b(q, u) = 0 \quad \forall q \in Q, \quad (6.1.2)$$

$$(T_t, \theta) + w^*(u, T, \theta) + (\kappa \nabla T, \nabla \theta) = (\Upsilon, \theta) \quad \forall \theta \in Y. \quad (6.1.3)$$

Since (6.1.3) is a convection-diffusion equation, for convection dominated flows, the direct Galerkin approximation will develop spurious oscillations. To stabilize the solution, we use SDFEM formulation for the discrete version of (6.1.3). SDFEM assumes that $\kappa \nabla u \in H^1(K)$ for all $K \in \mathcal{T}_h$. Since κ is discontinuous on $\partial\Omega_s$, this does not hold in our case. For the brevity of the presentation, we simply replace κ with $\kappa_{eff} \in R$, where κ_{eff} is the coefficient for the homogenized media [51]:

$$\frac{1}{\kappa_{eff}} := \frac{\frac{1}{\kappa_f} + \frac{1}{\kappa_s}}{2}.$$

In general, if the discontinuity of κ is not resolved by the mesh, then the term $(-\nabla \cdot (\kappa \cdot \nabla T_h), u_h \cdot \nabla \theta_h)_K$ should be replaced with

$$(\kappa \cdot \nabla T_h, \nabla (u_h \cdot \nabla \theta_h))_K - \int_{\partial K} \kappa \frac{\partial T_h}{\partial \mathbf{n}_{\partial K}} u_h \cdot \nabla \theta_h.$$

Thus, we consider the following algorithm:

The discrete model. Assume that (X_h, Q_h) is a div-stable pair.

Problem 10. Find $(u_h^{n+1}, p_h^{n+1}, \lambda_h^{n+1}, T_h^{n+1}) \in (X_h, Q_h, L_h, Y_h)$, $n = 0, 1, \dots, N - 1$ satisfying

$$\begin{aligned} \left(\frac{u_h^{n+1} - u_h^n}{\Delta t}, v_h \right) + a^h(u_h^{n+1}, v_h) + b(p_h^{n+1}, v_h) \\ + c(\lambda_h^{n+1}, v_h) + d^*(u_h^n, u_h^{n+1}, v_h) = (f^{n+1}, v_h) \quad \forall v_h \in X_h, \end{aligned} \quad (6.1.4)$$

$$b(q_h, u_h^{n+1}) = 0 \quad \forall q_h \in Q_h, \quad (6.1.5)$$

$$c(\mu_h, u_h^{n+1}) = 0 \quad \forall \mu_h \in L_h, \quad (6.1.6)$$

$$\left(\frac{T_h^{n+1} - T_h^n}{\Delta t}, \theta_h \right) + w^*(u_h^{n+1}, T_h^{n+1}, \theta_h) + \kappa_{eff}(T_h^{n+1}, \theta_h)_1 \quad (6.1.7)$$

$$\begin{aligned} + \sum_{K \in \mathcal{T}_h} \delta_K \left(-\kappa_{eff} \Delta T_h^{n+1} + u_h^{n+1} \cdot \nabla T_h^{n+1} + \frac{T_h^{n+1} - T_h^n}{\Delta t}, u_h^{n+1} \cdot \nabla \theta_h \right)_K \\ = (\Upsilon^{n+1}, \theta_h) + \sum_{K \in \mathcal{T}_h} \delta_K (\Upsilon_h^{n+1}, u_h^{n+1} \cdot \nabla \theta_h)_K \quad \forall \theta_h \in R_h, \end{aligned}$$

where u_h^0, T_h^0 are the approximations of u^0, T^0 .

6.2 WELL-POSEDNESS, STABILITY AND CONVERGENCE

We derive the stability and convergence results for the temperature variable for two values of the thermal diffusion coefficient κ_{eff} :

A) $\kappa_{eff} \ll 1$;

B) Moderate or large κ_{eff} .

Theorem 6.2.1. Assume $\delta_K \leq \min \left\{ \frac{\Delta t}{8}, \frac{h_K^2}{4C_{inv}^2 \kappa_{eff}} \right\}$, where C_{inv} is the inverse inequality constant. Then there exists a unique $(u_h^n, p_h^n, \lambda_h^n, T_h^n) \in (X_h, Q_h, L_h, Y_h)$ solution of the Problem 10. Moreover, $\forall n = 1, \dots, N$, T_h^n satisfies

A)

$$\begin{aligned} \|T_h^N\|^2 &+ \Delta t \kappa_{eff} \sum_{n=0}^{N-1} |T_h^{n+1}|_1^2 + \Delta t \sum_{n=0}^{N-1} \sum_K \delta_K \|u_h^{n+1} \cdot \nabla T_h^{n+1}\|_K^2 \\ &\leq C e^{t_f} \left(\|T_h^0\|^2 + \|\Upsilon\|_{2,0}^2 + \sum_K \delta_K \|\Upsilon\|_{2,0,K}^2 \right), \end{aligned} \quad (6.2.1)$$

B)

$$\begin{aligned} \|T_h^N\|^2 &+ \Delta t \kappa_{eff} \sum_{n=0}^{N-1} |T_h^{n+1}|_1^2 + \Delta t \sum_{n=0}^{N-1} \sum_K \delta_K \|u_h^{n+1} \cdot \nabla T_h^{n+1}\|_K^2 \\ &\leq C \left(\|T_h^0\|^2 + \|\Upsilon\|_{2,-1}^2 + \sum_K \delta_K \|\Upsilon\|_{2,0,K}^2 \right). \end{aligned} \quad (6.2.2)$$

Proof. Pick $\theta_h = T_h^{n+1}$ in (6.1.7) to get

$$\begin{aligned} &\frac{\|T_h^{n+1}\|^2 - \|T_h^n\|^2 + \|T_h^{n+1} - T_h^n\|^2}{2\Delta t} + \kappa_{eff} |T_h^{n+1}|_1^2 + \sum_K \delta_K \|u_h^{n+1} \cdot \nabla T_h^{n+1}\|_K^2 \\ &+ \sum_K \delta_K \left(-\kappa_{eff} \Delta T_h^{n+1} + \frac{T_h^{n+1} - T_h^n}{\Delta t}, u_h^{n+1} \cdot \nabla T_h^{n+1} \right)_K \\ &\leq \sum_K \delta_K (\Upsilon^{n+1}, u_h^{n+1} \cdot \nabla T_h^{n+1})_K + (\Upsilon^{n+1}, T_h^{n+1}), \end{aligned} \quad (6.2.3)$$

where the trilinear term vanished due to skew-symmetrization.

The local inverse inequality

$$\|\Delta v_h\|_K \leq C_{inv} h_K^{-1} |v_h|_{1,K}$$

and standard inequalities yield

$$\begin{aligned} &\sum_K \delta_K \left(-\kappa_{eff} \Delta T_h^{n+1} + \frac{T_h^{n+1} - T_h^n}{\Delta t}, u_h^{n+1} \cdot \nabla T_h^{n+1} \right)_K \\ &\leq \sum_K \delta_K \left(\kappa_{eff} C_{inv} h_K^{-1} |T_h^{n+1}|_{1,K} + \frac{\|T_h^{n+1} - T_h^n\|_K}{\Delta t} \right) \|u_h^{n+1} \cdot \nabla T_h^{n+1}\|_K \\ &\leq \sum_K 2\delta_K \left(\kappa_{eff}^2 C_{inv}^2 h_K^{-2} |T_h^{n+1}|_{1,K}^2 + \frac{\|T_h^{n+1} - T_h^n\|_K^2}{\Delta t^2} \right) \\ &+ \frac{1}{4} \sum_K \delta_K \|u_h^{n+1} \cdot \nabla T_h^{n+1}\|_K^2. \end{aligned} \quad (6.2.4)$$

We further obtain

$$\begin{aligned}
& \sum_K \delta_K (\Upsilon^{n+1}, u_h^{n+1} \cdot \nabla T_h^{n+1})_K \\
\leq & \sum_K \delta_K \|\Upsilon^{n+1}\|_K^2 + \frac{1}{4} \sum_K \delta_K \|u_h^{n+1} \cdot \nabla T_h^{n+1}\|_K^2,
\end{aligned} \tag{6.2.5}$$

and

A)

$$\begin{aligned}
& (\Upsilon^{n+1}, T_h^{n+1}) = (\Upsilon^{n+1}, T_h^{n+1} - T_h^n) + (\Upsilon^{n+1}, T_h^n) \\
\leq & \left(\frac{1}{2} + \Delta t\right) \|\Upsilon^{n+1}\|^2 + \frac{\|T_h^{n+1} - T_h^n\|^2}{4\Delta t} + \frac{\|T_h^n\|^2}{2},
\end{aligned} \tag{6.2.6}$$

B)

$$(\Upsilon^{n+1}, T_h^{n+1}) \leq \frac{\|\Upsilon^{n+1}\|_{-1}^2}{2\kappa_{eff}} + \kappa_{eff} \frac{\|T_h^{n+1}\|^2}{2}. \tag{6.2.7}$$

Combining all the bounds above gives

A)

$$\begin{aligned}
& \frac{\|T_h^{n+1}\|^2 - \|T_h^n\|^2}{2\Delta t} + \frac{\kappa_{eff}}{2} |T_h^{n+1}|_1^2 + \frac{1}{2} \sum_K \delta_K \|u_h^{n+1} \cdot \nabla T_h^{n+1}\|_K^2 \\
+ & \sum_K \left(\frac{1}{4} - \frac{2\delta_K}{\Delta t}\right) \frac{\|T_h^{n+1} - T_h^n\|_K^2}{\Delta t} \\
+ & \sum_K \left(\frac{\kappa_{eff}}{2} - 2\delta_K \kappa_{eff}^2 C_{inv}^2 h_K^{-2}\right) |T_h^{n+1}|_{1,K}^2 \\
\leq & \frac{\|T_h^n\|^2}{2} + \left(\frac{1}{2} + \Delta t\right) \|\Upsilon^{n+1}\|^2 + \sum_K \delta_K \|\Upsilon^{n+1}\|_K^2.
\end{aligned}$$

B)

$$\begin{aligned}
& \frac{\|T_h^{n+1}\|^2 - \|T_h^n\|^2}{2\Delta t} + \frac{\kappa_{eff}}{2} |T_h^{n+1}|_1^2 + \frac{1}{2} \sum_K \delta_K \|u_h^{n+1} \cdot \nabla T_h^{n+1}\|_K^2 \\
& + \sum_K \left(\frac{1}{4} - \frac{2\delta_K}{\Delta t} \right) \frac{\|T_h^{n+1} - T_h^n\|_K^2}{\Delta t} \\
& + \sum_K \left(\frac{\kappa_{eff}}{2} - 2\delta_K \kappa_{eff}^2 C_{inv}^2 h_K^{-2} \right) |T_h^{n+1}|_{1,K}^2 \\
& \leq \frac{\|\Upsilon^{n+1}\|_{-1}^2}{2\kappa_{eff}} + \sum_K \delta_K \|\Upsilon^{n+1}\|_K^2.
\end{aligned}$$

Picking $\delta_K \leq \min \left\{ \frac{\Delta t}{8}, \frac{h_K^2}{4C_{inv}^2 \kappa_{eff}} \right\}$ and summing over the timesteps yields

A)

$$\begin{aligned}
& \|T_h^N\|^2 + \Delta t \kappa_{eff} \sum_{n=0}^{N-1} |T_h^{n+1}|_1^2 + \Delta t \sum_{n=0}^{N-1} \sum_K \delta_K \|u_h^{n+1} \cdot \nabla T_h^{n+1}\|_K^2 \quad (6.2.8) \\
& \leq \|T_h^0\|^2 + \Delta t \sum_{n=0}^{N-1} \|T_h^n\|^2 + C \Delta t \sum_{n=0}^{N-1} \|\Upsilon^{n+1}\|^2 + \Delta t \sum_{n=0}^{N-1} \sum_K \delta_K \|\Upsilon^{n+1}\|_K^2.
\end{aligned}$$

B)

$$\begin{aligned}
& \|T_h^N\|^2 + \Delta t \kappa_{eff} \sum_{n=0}^{N-1} |T_h^{n+1}|_1^2 + \Delta t \sum_{n=0}^{N-1} \sum_K \delta_K \|u_h^{n+1} \cdot \nabla T_h^{n+1}\|_K^2 \\
& \leq \|T_h^0\|^2 + C \frac{\Delta t}{\kappa_{eff}} \sum_{n=0}^{N-1} \|\Upsilon^{n+1}\|_{-1}^2 + \Delta t \sum_{n=0}^{N-1} \sum_K \delta_K \|\Upsilon^{n+1}\|_K^2. \quad (6.2.9)
\end{aligned}$$

The Gronwall's inequality completes the proof. \square

Theorem 6.2.2. Assume $\delta_K \leq \min \left\{ \frac{\Delta t}{16}, \frac{h_K^2}{8C_{inv}^2 \kappa_{eff}} \right\}$, where C_{inv} is the inverse inequality constant. Then the temprature error $e_T^n := T^n - T_h^n$ satisfies

A)

$$\begin{aligned}
& \|e_T^N\|^2 + \kappa_{eff} \Delta t \sum_{n=0}^{N-1} |e_T^{n+1}|_1^2 \leq C e^{t_f} \left(\|e_T^0\|^2 + \frac{\Delta t}{\kappa_{eff}} \sum_{n=0}^{N-1} |e^{n+1}|_1^2 |T^{n+1}|_1^2 \right. \\
& + \inf_{\theta_h \in Y_h} \left(\frac{\Delta t}{\kappa_{eff}} \sum_{n=0}^{N-1} |u_h^{n+1}|_1^2 |T^{n+1} - \theta_h|_1^2 + |T_t - \theta_h|_{2,0}^2 + \kappa_{eff} |T - \theta_h|_{2,1}^2 \right. \\
& + \sum_{K \in \mathcal{T}_h} \delta_K (\Delta t^2 \|T_{tt}\|_{2,0,K}^2 + |T_t - \theta_h|_{2,0,K}^2 + \kappa_{eff}^2 |\Delta(T - \theta_h)|_{2,0,K}^2) \quad (6.2.10) \\
& \left. + \Delta t \sum_{n=0}^{N-1} \sum_{K \in \mathcal{T}_h} \delta_K h_K^{-2} (|e^{n+1}|_{1,K}^2 |T^{n+1}|_{1,K}^2 + |u_h^{n+1}|_{1,K}^2 |T^{n+1} - \theta_h|_{1,K}^2) \right).
\end{aligned}$$

B)

$$\begin{aligned}
& \|e_T^N\|^2 + \kappa_{eff} \Delta t \sum_{n=0}^{N-1} |e_T^{n+1}|_1^2 \leq C \left(\|e_T^0\|^2 + \frac{\Delta t}{\kappa_{eff}} \sum_{n=0}^{N-1} |e^{n+1}|_1^2 |T^{n+1}|_1^2 \right. \\
& + \inf_{\theta_h \in Y_h} \left(\frac{\Delta t}{\kappa_{eff}} \sum_{n=0}^{N-1} |u_h^{n+1}|_1^2 |T^{n+1} - \theta_h|_1^2 + \frac{|T_t - \theta_h|_{2,0}^2}{\kappa_{eff}} + \kappa_{eff} |T - \theta_h|_{2,1}^2 \right. \\
& + \sum_{K \in \mathcal{T}_h} \delta_K (\Delta t^2 \|T_{tt}\|_{2,0,K}^2 + |T_t - \theta_h|_{2,0,K}^2 + \kappa_{eff}^2 |\Delta(T - \theta_h)|_{2,0,K}^2) \quad (6.2.11) \\
& \left. + \Delta t \sum_{n=0}^{N-1} \sum_{K \in \mathcal{T}_h} \delta_K h_K^{-2} (|e^{n+1}|_{1,K}^2 |T^{n+1}|_{1,K}^2 + |u_h^{n+1}|_{1,K}^2 |T^{n+1} - \theta_h|_{1,K}^2) \right).
\end{aligned}$$

Proof. At time t_{n+1} , the true solution $T(x, t)$ satisfies

$$\begin{aligned}
& \left(\frac{T^{n+1} - T^n}{\Delta t}, \theta_h \right) + w^*(u^{n+1}, T^{n+1}, \theta_h) + \kappa_{eff} (T^{n+1}, \theta_h)_1 \quad (6.2.12) \\
& + \sum_{K \in \mathcal{T}_h} \delta_K \left(-\kappa_{eff} \Delta T^{n+1} + u^{n+1} \cdot \nabla T^{n+1} + \frac{T^{n+1} - T^n}{\Delta t}, u_h^{n+1} \cdot \nabla \theta_h \right)_K \\
& = (\Upsilon^{n+1}, \theta_h) + \sum_{K \in \mathcal{T}_h} \delta_K \left(\Upsilon_h^{n+1} + \frac{T^{n+1} - T^n}{\Delta t} - T_t(t^{n+1}), u_h^{n+1} \cdot \nabla \theta_h \right)_K
\end{aligned}$$

for all $\theta_h \in Y_h$. Subtracting (6.1.7) from (6.2.12) gives

$$\begin{aligned}
& \left(\frac{e_T^{n+1} - e_T^n}{\Delta t}, \theta_h \right) + w^*(e^{n+1}, T^{n+1}, \theta_h) + w^*(u_h^{n+1}, e_T^{n+1}, \theta_h) + \kappa_{eff}(e^{n+1}, \theta_h)_1 \\
& + \sum_{K \in \mathcal{T}_h} \delta_K \left(-\kappa_{eff} \Delta e_T^{n+1} + e^{n+1} \cdot \nabla T^{n+1} + u_h^{n+1} \cdot \nabla e_T^{n+1}, u_h^{n+1} \cdot \nabla \theta_h \right)_K \\
& + \sum_{K \in \mathcal{T}_h} \delta_K \left(\frac{e_T^{n+1} - e_T^n}{\Delta t}, u_h^{n+1} \cdot \nabla \theta_h \right)_K \\
& = \sum_{K \in \mathcal{T}_h} \delta_K \left(\frac{T^{n+1} - T^n}{\Delta t} - T_t(t^{n+1}), u_h^{n+1} \cdot \nabla \theta_h \right)_K.
\end{aligned} \tag{6.2.13}$$

Let us decompose the error at $t = t_n$ as

$$e_T^n = (T^n - \tilde{T}_h^n) + (\tilde{T}_h^n - T_h^n) := \phi_h^n + \psi^n,$$

where \tilde{T}_h^n is an interpolant of T^n . Choosing $\theta_h = \phi_h^{n+1}$ gives

$$\begin{aligned}
& \frac{\|\phi_h^{n+1}\|^2 - \|\phi_h^n\|^2 + \|\phi_h^{n+1} - \phi_h^n\|^2}{2\Delta t} + \kappa_{eff} |\phi_h^{n+1}|_1^2 \\
& + \sum_{K \in \mathcal{T}_h} \delta_K \|u_h^{n+1} \cdot \nabla \phi_h^{n+1}\|_K^2 = - \left(\frac{\psi^{n+1} - \psi^n}{\Delta t}, \phi_h^{n+1} \right) \\
& - \kappa_{eff} (\psi^{n+1}, \phi_h^{n+1})_1 - w^*(e^{n+1}, T^{n+1}, \phi_h^{n+1}) - w^*(u_h^{n+1}, \psi^{n+1}, \phi_h^{n+1}) \\
& - \sum_{K \in \mathcal{T}_h} \delta_K \left(-\kappa_{eff} \Delta \psi^{n+1} + e^{n+1} \cdot \nabla T^{n+1} + u_h^{n+1} \cdot \nabla \psi^{n+1}, u_h^{n+1} \cdot \nabla \phi_h^{n+1} \right)_K \\
& + \sum_{K \in \mathcal{T}_h} \delta_K \left(-\kappa_{eff} \Delta \psi^{n+1} + \frac{\psi^{n+1} - \psi^n}{\Delta t}, u_h^{n+1} \cdot \nabla \phi_h^{n+1} \right)_K \\
& - \sum_{K \in \mathcal{T}_h} \delta_K \left(-\kappa_{eff} \Delta \phi_h^{n+1} + \frac{\phi_h^{n+1} - \phi_h^n}{\Delta t}, u_h^{n+1} \cdot \nabla \phi_h^{n+1} \right)_K \\
& + \sum_{K \in \mathcal{T}_h} \delta_K \left(\frac{T^{n+1} - T^n}{\Delta t} - T_t(t^{n+1}), u_h^{n+1} \cdot \nabla \phi_h^{n+1} \right)_K.
\end{aligned} \tag{6.2.14}$$

We bound the terms on RHS of (6.2.14) individually.

A)

$$\begin{aligned}
& \left(\frac{\psi^{n+1} - \psi^n}{\Delta t}, \phi_h^{n+1} \right) \leq \frac{\|\psi^{n+1} - \psi^n\|}{\Delta t} \|\phi_h^{n+1} - \phi_h^n\| + \frac{\|\psi^{n+1} - \psi^n\|}{\Delta t} \|\phi_h^n\| \\
& \leq C \frac{\|\psi^{n+1} - \psi^n\|^2}{\Delta t} + \frac{\|\phi_h^{n+1} - \phi_h^n\|^2}{4\Delta t} + C \frac{\|\psi^{n+1} - \psi^n\|^2}{\Delta t^2} + \frac{\|\phi_h^n\|^2}{2} \\
& \leq \frac{C}{\Delta t} \int_{t^n}^{t^{n+1}} \|\psi_t\|^2 dt + \frac{\|\phi_h^{n+1} - \phi_h^n\|^2}{4\Delta t} + \frac{\|\phi_h^n\|^2}{2}. \tag{6.2.15}
\end{aligned}$$

B)

$$\left(\frac{\psi^{n+1} - \psi^n}{\Delta t}, \phi_h^{n+1} \right) \leq \frac{C}{\kappa_{eff} \Delta t} \int_{t^n}^{t^{n+1}} \|\psi_t\|^2 dt + \tau \kappa_{eff} |\phi_h^{n+1}|_1^2 \tag{6.2.16}$$

$$\kappa_{eff} (\psi^{n+1}, \phi_h^{n+1})_1 \leq C \kappa_{eff} |\psi^{n+1}|_1^2 + \tau \kappa_{eff} |\phi_h^{n+1}|_1^2. \tag{6.2.17}$$

$$\begin{aligned}
w^*(e^{n+1}, T^{n+1}, \phi_h^{n+1}) & \leq C |e^{n+1}|_1 |T^{n+1}|_1 |\phi_h^{n+1}|_1 \\
& \leq \frac{C}{\kappa_{eff}} |e^{n+1}|_1^2 |T^{n+1}|_1^2 + \tau \kappa_{eff} |\phi_h^{n+1}|_1^2. \tag{6.2.18}
\end{aligned}$$

$$w^*(u_h^{n+1}, \psi^{n+1}, \phi_h^{n+1}) \leq \frac{C}{\kappa_{eff}} |u_h^{n+1}|_1^2 |\psi^{n+1}|_1^2 + \tau \kappa_{eff} |\phi_h^{n+1}|_1^2. \tag{6.2.19}$$

Similar to (6.2.4)

$$\begin{aligned}
& \sum_K \delta_K \left(-\kappa_{eff} \Delta \phi_h^{n+1} + \frac{\phi_h^{n+1} - \phi_h^n}{\Delta t}, u_h^{n+1} \cdot \nabla \phi_h^{n+1} \right)_K \\
& \leq \sum_K \delta_K \left(\kappa_{eff} C_{inv} h_K^{-1} |\phi_h^{n+1}|_{1,K} + \frac{\|\phi_h^{n+1} - \phi_h^n\|_K}{\Delta t} \right) \|u_h^{n+1} \cdot \nabla \phi_h^{n+1}\|_K \\
& \leq \sum_K 2\delta_K \left(\kappa_{eff}^2 C_{inv}^2 h_K^{-2} |\phi_h^{n+1}|_{1,K}^2 + \frac{\|\phi_h^{n+1} - \phi_h^n\|_K^2}{\Delta t^2} \right) \\
& + \frac{1}{4} \sum_K \delta_K \|u_h^{n+1} \cdot \nabla \phi_h^{n+1}\|_K^2, \tag{6.2.20}
\end{aligned}$$

and

$$\begin{aligned}
& \sum_{K \in \mathcal{T}_h} \delta_K \left(-\kappa_{eff} \Delta \psi^{n+1} + e^{n+1} \cdot \nabla T^{n+1} + u_h^{n+1} \cdot \nabla \psi_h^{n+1}, u_h^{n+1} \cdot \nabla \phi_h^{n+1} \right)_K \\
& + \sum_{K \in \mathcal{T}_h} \delta_K \left(\frac{\psi^{n+1} - \psi^n}{\Delta t}, u_h^{n+1} \cdot \nabla \phi_h^{n+1} \right)_K \tag{6.2.21} \\
& \leq C \sum_{K \in \mathcal{T}_h} \delta_K \left(\kappa_{eff}^2 \|\Delta \psi^{n+1}\|_K^2 + h_K^{-2} |e^{n+1}|_{1,K}^2 |T^{n+1}|_{1,K}^2 + h_K^{-2} |u_h^{n+1}|_{1,K}^2 |\psi^{n+1}|_{1,K}^2 \right) \\
& + \sum_{K \in \mathcal{T}_h} \frac{C}{\Delta t} \delta_K \int_{t^n}^{t^{n+1}} \|\psi_t\|_K^2 dt + \frac{1}{8} \sum_{K \in \mathcal{T}_h} \delta_K \|u_h^{n+1} \cdot \nabla \phi_h^{n+1}\|_K^2.
\end{aligned}$$

$$\begin{aligned}
& \sum_{K \in \mathcal{T}_h} \delta_K \left(\frac{T^{n+1} - T^n}{\Delta t} - T_t(t^{n+1}), u_h^{n+1} \cdot \nabla \phi_h^{n+1} \right)_K \\
& \leq C \sum_{K \in \mathcal{T}_h} \delta_K \Delta t \int_{t^n}^{t^{n+1}} \|T_{tt}\|_K^2 dt + \frac{1}{8} \sum_{K \in \mathcal{T}_h} \delta_K \|u_h^{n+1} \cdot \nabla \phi_h^{n+1}\|_K^2. \tag{6.2.22}
\end{aligned}$$

Letting $\delta_K \leq \min \left\{ \frac{\Delta t}{16}, \frac{h_K^2}{8C_{inv}^2 \kappa_{eff}} \right\}$, $\tau = \frac{1}{6}$ and $\tau = \frac{1}{8}$ in case A) and B), respectively, gives

$$\begin{aligned}
\text{A)} \quad & \frac{\|\phi_h^{n+1}\|^2 - \|\phi_h^n\|^2 + \|\phi_h^{n+1} - \phi_h^n\|^2}{2\Delta t} + \frac{\kappa_{eff}}{2} |\phi_h^{n+1}|_1^2 \\
& + \frac{1}{2} \sum_{K \in \mathcal{T}_h} \delta_K \|u_h^{n+1} \cdot \nabla \phi_h^{n+1}\|_K^2 \leq \frac{\|\phi_h^n\|^2}{2} \\
& + C \left(\frac{1}{\Delta t} \int_{t^n}^{t^{n+1}} \|\psi_t\|^2 dt + \kappa_{eff} |\psi^{n+1}|_1^2 + \frac{|e^{n+1}|_1^2 |T^{n+1}|_1^2}{\kappa_{eff}} + \frac{|u_h^{n+1}|_1^2 |\psi^{n+1}|_1^2}{\kappa_{eff}} \right. \\
& + \sum_{K \in \mathcal{T}_h} \delta_K \left(\frac{1}{\Delta t} \int_{t^n}^{t^{n+1}} \|\psi_t\|_K^2 dt + h_K^{-2} |e^{n+1}|_{1,K}^2 |T^{n+1}|_{1,K}^2 \right. \tag{6.2.23} \\
& \left. \left. + h_K^{-2} |u_h^{n+1}|_{1,K}^2 |\psi^{n+1}|_{1,K}^2 + \kappa_{eff}^2 \|\Delta \psi^{n+1}\|_K^2 + \Delta t \int_{t^n}^{t^{n+1}} \|T_{tt}\|_K^2 dt \right) \right).
\end{aligned}$$

$$\begin{aligned}
\text{B)} \quad & \frac{\|\phi_h^{n+1}\|^2 - \|\phi_h^n\|^2 + \|\phi_h^{n+1} - \phi_h^n\|^2}{2\Delta t} + \frac{\kappa_{eff}}{2} |\phi_h^{n+1}|_1^2 \\
& + \frac{1}{2} \sum_{K \in \mathcal{T}_h} \delta_K \|u_h^{n+1} \cdot \nabla \phi_h^{n+1}\|_K^2 \tag{6.2.24} \\
& \leq C \left(\frac{1}{\kappa_{eff} \Delta t} \int_{t^n}^{t^{n+1}} \|\psi_t\|^2 dt + \kappa_{eff} |\psi^{n+1}|_1^2 + \frac{|e^{n+1}|_1^2 |T^{n+1}|_1^2}{\kappa_{eff}} + \frac{|u_h^{n+1}|_1^2 |\psi^{n+1}|_1^2}{\kappa_{eff}} \right. \\
& + \sum_{K \in \mathcal{T}_h} \delta_K \left(\frac{1}{\Delta t} \int_{t^n}^{t^{n+1}} \|\psi_t\|_K^2 dt + h_K^{-2} |e^{n+1}|_{1,K}^2 |T^{n+1}|_{1,K}^2 \right. \\
& \left. \left. + h_K^{-2} |u_h^{n+1}|_{1,K}^2 |\psi^{n+1}|_{1,K}^2 + \kappa_{eff}^2 \|\Delta \psi^{n+1}\|_K^2 + \Delta t \int_{t^n}^{t^{n+1}} \|T_{tt}\|_K^2 dt \right) \right).
\end{aligned}$$

Summing over timesteps gives

A)

$$\begin{aligned}
& \|\phi_h^N\|^2 + \kappa_{eff} \Delta t \sum_{n=0}^{N-1} |\phi_h^{n+1}|_1^2 + \sum_{n=0}^{N-1} \|\phi_h^{n+1} - \phi_h^n\|^2 + \sum_{K \in \mathcal{T}_h} \delta_K \|u_h^{n+1} \cdot \nabla \phi_h^{n+1}\|_K^2 \\
& \leq \|\phi_h^0\|^2 + \Delta t \sum_{n=0}^{N-1} \|\phi_h^n\|^2 + C \left(\frac{\Delta t}{\kappa_{eff}} \sum_{n=0}^{N-1} (|e^{n+1}|_1^2 |T^{n+1}|_1^2 + |u_h^{n+1}|_1^2 |\psi^{n+1}|_1^2) \right. \\
& + |\psi_t|_{2,0}^2 + \sum_{K \in \mathcal{T}_h} \delta_K (\Delta t^2 \|T_{tt}\|_{2,0,K}^2 + |\psi_t|_{2,0,K}^2 + \kappa_{eff}^2 \|\Delta \psi\|_{2,0,K}^2) + \kappa_{eff} |\psi|_{2,1}^2 \\
& \left. + \Delta t \sum_{n=0}^{N-1} \sum_{K \in \mathcal{T}_h} \delta_K h_K^{-2} (|e^{n+1}|_{1,K}^2 |T^{n+1}|_{1,K}^2 + |u_h^{n+1}|_{1,K}^2 |\psi^{n+1}|_{1,K}^2) \right). \tag{6.2.25}
\end{aligned}$$

B)

$$\begin{aligned}
& \|\phi_h^N\|^2 + \kappa_{eff} \Delta t \sum_{n=0}^{N-1} |\phi_h^{n+1}|_1^2 + \sum_{n=0}^{N-1} \|\phi_h^{n+1} - \phi_h^n\|^2 + \sum_{K \in \mathcal{T}_h} \delta_K \|u_h^{n+1} \cdot \nabla \phi_h^{n+1}\|_K^2 \\
& \leq \|\phi_h^0\|^2 + C \left(\frac{\Delta t}{\kappa_{eff}} \sum_{n=0}^{N-1} (|e^{n+1}|_1^2 |T^{n+1}|_1^2 + |u_h^{n+1}|_1^2 |\psi^{n+1}|_1^2) \right. \\
& \quad + \frac{|\psi_t|_{2,0}^2}{\kappa_{eff}} + \sum_{K \in \mathcal{T}_h} \delta_K (\Delta t^2 \|T_{tt}\|_{2,0,K}^2 + |\psi_t|_{2,0,K}^2 + \kappa_{eff}^2 |\Delta \psi|_{2,0,K}^2) + \kappa_{eff} |\psi|_{2,1}^2 \\
& \quad \left. + \Delta t \sum_{n=0}^{N-1} \sum_{K \in \mathcal{T}_h} \delta_K h_K^{-2} (|e^{n+1}|_{1,K}^2 |T^{n+1}|_{1,K}^2 + |u_h^{n+1}|_{1,K}^2 |\psi^{n+1}|_{1,K}^2) \right). \tag{6.2.26}
\end{aligned}$$

Applying the Gronwall's inequality for Case 1, we get

$$\begin{aligned}
& \|\phi_h^N\|^2 + \kappa_{eff} \Delta t \sum_{n=0}^{N-1} |\phi_h^{n+1}|_1^2 + \sum_{n=0}^{N-1} \|\phi_h^{n+1} - \phi_h^n\|^2 + \sum_{K \in \mathcal{T}_h} \delta_K \|u_h^{n+1} \cdot \nabla \phi_h^{n+1}\|_K^2 \\
& \leq C e^{t_f} \left(\|\phi_h^0\|^2 + \frac{\Delta t}{\kappa_{eff}} \sum_{n=0}^{N-1} (|e^{n+1}|_1^2 |T^{n+1}|_1^2 + |u_h^{n+1}|_1^2 |\psi^{n+1}|_1^2) \right. \\
& \quad + |\psi_t|_{2,0}^2 + \sum_{K \in \mathcal{T}_h} \delta_K (\Delta t^2 \|T_{tt}\|_{2,0,K}^2 + |\psi_t|_{2,0,K}^2 + \kappa_{eff}^2 |\Delta \psi|_{2,0,K}^2) + \kappa_{eff} |\psi|_{2,1}^2 \\
& \quad \left. + \Delta t \sum_{n=0}^{N-1} \sum_{K \in \mathcal{T}_h} \delta_K h_K^{-2} (|e^{n+1}|_{1,K}^2 |T^{n+1}|_{1,K}^2 + |u_h^{n+1}|_{1,K}^2 |\psi^{n+1}|_{1,K}^2) \right). \tag{6.2.27}
\end{aligned}$$

The triangle inequality completes the proof. □

Corollary 1. *Assume*

$$T \in L^\infty(0, t_f; H^2(\Omega)) \cap L^\infty(0, t_f; H^1(\Omega)), T_{tt} \in L^2(0, t_f; L^2(\Omega))$$

(which may or may not hold depending on the regularity of u and Ω_f) and let $Y_h = P_2$. If δ_K is chosen to satisfy the conditions of the Theorem 6.2.2, then

A)

$$\|e_T^N\|^2 + \kappa_{eff} \Delta t \sum_{n=0}^{N-1} |e_T^{n+1}|_1^2 \leq C e^{t_f} \left(\|e_T^0\|^2 + \frac{\Delta t}{\kappa_{eff}} \sum_{n=0}^{N-1} |e^{n+1}|_1^2 + \Delta t^2 + \frac{h^2}{\kappa_{eff}} \right).$$

B)

$$\|e_T^N\|^2 + \kappa_{eff} \Delta t \sum_{n=0}^{N-1} |e_T^{n+1}|_1^2 \leq C \left(\|e_T^0\|^2 + \frac{\Delta t}{\kappa_{eff}} \sum_{n=0}^{N-1} |e^{n+1}|_1^2 + \Delta t^2 + \frac{h^2}{\kappa_{eff}} \right).$$

6.3 NUMERICAL EXPERIMENTS

We test the accuracy of the proposed algorithm for heat transfer on a two-dimensional flow problem. The solid region Ω_s consists of balls with centers at

$$(0.14, 0.496), (0.19, 0.54), (0.17, 0.433), (0.1, 0.44), (0.13, 0.56),$$

$$(0.35, 0.48), (0.34, 0.56), (0.45, 0.5), (0.52, 0.45), (0.57, 0.52)$$

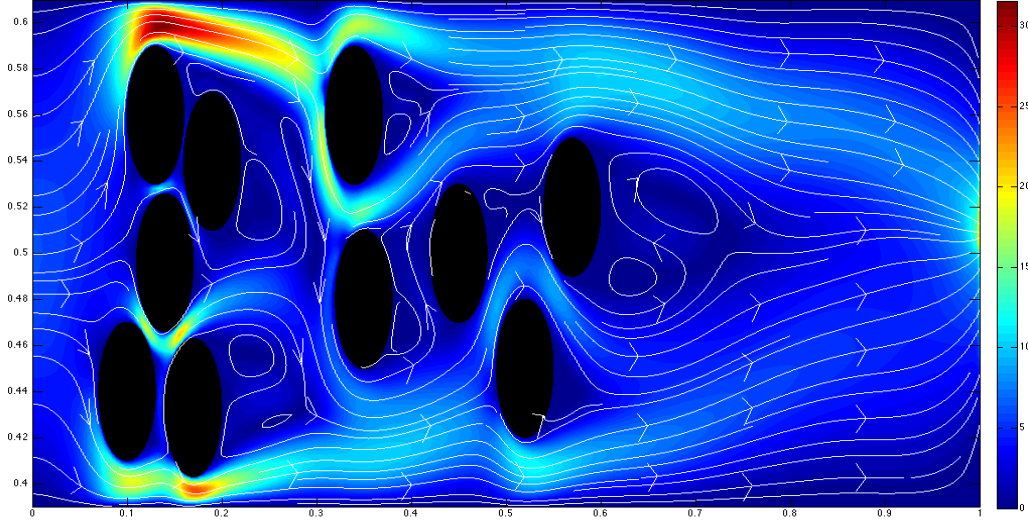
with $r = 0.03$. The boundary conditions are no-slip on the top and bottom boundaries, a parabolic inflow given by

$$U_{in} = ((500 + 5t)(y - 0.39)(0.61 - y), 0)^T$$

and do-nothing outflow. The flow and model parameters are $\nu = 0.005$, $f = (\exp(xy + t), 0)^T \chi_f$, $t_f = 0.1$, $\Delta t = 0.01$ and $\varepsilon = 1e - 15$.

For the heat part of the problem, we take $\Upsilon = 1000\chi_s$ and $T = 0$ at the inlet, $\frac{\partial T}{\partial \mathbf{n}} = 0$ elsewhere on the boundary. The SDFEM parameter δ_K is chosen to be $10^{-3}h_K$. As the theoretical results indicate, the convergence of the algorithm is highly sensitive to the value of the thermal diffusivity coefficient κ_{eff} and we run the experiments for various values of κ_{eff} .

Figure 6.1: The body-fitted, resolved temperature field contours at $t = t_f$



The simulations are performed on three uniform mesh refinements with diameters, 0.37, 0.2 and 0.147, respectively. The results are compared with the resolved solution, obtained by solving the system on a very fine mesh. We compare the temperature contours at $t = t_f$ and temperatures at the channel outlet.

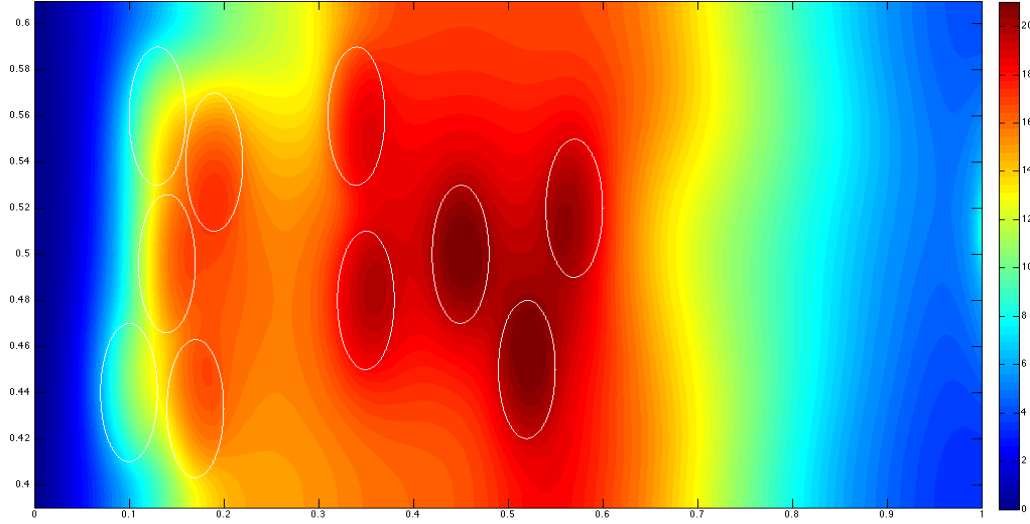
1) Moderate κ_{eff} . We first test with $\kappa_{eff} = \frac{1}{6}$. With this value of κ_{eff} , on all meshes, the mesh Péclet number satisfies

$$0.252 \leq Pe := \frac{\|u\|_{\infty} h}{2\kappa_{eff}} \leq 0.666,$$

and therefore the heat transfer is not convection dominated. Further, as the value of κ_{eff} is moderate, we also expect good convergence of our scheme.

The poor approximation of the velocity field, in turn, produces very inaccurate temperature approximations. E.g., on the coarsest mesh, the Brinkman model predicts nearly zero temperature in the region between two clusters of balls, while

Figure 6.2: The body-fitted, resolved temperature field contours at $t = t_f$, $\kappa_{eff} = \frac{1}{6}$



in the true case we observe $T \geq 14$ in that region. The proposed algorithm yields more accurate temperature contours, with values $T_h \geq 12$ in the above-mentioned region. Further, the undershoot in the peak speed values is also reflected in undershoot of the temperature values.

In some applications, one of the quantities of interest is the temperatures at the outlet of the channel. The Figure 6.7 reveal that our model is again more accurate than the Brinkman model.

We also list the errors in L^2 norm for the temperature variable in the Table 6.1, which demonstrates the higher accuracy of our algorithm.

2) Small κ_{eff} . The next test was performed with $\kappa_{eff} = 2e - 4$. As the convergence estimate (6.2.11) predicts, both algorithms yielded large errors. Similar results were reported in [30]. The effective stabilization of convection-diffusion equations to these types of problems still remains an open problem.

	Brinkman	Model
h		
0.037	3.04802	0.894945
0.02	0.604953	0.184266
0.0147	0.393514	0.136332

Table 6.1: Errors in $L^2(\Omega)$ norm, at $t = t_f$

Figure 6.3: From top to bottom: speed contours of our model on meshes with $h \simeq 0.037$, $h \simeq 0.02$, $h \simeq 0.0147$

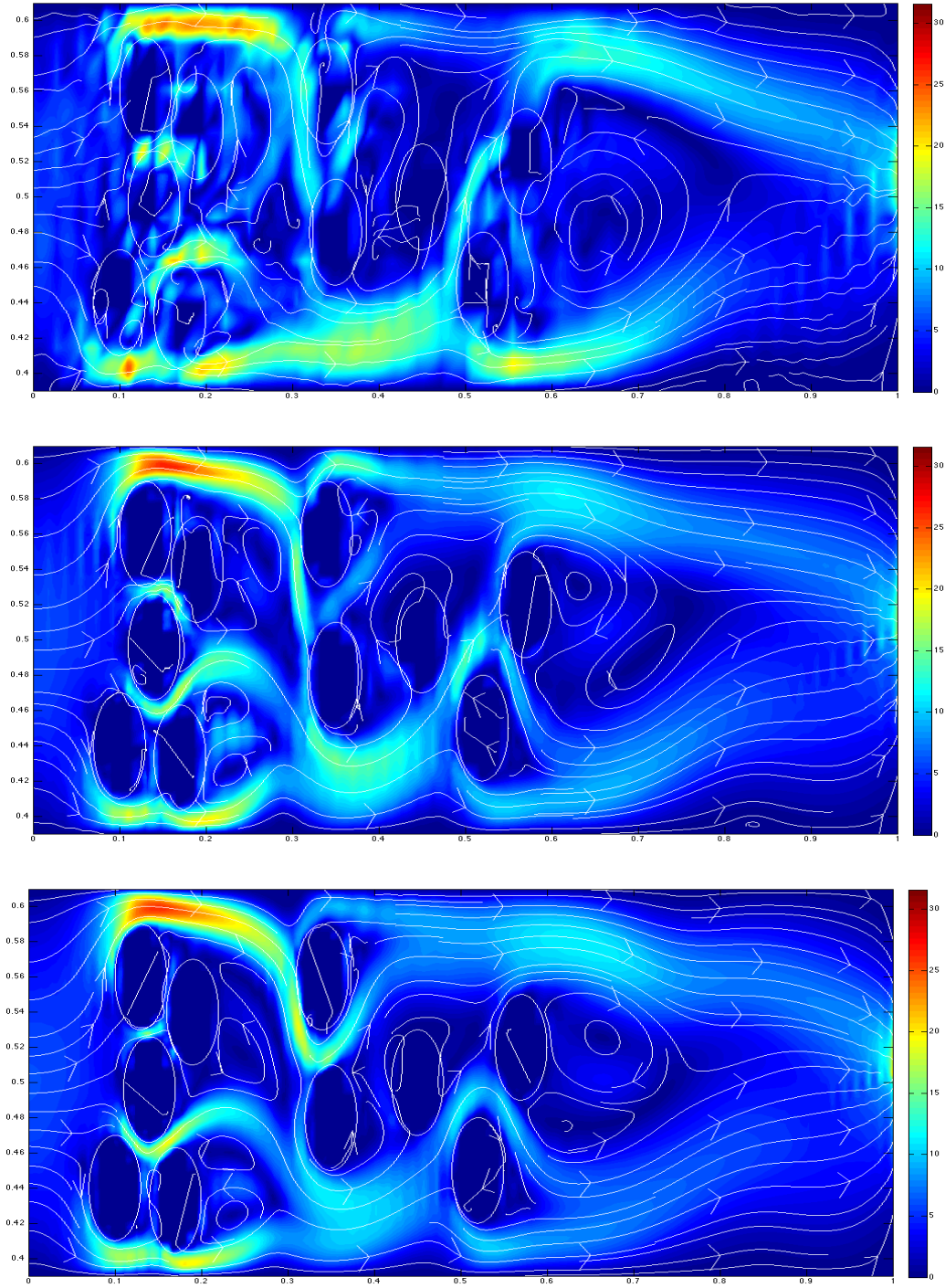


Figure 6.4: From top to bottom: speed contours of Brinkman model on meshes with $h \simeq 0.037$, $h \simeq 0.02$, $h \simeq 0.0147$

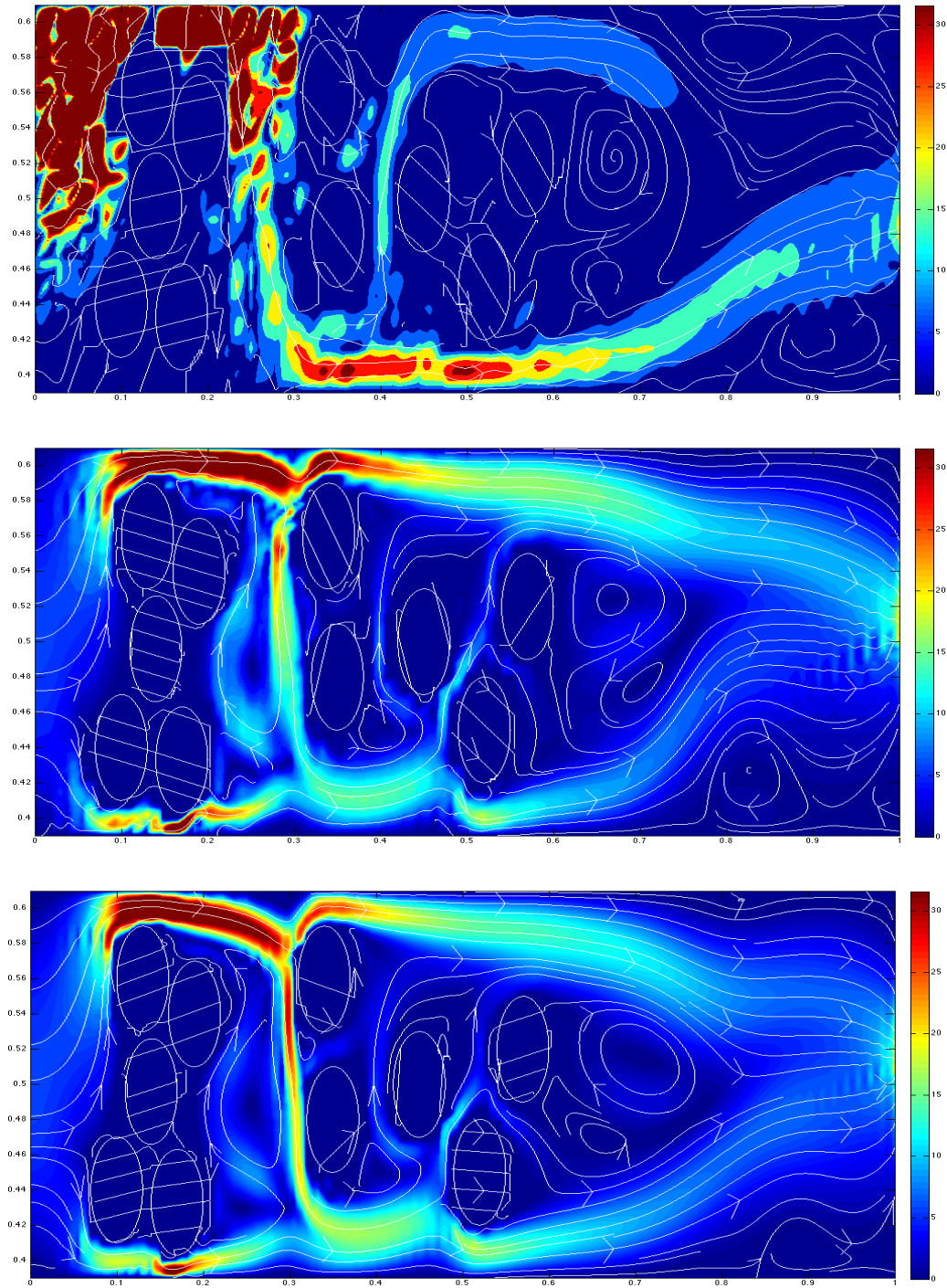


Figure 6.5: From top to bottom: temperature contours of our model for $\kappa_{eff} = \frac{1}{6}$ on meshes with $h \simeq 0.037$, $h \simeq 0.02$, $h \simeq 0.0147$

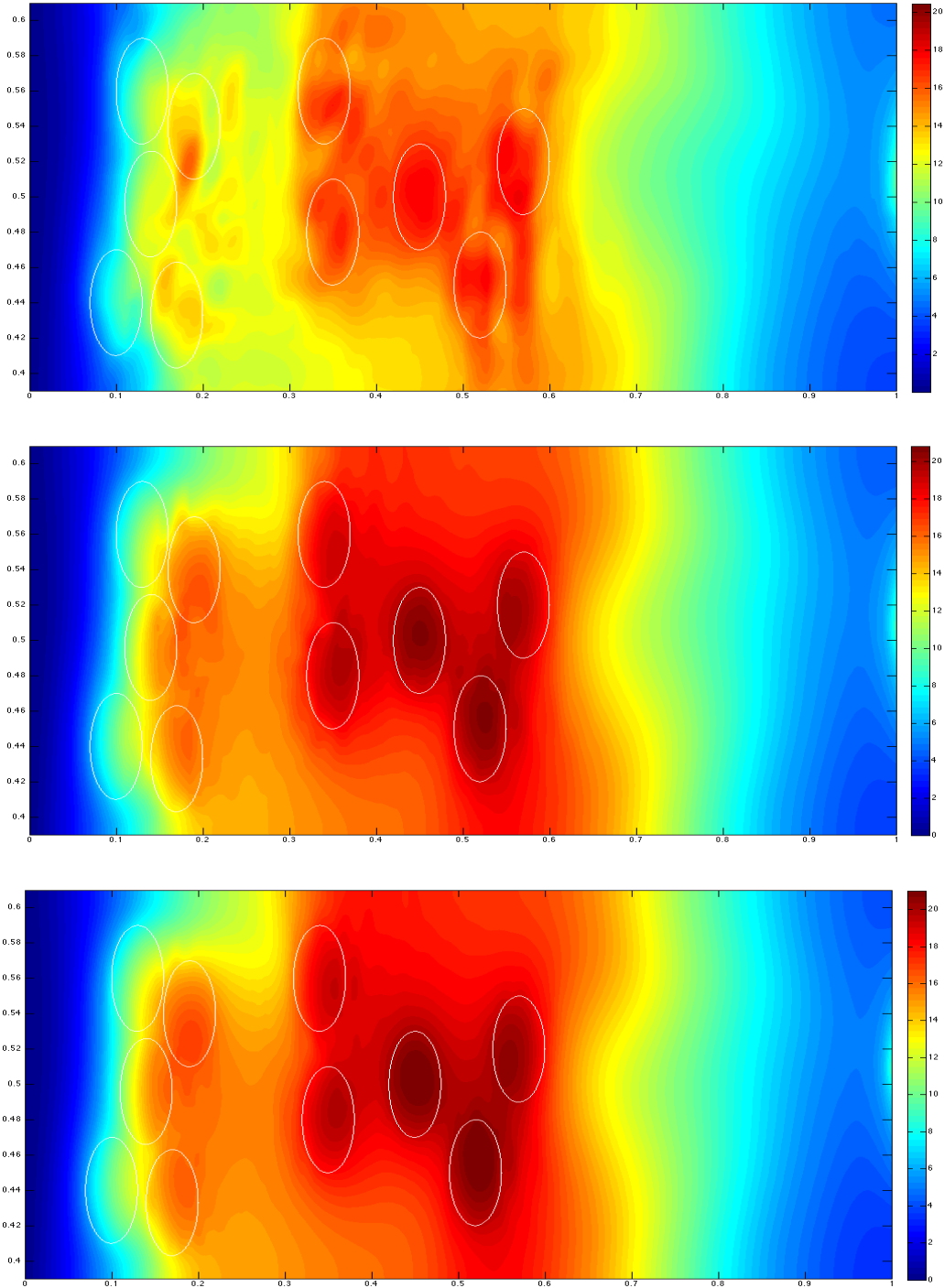


Figure 6.6: From top to bottom: temperature contours of the Brinkman model for $\kappa_{eff} = \frac{1}{6}$ on meshes with $h \simeq 0.037$, $h \simeq 0.02$, $h \simeq 0.0147$

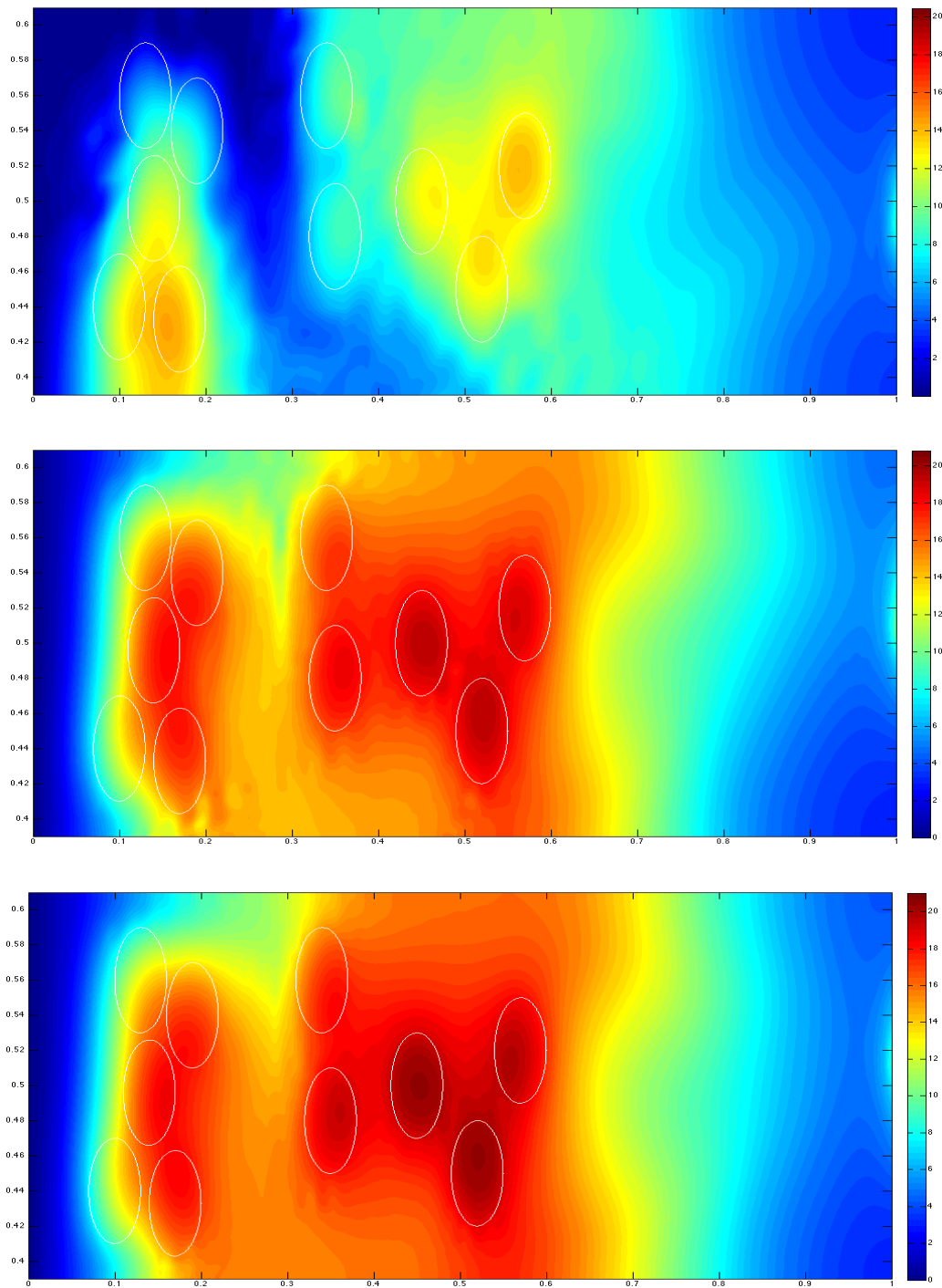
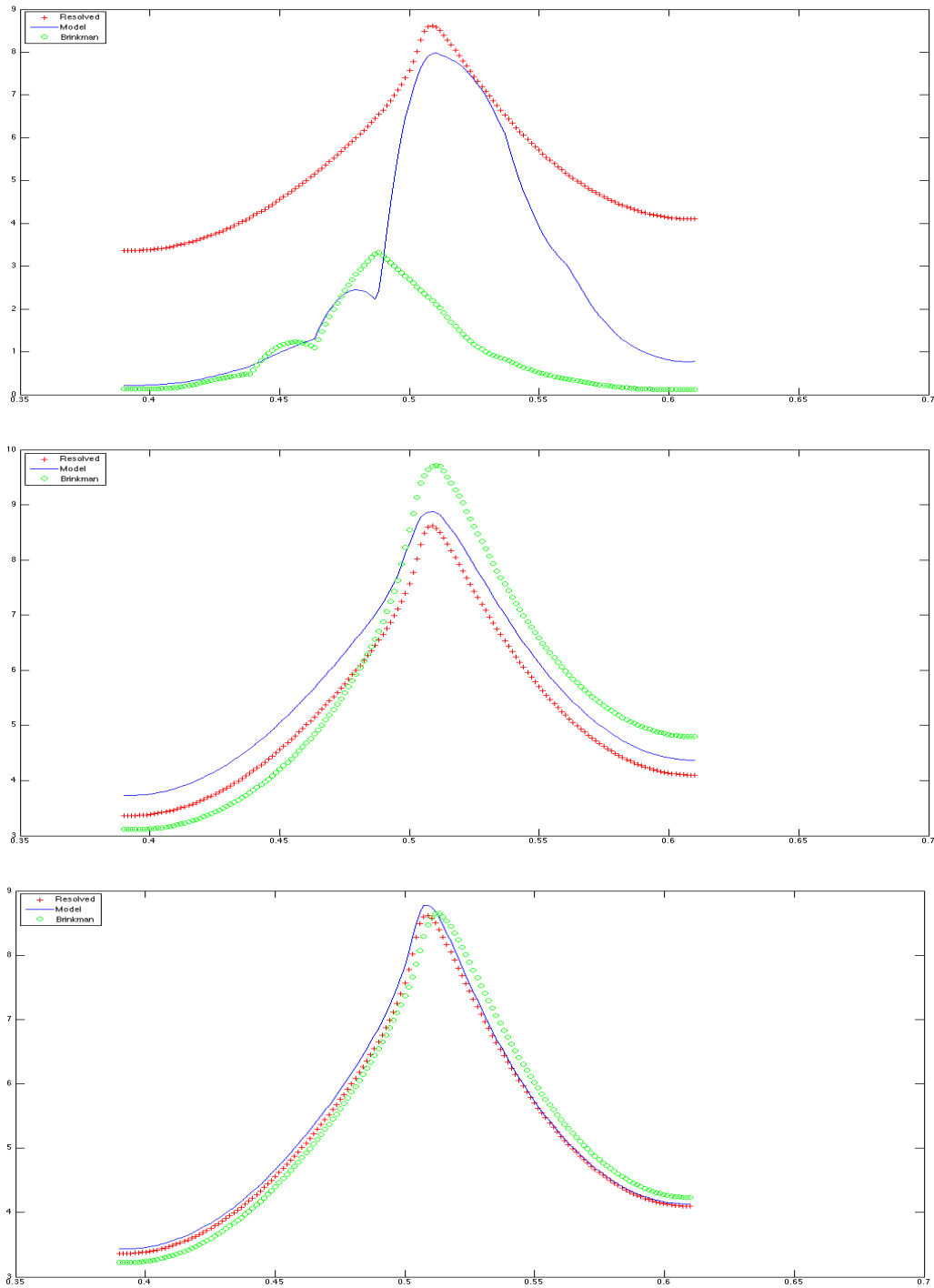


Figure 6.7: From top to bottom: outlet temperatures for $\kappa_{eff} = \frac{1}{6}$ on meshes with $h \simeq 0.037$, $h \simeq 0.02$, $h \simeq 0.0147$



7.0 CONCLUSIONS AND FUTURE PROSPECTS

7.1 CONCLUSIONS

In Chapter 4, we proposed a modification of Brinkman model for small Re fluid flow. It avoids using computationally expensive body-fitted meshes and approximates the flow much more accurately than the original model. The analysis is valid for both 2d and 3d flows. We showed that the model is well-posed on any shape regular mesh. It converges at a rate $\mathcal{O}(\sqrt{\varepsilon})$ in $H^1(\Omega_s)$. Also, we proved a convergence result, where the convergence of the velocity is decoupled from that of the Lagrange multiplier.

In Chapter 5, we formulated new algorithm that applies strong penalization of no-flow without polluting the flow in the pores, while the weak no-flow is implemented using minimally chosen LM space. The new, mesh-conforming penalization region gave positive effects on the results of the computations, including the improved pressure fields and smaller global velocity errors. Another advantage of the algorithm over [50] is that it does not require the careful selection of the penalty parameter ε , it can be chosen small (of course, it effects the condition number of the matrix).

In Chapter 6, we investigated SDFEM for heat transfer, where the convecting velocity is found by the algorithm of Chapter 5. Overall, compared to the Brinkman volume penalization model, the improvements in velocity approximations carry

over to the improved temperature approximations, as well as the drawbacks. We obtained more accurate temperature profiles, outlet temperatures and smaller L^2 errors through our model for moderate or large values of κ_{eff} .

7.2 FUTURE PROSPECTS

The developed algorithms give rise many interesting, new research problems, which will be studied as next steps of these works. The following list discusses some of them:

1. I would like improve the model for fluid flow by adapting ideas from XFEM [35]. For the triangles that intersect the fluid-solid interface, I am considering adding modified, continuous XFEM type functions to capture the geometry of the subregions more accurately.
2. Once the step one is successfully done, I would like adapt the algorithms to higher Re flows.
3. The performed numerical experiments for the developed algorithms have been two dimensional. In the future, I want to implement the three dimensional tests for my approaches.
4. The assembly of the system associated with the developed algorithms require efficient computations of integrals over global mesh cells intersected with spheres. This is a computational geometry question. I want to develop a quadrature rules over such domains for quadrilateral and triangular meshes.
5. In many applications, the solids are in constant motion, which sometimes take place over different time scales compared to fluid flow. Upon satisfactory completion of the above steps, I am planning to extend the algorithms to the case

of moving solids, which will add additional set of equations corresponding to the motion of obstacles.

6. An important aspect of the study of the flow problems is the quantification of various uncertainties. I want to extend my models to include the various uncertainties in the problem parameters.
7. To the authors knowledge, SDFEM for convection-diffusion problems is not addressed for the discontinuous κ case. I would like carry out the analysis of SDFEM for this case.

BIBLIOGRAPHY

- [1] *Millennium Prize Problems*, <http://www.claymath.org/millennium/>, 2010.
- [2] R. Adams, *Sobolev Spaces*, Vol. 65, Pure & App. Math., Academic Press, NY, 1975.
- [3] G. Allaire, *Homogenization of the Navier-Stokes equations in open sets perforated with tiny holes I. Abstract framework, a volume distribution of holes*, Arch. Rational Mech. Anal., 113 (1990), pp. 209-259.
- [4] P. Angot, *Analysis of Singular Perturbations on the Brinkman Problem for Fictitious Domain Models of Viscous Flows*, Math. Meth. Appl. Sci., 22 (1999), pp. 1395-1412.
- [5] P. Angot, C-H. Bruneau and P. Fabrie, *A penalization method to take into account obstacles in incompressible viscous flows*, Numer. Math., 81 (1999), pp. 497-520.
- [6] G.V. Baron, R.G. Willaert and L. De Backer, *Immobilised cell reactors: In Immobilised Living Cell Systems: Modelling and Experimental Methods*, Wiley, 1996.
- [7] J. Bear, *Dynamics of fluids in porous media*, Dover, 1972.
- [8] J. Bear and Y. Bachmat, *Introduction to Modeling of Transport Phenomena in Porous Media*, Kluwer Academic, Dordrecht, 1990.
- [9] L.C. Berselli, T. Iliescu and W.J. Layton, *Mathematics of Large Eddy Simulation of Turbulent Flows*, Springer, 2006.
- [10] P. B. Bochev, M. D. Gunzburger and J. N. Shadid, *Stability of the SUPG Finite Element Method for Transient Advection-Diffusion Problems*, Comp. Meth. Appl. Mech. Engr., 193(23-25) (2004), pp. 2301-2323.

- [11] S. Brenner and L.R. Scott, *The Mathematical Theory of Finite Element Methods*, Springer-Verlag, 2008.
- [12] H.C. Brinkman, *A calculation of the viscous force exerted by a flowing fluid on a dense swarm of particles*, Appl. Sci. Res., A1 (1947), pp. 27-34.
- [13] F. Brezzi and M. Fortin, *Mixed and hybrid finite elements methods*, Springer-Verlag, 1992.
- [14] R. Caulkin, A. Ahmad, M. Fairweather, X. Jia and R.A. Williams, *An investigation of sphere packed shell-side columns using a digital packing algorithm*, Computers and Chem. Engr., 31(12) (2007), pp. 1715-1724.
- [15] P. Ciarlet, *Analysis of the Scott-Zhang interpolation in the fractional order Sobolev spaces*, J. of Num. Math., 21 (3) (2013), pp. 173-180.
- [16] M.J.S. De Lemos, *Turbulence in Porous Media: Modeling And Applications*, Elsevier, 2006.
- [17] A. Ern and J-L. Guermond, *Theory and Practice of Finite Elements*, Springer, 2004.
- [18] G. P. Galdi, *An Introduction to the Mathematical Theory of the Navier-Stokes Equations: Volume 2: Nonlinear Steady Problems*, Springer, 1994.
- [19] G. P. Galdi, *An Introduction to the Navier-Stokes Initial-Boundary Value Problem*, Birkhauser, 2000.
- [20] P-L. George and H. Borouchaki, *Mesh Generation*, Wiley, second ed., 2008.
- [21] V. Girault and R. Glowinski, *Error analysis of a fictitious domain method applied to a Dirichlet problem*, Japan J. Indust. Appl. Math., 12(3) (1995), pp. 487-514.
- [22] V. Girault and P. A. Raviart, *Finite element methods for Navier-Stokes equations*, Springer-Verlag, 1979.
- [23] V. Girault and P. A. Raviart, *Finite element methods for Navier-Stokes equations: theory and algorithms*, Springer-Verlag, 1986.
- [24] V. Girault and L. R. Scott, *A quasi-local interpolation operator preserving the discrete divergence*, CALCOLO 40 (2003), pp. 1-19.

- [25] R. Glowinski, T.W. Pan and J. Périaux, *Distributed Lagrange multiplier methods for incompressible viscous flow around moving rigid bodies*, in *Comput. Methods Appl. Mech. Engrg.*, 151 (1998), pp. 181-194.
- [26] H. S. Fogler, *Elements of Chemical Reaction Engineering*, Prentice Hall, second ed., 2006.
- [27] M. Hamdan, *Single-phase flow through porous channels: A review of flow models and channel entry conditions*, *Appl. Math. Comput.*, 62 (1994), pp. 203-222.
- [28] F. Hecht, *New development in freefem++*, *J. Numer. Math.*, 20(3-4) (2012), pp. 251-265.
- [29] T. J. R. Hughes and A. Brooks. *Streamline upwind/ Petrov-Galerkin formulation for convection dominated flows with particular emphasis on the incompressible Navier-Stokes equations*, *Comp. Meth. Appl. Mech. Engrg.*, 32 (1982), pp. 199–259.
- [30] V. John, T. Mitkova, M. Roland, K. Sundmacher, L. Tobiska and A. Voigt, *Simulations of population balance systems with one internal coordinate using finite element methods*, *Chem. Engr. Sci.*, 64 (2009), pp. 733-741.
- [31] R. Ingram, *Approximating fast, viscous fluid flow in complicated domains*, PhD Thesis, University of Pittsburgh (2011).
- [32] K. Khadra, S. Parneix, P. Angot, and J.-P. Caltagirone, *Fictitious domain approach for numerical modelling of Navier-Stokes equations*, *Int. J. Num. Meth. Fluids*, 34 (2000), pp. 651-684.
- [33] S. F. Magram, *Drinking Water Denitrification in a Packed Bed Anoxic Reactor: Effect of Carbon Source and Reactor Depth*, *Journal of Applied Sciences*, 10 (2010), pp. 558-563.
- [34] N. Martys, D. P. Bentz and E. J. Garboczi, *Computer simulation study of the effective viscosity in Brinkman equation*, *Phys. Fluids*, 6 (1994), pp. 1434–1439.
- [35] N. Moës, J. Dolbow and T. Belytschko, *A finite element method for crack growth without remeshing*, *Int. J. Num. Meth. Engrg.*, 46 (1999), pp. 131-150.
- [36] R. Moormann, *A safety re-evaluation of the AVR pebble bed reactor operation and its consequences for future HTR concepts*, Forschungszentrum Jülich,

Zentralbibliothek, Verlag, Berichte des Forschungszentrums Jülich JUEL-4275, 2008.

- [37] R. Moorman, *AVR prototype pebble bed reactor: A safety re-evaluation of its operation and consequences for future reactors*, Kerntechnik 74 (2009), No. 1 in press.
- [38] C. S. Peskin, *The immersed boundary method*, Acta Numerica, 11 (2002), pp. 1-39.
- [39] A. Quarteroni, *Numerical Models for Differential Problems*, Springer-Verlag, 2009.
- [40] V. V. Ranade, R. Chaudhari and P. R. Gunjal, *Trickle Bed Reactors, Reactor Engineering and Applications*, Elsevier, 2011.
- [41] C.H. Rycroft, G.S. Grest, J.W. Landry and M.Z. Bazant, *Dynamics of random packings in granular flow*, Phys. Rev. E, 73(3) (2006), 051306.
- [42] C.H. Rycroft, G.S. Grest, J.W. Landry and M.Z. Bazant, *Analysis of granular flow in a pebble-bed nuclear reactor*, Phys. Rev. E, 74(3) (2006), 021306.
- [43] P. Sagaut, *Large Eddy Simulation for Incompressible Flows: an Introduction*, Springer-Verlag, third ed., 2006.
- [44] S. Salsa, *Partial Differential Equations in Action - From Modelling to Theory*, Springer, Milan, 2008.
- [45] E. M. Saiki and S. Biringen, *Numerical Simulation of a Cylinder in Uniform Flow: Application of a Virtual Boundary Method*, J. Comp. Phys., 123 (1996), pp. 450-465.
- [46] F. H. Scott, *Elements of Chemical Reaction Engineering*, Prentice Hall, 2005.
- [47] L. R. Scott and Sh. Zhang, *Finite element interpolation of nonsmooth functions satisfying boundary conditions*, Mathematics of Computation, 54(190) (1990), pp. 483-493.
- [48] J. D. Seader and E. J. Henley, *Separation process principles*, Wiley, second ed., 2006.
- [49] L.E. Sissom and D.R. Pitts, *Elements of Transport Phenomena*, McGraw-Hill, Kogakush Japan. 10, 1972.

- [50] A. Takhirov, *Stokes-Brinkman Lagrange multiplier/Fictitious domain method for flows in Pebble Bed Geometries*, SIAM J. Num. Anal., 51(5) (2013), pp. 2874-2886.
- [51] L. Tartar, *The General Theory of Homogenization: A Personalized Introduction*, Springer, 2009.
- [52] R. Temam, *Navier Stokes Equations*, North-Holland, Amsterdam, 2001.
- [53] N. Walkington and J. Howell, *Inf-Sup Conditions for Twofold Saddle Point Problems*, Numer. Math., 118 (2011), pp. 663-693.